

**ON-LINE MONITORING OF BASE METALS
SOLUTIONS IN FLOTATION USING
DIFFUSE REFLECTANCE
SPECTROPHOTOMETRY**

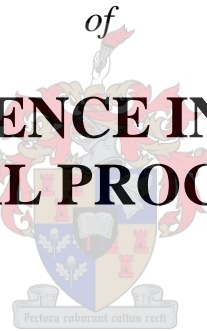
by

Mohau Justice Phiri

Thesis submitted in partial fulfilment
of the requirements for the degree

of

**MASTER OF SCIENCE IN ENGINEERING
(MINERAL PROCESSING)**



in the Department of Processing Engineering
at the University of Stellenbosch

Supervised by
Prof. C. Aldrich

STELLENBOSCH

DECEMBER 2010

DECLARATION

I, the undersigned, hereby declare that the work contained in this thesis is my own original work and that I have not previously in its entirety or in part submitted it at any university for the degree.

Mohau Justice Phiri

Date

.....

.....

ABSTRACT

This work evaluates the use of inverse least squares (ILS) and classical least squares (CLS) models for calibration of a diffuse reflectance spectrophotometer for on-line monitoring of the aqueous phase in a flotation cells. Both models use a Beer's law for the quantification of the metals. The formulated statistical models are compared to a proprietary Blue Cube model in terms of prediction ability to determine the potential applicability of the models. A diffuse reflectance spectrophotometry was used for simultaneous analysis of copper (Cu), cobalt (Co) and zinc (Zn) in the solutions.

The laboratory set-up of Blue Cube instrument was used for the experimental analyses. The concentrations and matrix compositions of the samples are simulated according to Skorpion zinc mine plant conditions. The calibration samples were prepared using a simplex-centroid mixture design with the triplicates of the centroid run. The unknown or test samples were prepared randomly within the same concentration of the calibration samples. The effects of temperature and nickel concentration on absorption of the metals were evaluated in the following range, 20 – 80 °C and 125 – 400 ppm, respectively.

The statistical models (ILS and CLS) were calibrated from visible and near infrared (VNIR) spectra data of the calibration samples. A modified Beer's method was used as a preprocessing technique to convert the raw data into absorbance values. The manual wavelength selection procedure was used to select the wavelengths to be used in both models. The quality of the models was evaluated based on R^2 and % root mean squared error (RMSE) values with 0.90 and 10% used as the guideline for the respective statistical parameters.

Both ILS and CLS models showed good results for all three metals (Cu, Co and Zn) during their calibration steps. It was further shown that both models give worse predictions for Zn as compared to other metals due to its low relative intensity in the mixture. The derivative orders of absorbance spectra that were used to enhance the prediction results of Zn had no positive effect but they rather lowered accuracy of predictions. An increase in temperature was found to increase the intensities of the absorption spectra of all the metals while an increase in nickel concentration decreases the prediction ability of model.

The developed statistical models were compared to a Blue Cube model in terms of prediction ability using analysis of variance (ANOVA) test. The ANOVA results revealed that there is no statistical difference between the developed models and Blue Cube model since the F-values for all the metals were below the critical F-value. Furthermore, the partial least squares (PLS) model shows an increased accuracy results for prediction of zinc metal as compared to both the ILS and CLS models. Finally, good comparisons of the statistical models results with atomic absorption spectroscopy (AAS) analyses were establish for the unknown samples.

The study demonstrates that chemometric models (ILS and CLS) developed here can be used for quantification of several metals in real hydrometallurgical solutions as samples were simulated according to a plant conditions. However, in order to have confidence in the results of the models, a factorial-mixture design must be used to study the effect of temperature and nickel concentration. Moreover the models must be further tested and validated on the real samples from a plant.

OPSOMMING

Hierdie werkstuk evalueer die gebruik van inverse kleinste kwadraatmetodes (IKK) en klassieke kleinste kwadraatmetodes (KKK) vir die kalibrasie van 'n diffuse reflektansiespektrofotometer vir die aanlyn monitering van die waterige fase in flottasieselle. Beer se wet word vir die kwantifisering van metale vir albei modelle gebruik. Die omskrewe data-gebaseerde modelle is op grond van voorspellingsvermoë vergelyk met 'n Blue Cube model, sodat die moontlike toepaslikheid van hierdie modelle bepaal kan word. 'n diffuse reflectantie spektrofotometrie is ingespan vir die gelyktydige analise van koper (Cu), kobalt (Co) en sink (Zn) in oplossing.

Eksperimentele analises is met behulp van 'n laboratoriumopstelling met 'n Blue Cube instrument uitgevoer. Die konsentrasies en matriks-samestellings van monsters is gesimuleer om Skorpion sinkmyn aanlegkondisies na te boots. Kalibrasie monsters is voorberei volgens 'n simpleks-sentroïed mengselontwerp met drievoudige sentroïede lopies. Onbekende (toets) monsters is ewekansig voorberei binne dieselfde konsentrasie spesifikasies as die kalibrasie monsters. Die invloed van temperatuur en nikkelskonsentrasie op die absorpsie van die metale is in die bestek van 20 – 80 °C en 125 – 400 dpm, onderskeidelik, bepaal.

Die data-gebaseerde modelle (IKK en KKK) is met sigbare en naby infrarooi (SNIR) spektra data van die kalibrasie monsters gekalibreer. 'n Gewysigde Beer metode is vir data voorbereiding benut om rou data na absorpsie waardes om te skakel. Die handgolfleengte-seleksieprosedure is vir beide modelle gebruik om die golfleengtes te kies. Die kwaliteit van die modelle is op grond van R^2 en % wortel gemiddelde kwadratiese fout (WGKF) geëvalueer, met waardes van 0.90 en 10% (onderskeidelik) as riglyne vir hierdie statistiese parameters.

Beide IKK en KKK modelle het vir hul kalibrasie stappe vir al drie metale (Cu, Co en Zn) goeie resultate getoon. Dit is verder getoon dat albei modelle die slegste voorspellings lewer vir Zn (vergeleke met die ander metale) as gevolg van Zn se lae relatiewe intensiteit in die mengsel. Afgeleide ordes van absorpsie spektra is gebruik om die Zn voorspellings te versterk, maar het geen positiewe effek gehad nie; intendeel, voorspellingakkuraatheid is

verlaag. 'n Verhoging in temperatuur het die intensiteite van die absorpsie spektra van alle metale verhoog, terwyl 'n verhoging in nikkelkonsentrasie die voorspellingakkuraatheid van die modelle verlaag het.

Die ontwikkelde data-gebaseerde modelle is met 'n Blue Cube model vergelyk in terme van voorspellingsvermoë met behulp van variansie-analise (ANOVA). Die ANOVA resultate toon dat daar geen statistiese verskil tussen die ontwikkelde modelle en die Blue Cube model is nie, aangesien die F-waardes vir al die metale onder die kritiese F-waarde is. Die gedeeltelike kleinste kwadraatmodel (GKK) toon verder verhoogde voorspellingakkuraatheid vir sinkmetaal tenoor beide die IKK en KKK modelle. Ten slotte, goeie ooreenstemming van die data-gebaseerde modelresultate met atoomabsorpsie spektroskopie (AAS) analise is vir die onbekende monsters gevind.

Hierdie werkstuk toon dat die chemometriese modelle (IKK en KKK) wat hier ontwikkel is, gebruik kan word vir die kwantifisering van verskeie metale in werklike hidrometallurgiese oplossings, aangesien monsters gesimuleer is volgens aanlegkondisies. Om egter verdere vertroue te hê in die modelresultate, sal 'n faktoriaal-mengselontwerp toegepas moet word om die effek van temperatuur en nikkelkonsentrasie te ondersoek. Voorts moet die modelle verder getoets en gevalideer word op werklike monsters van 'n aanleg.

DEDICATION

*In loving memory of my parents,
Mosala & 'Masebongile Phiri*

ACKNOWLEDGEMENTS

There are a number of people who have contributed to the completion of this research. Each individual has played an essential role in its finalization before the targeted time as follows:

My supervisor, Prof. C. Aldrich, for the courage he has shown when the work seemed difficult, and most importantly for the advice given on how to tackle problems in modelling.

My sponsor, Lets'eng Diamond Mine Company, for the financial support they have given throughout my MSc studies at Stellenbosch University.

Blue Cube Systems Company, for providing technical assistance with the optical fibre sensor. More importantly, the indispensable discussion from Frans Jansen and Francois du Plessis was most valuable.

Mpho Phiri, for her assistance during the preparation of the sample's solutions and for her valuable discussion on the solution chemistry section of this thesis.

Dr. M. Sekota, for her contribution and explanation on the transition chemistry of the metals in this study.

Lidia Auret, for her demonstration on data visualisation using Matlab software program. Additionally, her advice concerning the modelling were highly appreciated.

Dana Kell, for her invaluable suggestions and comments throughout the proof reading and editing of this thesis.

My family, for standing with me by the prayers and the support they had shown during the years of my studies.

My friends, Lebohang Hlalele and Mthobi Erasmus, for the words of encouragement they had given during the tough times of the research work.

The most sincere thanks must be given to Almighty God for the strength He has given me to manage the work of this project. Most importantly, I thank Him for the special combination of talents, inspiration and creativity which allowed this project to be completed.

Table of Contents

DECLARATION.....	i
OPSOMMING	iv
DEDICATION	vi
ACKNOWLEDGEMENTS.....	vii
LIST OF TABLES	xii
LIST OF FIGURES	xiii
ABBREVIATIONS	xv
NOMENCLATURE	xvi
1 INTRODUCTION	1
1.1 Flotation Principles Overview	1
1.2 Importance of an On-line Analyses.....	3
1.3 Control in Mineral Processing	4
1.4 Motivation of the Study.....	5
1.5 Objectives of the Study.....	5
1.6 Layout of the Thesis	6
2 REVIEW OF ON-LINE SPECTROSCOPY IN MINERAL PROCESSING.....	8
2.1 On-line Spectroscopy Measurements	8
2.1.1 On-stream Analysers	10
2.1.2 Diffuse Reflectance Spectrophotometry.....	12
2.1.2.1 Principles of the spectrophotometry.....	12
2.1.2.2 Chemically Modified Optical Sensor	13
2.1.2.3 Optical Fibre Sensors	14
2.2 Factors affecting the performance of Spectroscopy	17
2.2.1 Particle Size of Mineral	17
2.2.2 Mineral Composition.....	18
2.2.3 Temperature of Sample	18

3	REVIEW OF CALIBRATION MODELS.....	20
3.1	Classical Least Squares Methods	21
3.1.1	Theory.....	21
3.1.2	Application in Spectral Analysis.....	22
3.2	Inverse Least Squares Methods.....	26
3.2.1	Theory.....	26
3.2.2	Application in Spectral Analysis.....	28
4	EXPERIMENTAL WORK.....	32
4.1	Review on Experimental Design.....	33
4.1.1	Motivation for Experimental Design.....	33
4.1.2	The Concept of Mixture Design.....	35
4.1.3	Simplex-centroid design of three components mixture.....	37
4.2	Laboratory Samples Preparation.....	38
4.2.1	Calibration and Test Samples	39
4.2.2	Samples for Nickel effect	40
4.2.3	Samples for Temperature Effect	41
4.2.4	Blank Samples.....	41
4.3	Experimental Set-up	42
4.3.1	Instrument Description	42
4.3.2	Internal Calibration of the Instrument	43
4.4	Methodology	44
4.4.1	Analytical Procedure: Calibration and Test Samples	44
4.4.2	Effect of Nickel.....	46
4.4.3	Effect of Temperature on Samples.....	46
5	RESULTS AND DISCUSSION.....	48
5.1	Model Development	49
5.1.1	Data assessment	49

5.1.1.1	Measurements Consistency.....	50
5.1.1.2	Comparison of Calibration and Test data.....	51
5.1.2	Preprocessing Step	54
5.1.3	Calibration Step.....	56
5.1.4	Influence of number of calibration samples	60
5.2	Model Validation.....	61
5.2.1	Residual Plots.....	62
5.2.2	Influence of mixture component on calibration step.....	63
5.3	Testing of the model; Prediction Step	66
5.4	Derivative Spectroscopy.....	71
5.4.1	Mathematical background.....	71
5.4.2	Data Manipulation.....	73
5.4.3	Optimisation of the Model.....	75
5.5	Robustness of the Model	76
5.5.1	Effect of Temperature.....	76
5.5.1.1	Model Predictive ability	77
5.5.1.2	Influence on Spectra.....	79
5.5.2	Effect of Contaminants	82
5.5.2.1	Model Predictive ability	82
5.5.2.2	Influence on Spectra.....	85
5.6	Potential Applicability of the developed Models.....	87
5.6.1	Blue Cube Model	87
5.6.2	Partial Least Squares Model	91
5.6.2.1	Background of the PLS Model	91
5.6.2.2	Data Interpretation with PLS model.....	93
5.6.3	Atomic Absorption Spectroscopy (AAS)	98
6	CONCLUSIONS AND RECOMMENDATIONS	101

6.1	Conclusions.....	101
6.2	Recommendations	103
	REFERENCE.....	104
	APPENDIX A: TEST SAMPLES.....	112
	APPENDIX B: PERFORMANCE OF CLS MODEL	112
	B.1 Calibration Step of CLS model.....	112
	B.2 Prediction Step of CLS Model.....	113
	APPENDIX C: DERIVATIVE SPECTROSCOPY	114
	APPENDIX D: FACTORS AFFECTING CLS MODEL	115
	D.1 Effect of the temperature.....	115
	D.2 Effect of the Nickel concentration	116
	APPENDIX E: SUPPLEMENTARY METHODS	117
	E.1 PLS model evaluation.....	117
	E.2 AAS experiments	119
	APPENDIX F: PUBLICATIONS	120
	Presentations.....	120
	Peer-reviewed Journal.....	120

LIST OF TABLES

Table 3.1: Comparison of CLS and ILS in terms of spectral analysis	31
Table 4.1: The metals' concentrations as found at Skorpion Zinc flotation plant.....	39
Table 4.2: Preparation of stock solution using sulphuric acid	39
Table 4.3: Sample solutions used for calibration procedure.....	40
Table 4.4: Sample solutions for determination of nickel interference effect.....	41
Table 4.5: Sample Solutions for determination of temperature effect	41
Table 5.1: Repeatability of Individual Measurements from Raw Data.....	50
Table 5.2: Selected wavelength region for each individual metal	57
Table 5.3: Results from the calibration steps of ILS and CLS model.....	58
Table 5.4: Absorbance response from the calibration samples.....	63
Table 5.5: Sequential fit and statistics of the models	64
Table 5.6: Results from the prediction steps of ILS and CLS model.....	69
Table 5.7: Selection of wavelength region from derivate spectra for ILS model	74
Table 5.8: Precision of ILS model for Cu, Co and Zn at various temperatures.....	79
Table 5.9: Summary statistics for the comparison of the models	89
Table 5.10: Results of ANOVA test for comparison of the models.....	90
Table 5.11: Multiple comparisons of pair of the models and theoretical data.....	91
Table 5.12: Statistically comparisons for prediction ability of CLS, ILS and PLS model.....	98

LIST OF FIGURES

Figure 1.1: Flow sheet for industrial flotation process of typical mineral.....	3
Figure 2.1: Attenuation of an incident beam through absorption of radiation by sample	12
Figure 2.2: Chromite variation before and after implementation of Blue Cube optical sensor	17
Figure 2.3: UV-VIS absorption of nickel complex and its dependence on temperature (after Kumagai <i>et al</i> , (2008)).....	19
Figure 4.1: Illustration of interactions effect in mixture design.....	36
Figure 4.2: Three factor simplex-centroid mixture design	37
Figure 4.3: Blue Cube optical fibre sensor instrument	43
Figure 4.4: Laboratory set-up of Blue Cube instrument showing sample holder	44
Figure 4.5: Blue Cube laboratory set-up during the drainage of used solution	45
Figure 4.6: Schematic diagram of Blue Cube laboratory set-up.....	46
Figure 5.1: Raw spectra of pure Cu, Co, Zn and their mixture.....	49
Figure 5.2: Consistency of measurements during calibration and prediction steps	51
Figure 5.3: Sammon mapping for the calibration and test data	52
Figure 5.4: Comparison of calibration (A) and test data (B) for each wavelength number ...	53
Figure 5.5: Absorption spectra of pure Cu, Co and Zn together with their mixture	55
Figure 5.6: Absorption spectra showing maximum peaks of pure Zn and Co	56
Figure 5.7: Calibration graph for the Cu metal using ILS model	59
Figure 5.8: Calibration graph for the Co metal using ILS model	59
Figure 5.9: Calibration graph for the Zn metal using ILS model.....	60
Figure 5.10: The effect of calibration samples on prediction ability of ILS model	61
Figure 5.11: Normality plot of the studentised residuals of calibration samples	62
Figure 5.12: Absorbance contour plot for the components of the linear mixture model	65
Figure 5.13: Stock solution for pure Cu, Zn and Co metals	66
Figure 5.14: Graph for the prediction of Cu metal using ILS model	67
Figure 5.15: Graph for the prediction of Co metal using ILS model	68
Figure 5.16: Graph for the prediction of Zn metal using ILS model	68
Figure 5.17: Electron Configuration of in the outer d-orbital of Cu, Co and Zn ions.....	70
Figure 5.18: First, second, third and fourth derivative spectroscopy of Cu, Co and Zn metals	74
Figure 5.19: Evaluation performance of derivative spectroscopy.....	75

Figure 5.20: Prediction ability of ILS model for copper metal at various temperatures	77
Figure 5.21: Prediction ability of ILS model for cobalt metal at various temperatures	78
Figure 5.22: Prediction ability of ILS model for zinc metal at various temperatures	78
Figure 5.23: Influence of temperature on absorption spectra of the metals	80
Figure 5.24: Effect of water on the absorption spectra of Co and Zn metals	81
Figure 5.25: Energy levels for orbitals of an atom.....	82
Figure 5.26: Prediction ability of ILS model for copper metal in presence of nickel.....	83
Figure 5.27: Prediction ability of ILS model for cobalt metal in presence of nickel	83
Figure 5.28: Absorption spectra of solution of Cu and Co in the presence of nickel	84
Figure 5.29: Prediction ability of ILS model for zinc metal in presence of nickel.....	85
Figure 5.30: Absorption spectra of pure Cu, Co, Zn and Ni metals.....	86
Figure 5.31: Absorption spectra of nickel in increasing concentration.....	86
Figure 5.32: Comparison of developed models and Blue Cube for a Cu metal	88
Figure 5.33: Comparison of developed models and Blue Cube for a Co metal	88
Figure 5.34: Comparison of developed models and Blue Cube for a Zn metal.....	89
Figure 5.35: Score plot for detection of the outliers.....	94
Figure 5.36: The explained variance in the calibration data	95
Figure 5.37: Cross- validation method for the PLS model.....	96
Figure 5.38: Prediction results of the unknown samples.....	97
Figure 5.39: Comparison of the ILS, CLS and PLS model	97
Figure 5.40: Calibration graph of the Cu metal for AAS analysis.....	99
Figure 5.41: Predicted results for copper using the AAS technique	99

ABBREVIATIONS

AAS	Atomic absorption spectroscopy
ACLS	Augmented classical least squares
ANOVA	Analysis of variance
CLS	Classical least squares
CV	Cross validation
CMOS	Chemically modified optical sensor
DRS	Diffuse reflectance spectrophotometry
GILS	Genetic inverse least squares
HPLC	High pressure liquid chromatography
ILS	Inverse least squares
IR	Infrared
LIBS	Laser-induced breakdown spectroscopy
PACLS	Prediction augmented classical least squares
PCA	Principal component analysis
PCR	Principal component regression
PLS	Partial least squares
RMSE	Root mean square error
SSA	Singular spectrum analysis
STDV	Standard deviation
UV	Ultraviolet
VIS	Visible
VNIR	Visible and near infrared
XPS	X-ray photoelectron spectroscopy
XRF	X-ray fluorescence

NOMENCLATURE

A	Absorbance
A	Absorbance spectra matrix
A_u	Absorbance of the unknown spectra matrix
β_i	Regression coefficient for a mixture regression model
B	Regression coefficient
b	Sample path length
C	Concentration of a sample
C	Concentration matrix of calibration samples
C_u	Concentration matrix of unknown samples
E	Residual matrix for absorbance
E_A	Errors matrix for calibration
E_U	Errors matrix for prediction
e	Error of individual spectrum
ε	Molar absorptivity of the analyte
d _{os}	Distance in original space
d _{ps}	Distance in projection space
F	Residual matrix for concentration
I	Transmitted intensity
I ₀	Incident intensity
K	Calibration coefficient for classical model
P	Calibration coefficient for inverse model
P	Loading matrix for absorbance
Q	Loading matrix for concentration
R ²	Correlation coefficient
T	Score matrix for absorbance
T	Transmittance
U	Score matrix for concentration
x_1, x_2, x_3	Coded values for regression model factors
y	Response value for mixture regression model
Y _{pred}	Predicted value by the model

Y_{mean}

Mean of the predicted values

Y_{theor}

Theoretical value

CHAPTER 1: INTRODUCTION

This chapter introduces the process of flotation and gives a number of reasons why a complex process like flotation must be monitored by on-line methods for better process control. A brief background on the on-line control methods such as on-stream analysers, image processing techniques and diffuse reflectance spectrophotometry (DRS) is given. From the basis of the success of DRS, the motivation and objectives of the study are laid out. The methods used for data collection and analysis are briefly discussed. The chapter concludes by giving the layout of the thesis.

1 INTRODUCTION

The consumption of valuable minerals is ever increasing in modern societies due to their usage in everyday life. Commodities, such as iron, coal and oil are used in large quantities to fuel economic growth in developing and developed countries alike. In addition, minerals produced in smaller quantities, like copper, gold and nickel, are also essential in everyday usage. Mining and mineral processes have become essential tools for obtaining the minerals that contribute to the growth of countries' economy. Of all the unit processes required to produce these commodities, froth flotation is the widely used one. Froth flotation contributes a major portion to mineral processing, not only because it is a mature process, but can also be easily implemented on large scale to process different mineral ores. It is used mainly for the separation of a large range of sulphides, carbonates and oxides prior to further refinement.

1.1 Flotation Principles Overview

Froth flotation makes use of the differences in physico-chemical surface properties of various mineral particles to achieve separation. In order for a process to take place, an air-bubble

must attach itself to particles so as to lift them to the water's surface (Wills, 1997). The flotation process involves many mechanisms that affect the froth's characteristics, which in turn determines flotation performance. It is also influenced by many manipulated variables, thus making it one of the most difficult processes to understand to date (Sauter and Ragot, 2008). Reagents such as frothers, collectors, activators and depressants have an effect on the chemical environment of the flotation pulp since they can enhance or reduce the chances of bubble-mineral aggregate formation.

It is important to control these reagents so that the good froth properties can be achieved. A brief description of each reagent is given as follows (Bartolacci *et al*, 2006):

Frother reduces the average bubble size within the pulp and leads to the formation of a separate froth phase above the pulp. However, it can cause froth instability due to excessive addition.

Collector makes the valuable mineral hydrophobic so that it can be uplifted by air bubbles which further control the froth mobility and drainage rate.

Activator regulates the chemical nature of mineral surfaces so that they become hydrophobic due to the action of the collector. It has been reported that too much activator can lead to froth collapse (Ylinen, 2000).

Depressant is used to increase the selectivity of flotation by rendering certain minerals hydrophilic, thus preventing their flotation and is used to control the pH of the system.

Despite decades of research, flotation is a complex process that is still not understood sufficiently well to model and control on an advanced basis and one of the main reasons is the lack of on-line sensors that can be used to measure the state of the flotation system. Computer vision, (Aldrich *et al*, 2010), is a possible exception to this, but the technique has not yet proved useful to assess the metallurgical composition of the aqueous phase of the flotation system. Basically, there are two control methods commonly used, namely off-line and on-line. In this work, the focus will be on the latter due to their quick analysis time over the former when employed on an industrial scale. Furthermore, the urgent need for better information has led to increased effort to develop analytical sensors. This type of sensors have brought a lot of improvement in the control and monitoring of complex process like flotation as will be illustrated in the section that follows.

1.2 Importance of an On-line Analyses

Most sulphide ores have traditionally been processed using pyrometallurgical process to produce a matte that goes through further refining, however copper, nickel, zinc and all other minor minerals can be produced using other extractive metallurgy. Recent advances in hydrometallurgy have resulted in mineral processing operations that can be applied in this area. Most of the sulphides of low grade have traditionally been processed by concentrating through a froth flotation process, since the reagents used are very selective to a specific mineral to be processed.

The on-line determination of these metals plays a significant role during the extraction processes. There will be improvements in the whole plant system efficiency. When evaluating the significance of on-line analytical methods Figure 1.1 will be used. The figure shows the schematic diagram of the flotation process of a typical ore.

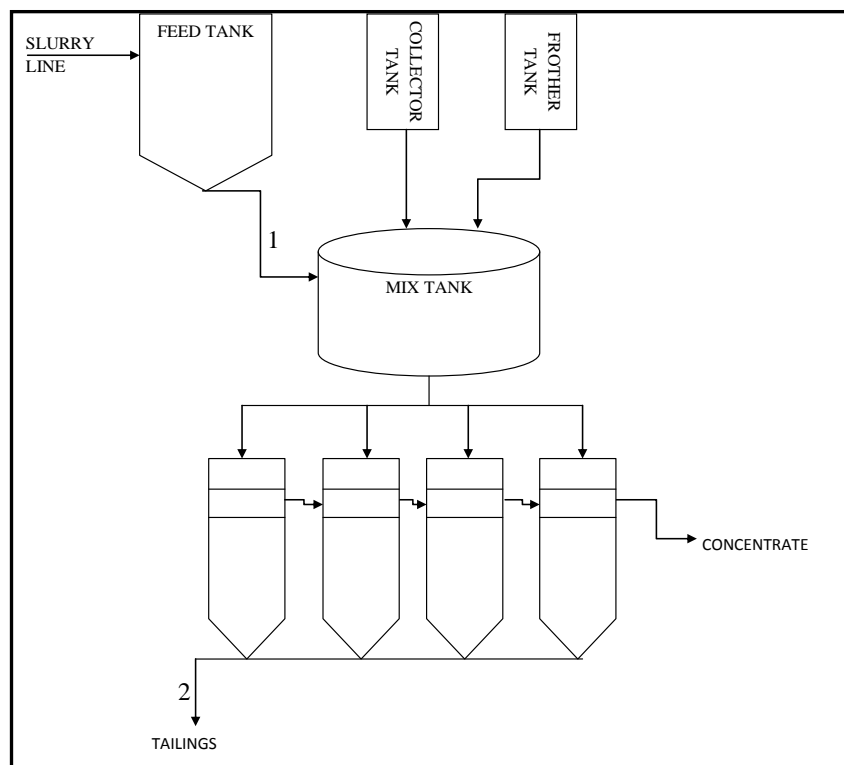


Figure 1.1: Flow sheet for industrial flotation process of typical mineral

From Figure 1.1, it can be observed that if the quantity of the mineral in stream labelled 1 from the feed tank is known, the amount of chemical reagents (collector and frother) used during the flotation process will be proportional to mineral content in that particular stream.

Thus a high recovery of mineral can be achieved through an effective process. The plant will save a great deal of money from the cost of reagents. Furthermore, by knowing the mineral content in stream labelled 2, the efficiency of the flotation process can be determined. Then the whole plant performance can be improved due to the fact that mineral content will be easily quantified in the solution. Both streams 1 and 2 can be determined by an online analysis method, which will be developed in this research project. These methods can perform fast analysis, thus can detect plant disturbances within a short period of time.

The on-line measurements are non-intrusive, hence there is no interference with the process, and thus plant operations run smoothly without interruptions. Moreover on-line analysis reduces the health hazards that are usually experienced during the sampling process for laboratory analysis (Sowerby, 2002). Moreover, the laboratory analyses were subjected to large sampling errors whereas on-line methods provide high quality sampling data through the analysis of large continuous volumes of material at hand (Gaft *et al*, 2007).

1.3 Control in Mineral Processing

Due to the benefits brought by on-line analysis, there are a number of techniques that had been developed for process control. These mostly include include on-stream analysers based on the use of data from the electromagnetic spectrum, such as optical or (near) infrared sensors. Furthermore, Bartolacci *et al*, (2006) observed that human eyes, are insufficient monitors for highly complex processes like flotation, hence an on-line machine vision system is needed for those particular applications. The on-stream analysers like XRF analysers make sampling time longer by about 15 minutes when employed on large plants, where there are several slurry lines. Moreover, some of the computational algorithms used to interpret the signals are yet sufficiently robust for automated use in real plant situations.

Optical fibre sensors have found a wide application in many industries including the pharmaceutical, food processing, and mineral processing. There are several reasons for this wide application. For example, the instruments are relatively low cost and can easily be operated without any health hazards. Additionally and most importantly, the sensors use diffuse reflectance spectroscopy for their measurements. In this technique, light is scattered

and reflected through the sample of interest (Lottering and Aldrich, 2006; Haavisto *et al*, 2008).

De Waal and Du Plessis (2005) used the optical fibre sensor to determine the mineral composition of heavy sands. The research work done by Haavisto *et al*, (2008) on the optical monitoring of the flotation process formed the basis in application of optical fibre in mineral processing. In their work, an optical fibre sensor was combined together with statistical models to control and monitor the copper-zinc flotation plant and an XRF analyser was used to update the calibration model. The methods developed in each application are plant specific, however they can be extended to other and different plant conditions.

1.4 Motivation of the Study

The Blue Cube Systems Pty (Ltd) is located in Stellenbosch, South Africa and has become an established manufacturer of on-line, mineral industry instruments for analysis of dry, slurry and aqueous solution samples. The Blue Cube instruments provide a reliable means to predict unknown samples in real industrial applications. However, little is known with regards to these instruments, as the models used to calibrate them are proprietary information.

Thus the focus of this study is to assess the potential application of diffuse reflectance spectrophotometry (DRS) as an on-line analytical tool in the Skorpion zinc flotation plant situated in Namibia. The data measurements and interpretation are considered in this research to get a better understanding of the principles behind the DRS, such as used by Blue Cube, to contribute to improvements of plant performance.

1.5 Objectives of the Study

As diffuse reflectance spectrophotometry has not been used for on-line estimation of copper (Cu), cobalt (Co) and zinc (Zn) before, the main goal of this study is to assess the feasibility of on-line sensors in this context. Specific objectives that will be pursued are the following:

- i. Calibration of diffuse reflectance spectrophotometry on a laboratory scale using standard solutions that are prepared according to statistically designed experiments.

- ii. Assessment of the classical least squares (CLS) and inverse least squares (ILS) techniques to calibrate the sensor.
- iii. Assessment of the effect of temperature and contaminants on the response of the sensor.
- iv. Finally, comparison of the different statistical calibration models in terms of predictive ability related to test samples.

In order to achieve the stated objectives, the method that will be employed involves analysis of standard solutions on a laboratory scale and measurements of their absorption spectra. In this application, the reflected visible light from different solutions was measured using the Blue Cube optical fibre sensor coupled to spectrophotometer, which recorded the spectra of the metals. The spectra were captured via a desktop computer and processed using CLS & ILS techniques. The statistical models developed will be used to determine the concentration of the unknown solutions. The results of these models will be verified by partial least squares (PLS) model and atomic absorption spectrometry (AAS) technique.

1.6 Layout of the Thesis

The layout of the thesis can be summarised as follows:

- Chapter 1 deals with the natural occurrences and use of base metals, more importantly highlighting their essential role in our society and also stated the significance of on-line as compared to off-line methods. Finally, the research objectives and background of the problem to be addressed were examined.
- Chapter 2 presents the literature review of work performed in the field of online analysis for hydrometallurgical solutions and provides the reader with an overview of the work done to date, thus indicating the strengths and some weaknesses of existing on-line techniques. In addition, there is essential theory on spectroscopy concepts, which will help the reader to understand why some factors were investigated in the

study. It further provides a better understanding of the concept of the Blue Cube optical fibre sensor.

- Chapter 3 is concerned with the theory of calibration models, specifically investigating both classical and inverse least squares (CLS & ILS) techniques. The points discussed include the mathematical background of each technique and their application in aqueous media. The chapter is concluded by indicating the advantages and disadvantages of the techniques over one another.
- The focus of Chapter 4 is mainly on the methodology of the project. The experimental design used for calibration purpose is laid out. The major part of this chapter is closely concerned with the laboratory experimental work whereby the synthetic samples are used to develop and validate the calibration model. The features and operations of the laboratory set-up of the Blue Cube optical fibre sensor instrument are given in details.
- Chapter 5 investigates the results and discusses the laboratory tests. The results are compared to the theoretical knowledge so as to evaluate the applicability of the developed models on the large industrial scale.
- The last chapter contains the conclusion of the research. Lastly future work is recommended towards improvement in the accuracy and precision of both the ILS and CLS models.

CHAPTER 2: LITERATURE REVIEW

The following literature survey details the strengths and weaknesses of on-line methods or techniques, namely on-stream analysers and diffuse reflectance spectrophotometry (DRS). The survey illustrates that on-stream instruments have high accuracy owing to their elemental composition analysis because each element is determined at specific wavelength. However, they pose hazards to operating personnel and sometimes require intense computational work with complex algorithms. On the other hand, DRS techniques use statistical models which produce high accuracy with less computational work. However, the techniques have a large operating window for spectral analysis that can be affected by interference from external sources. The chapter wraps up by examining the factors that affect spectroscopical methods.

2 REVIEW OF ON-LINE SPECTROSCOPY IN MINERAL PROCESSING

2.1 On-line Spectroscopy Measurements

The massive demand for copper (Cu), cobalt (Co) and zinc (Zn) metals have led to the development and growth of extractive metallurgical plants to produce these metals in very large quantities; hence in order to ensure that such a goal is met, the unit operations and processes must be maintained at optimum conditions. This can be successfully done by use of on-line analysis to avoid the loss of any metal along the process.

The efficiency of the plant depends on the routine analysis of each element after each and every unit operation so that process engineers can have the best tools to optimise and control the process (Gaft *et al*, 2007). On-line analysis is most suited for this case to provide immediate and continuous data and feedback necessary for implementation as suggested by

Sowerby (2002) and Gaft *et al* (2007). In one flotation application, it was observed that on-line spectroscopic techniques produce grade measurements for 24 hours as opposed to plant operators who cannot check it regularly (Bartolacci *et al*, 2006).

Moreover, on-line analysis using optical sensors have many advantages in leaching or froth flotation plants because there is a broad range of analysis, meaning that metals of interest will be read simultaneously and results will be available on-line. Ultimately this provides a good opportunity to improve the process (Gaft *et al*, 2007). On the other hand, the manual sampling and laboratory analyses which are done by the plant operator require a great deal of time and relatively expensive equipment (ICP-MS or AAS) to perform (Paula *et al*, 2004).

Furthermore, manual analyses in the laboratory are subjected to large sampling errors whereas sensors provide high quality sampling data through the analysis of large continuous volume of material at hand (Gaft *et al*, 2007). The on-stream analysers, like XRF instrument, have very high accuracy since they can determine the elemental composition of a sample at hand. High accuracy and speed mean the plants can reduce their reagent consumption and ultimately achieve higher financial returns.

Finally, on-line analysis methods are suitable where the sampling or measurement is particularly difficult. For instance, the measuring of dissolved oxygen during the leaching process of nickel and copper via the off-line methods yield poor predictions because the atmospheric oxygen may interfere with the measurements. Therefore, in order to get accurate results the oxygen must be measured within the vessel so as to obtain a real time concentration, thus allowing the process to be monitored effectively.

In conclusion, the use of spectroscopy in mineral processing had given attention for the last decade because these techniques or instruments require very little (if any) sample preparation. Moreover, there is no contact with a sample to be analysed. These benefits had not only added stability in plant performance but also given rise to the development of more on-line techniques. In this review, the focus will be given mainly on two techniques namely, on-stream analysers and diffuse reflectance spectrophotometry (DRS). The latter will be dealt more in details as this study is formulated based on its principle. The fundamental principles and applications of DRS in mineral processing will be also discussed.

2.1.1 On-stream Analysers

Among the techniques and instruments used in mineral processing, X-ray fluorescence (XRF) analysers are one of the most developed machines with many industrial applications. The main advantage of XRF analysers is their ability to determine the elemental composition of any given substance (Haavisto and Kaartinen, 2009). Each element in the sample corresponds to a specific reflected fluorescent using X-rays to radiate the sample. When an XRF analyser was used as an on-line analysis tool, the plant operators were relieved from a great deal of tedious work done for laboratory samples analyses. The XRF can perform simultaneous analysis of all elements, whereas operators must run each element individually.

Remes *et al.*, (2007) used an XRF analyser in a flotation process to determine the amount of copper for both concentrates and tailings streams. In their study, they evaluated the effect of measurement and cycling time for the analyser, which were related to the profits of a plant. The first-order kinetic model was developed to derive the relationship and it was found that measurement cycles affect the plant's economical returns while the measurement time does not. There was an assay delay of about 20 minutes between two consecutive XRF measurements, thus leading to a decrease in plant performance. In addition, Haavisto and Kaartinen, (2009) stated that an XRF analyser alone cannot detect plant disturbance within 10 minute periods. This means that faster measurements and control were needed to improve the plant performance.

Gaft *et al.*, (2007) reported that the laser induced breakdown spectroscopy (LIBS) machine, which has much shorter sampling time, was used to measure magnesium, iron and aluminium in phosphate rocks for the purpose of ore sorting. The LIBS machine was tested successfully in both laboratory and plant analyses using real samples for the laboratory optimisation. When the developed technique was compared to routine analytical laboratory analyses, it was identified that laboratory analyses were more accurate than an on-line analyser. However the LIBS machine shows to operate for about year without experiencing any mechanical problems. The major drawback of the technique is that the machine analyses only the surface of the sample, hence there is lack of representative data of the entire sample.

In another study by Biesinger *et al.*, (2007), X-ray photoelectron spectroscopy (XPS) was used to evaluate surface chemical mechanisms in a copper flotation process. The main aim of their study was to examine whether the loss of valuable mineral was due to surface chemistry. Samples were collected from different stages of the process, that is, feed stream, rougher, concentrates and tailings. The XPS spectra and images were used to control and monitor the plant performance (Biesinger *et al.*, 2007). The XPS was found to be a semi-quantitative technique; hence back-up analysis from laboratory experiments was needed for effective monitoring of copper content along the process.

In a search for a method that can perform full quantitative analysis, Coughill *et al.*, (2002) described a laser technique for the measurement of particle size in mineral slurries. They argued that the technique had much improved advantages as compared to previous techniques since the particle analyser had the ability to operate on undiluted and non-electrically conducting slurries. The analyser was developed from the laboratory using real samples from the plant. Ultimately the tests indicated that solid content has no effect on the measurements of the mineral under study.

Coughill *et al.*, (2002) stated that the CSIRO particle size analyser was tested on lead/zinc ore, magnetite ore, titanium oxide ore and iron ore. All the slurries tested displayed a strong correlation, about 95%, between the laboratory and the analyser results. Furthermore, lower detection limits were observed for all the minerals measured. However, the analyser takes approximately five minutes to perform the measurements due to the low frequency of ultrasonic and de-aeration periods. This can cause the plant to suffer from fast disturbances usually experienced in slurry plants.

In general, the on-stream analysers are quite effective in monitoring and controlling plant processes, because they can determine elemental composition of a sample with high accuracy. The major difficulty in their usage includes exposure of radiation via the instruments necessary for on-stream analysing. Hence, the plant personnel require extensive training. Moreover, their sampling time is questionable when faster disturbances are experienced in plant situations (Haavisto and Kaartinen, 2009, Remes *et al.*, 2007).

2.1.2 Diffuse Reflectance Spectrophotometry

2.1.2.1 Principles of the spectrophotometry

Diffuse reflectance spectrophotometry (DRS) involves the applications whereby the reflected, scattered or emitted light from the sample is measured as a function of wavelength. The optical methods employed in DRS techniques are based on ultraviolet (180 – 380 nm), visible (380 – 780 nm) and near infrared (780 – 2500 nm) radiation (Skoog *et al*, 2008). This study makes use of the combined visible and near infrared (VNIR) reflectance spectroscopy and the wavelengths range from 400-1000 nm. The fundamental concept in DRS is the interaction of radiation of light with the measured sample. The incident intensity (I_0) from the light source is passed through the sample of interest and the absorption of radiation by a sample results in transmitted intensity (I) as shown in Figure 2.1.

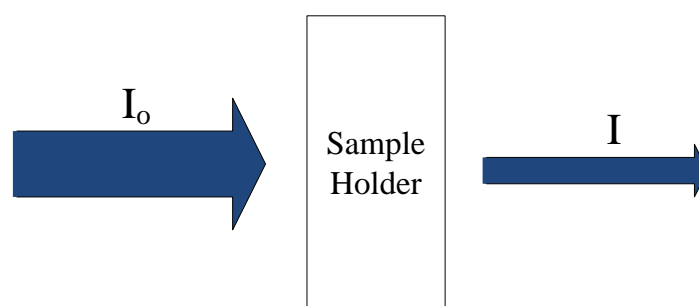


Figure 2.1: Attenuation of an incident beam through absorption of radiation by sample

The interaction of light and sample can be related together to give absorbance (A) or transmittance (T) of the absorbing sample as given by equation 2.1. Moreover if the light is travelling through a homogeneous and non-scattering medium, as it is the case in this study, the relationship of absorbance is given by Beer-Lambert law as illustrated in equation 2.2. The absorbance of the absorbing sample is directly proportional to its concentration (C) and path length (b).

$$A = \log \frac{1}{T} = \log \frac{I_0}{I} \quad (2.1)$$

$$A = \epsilon b C \quad (2.2)$$

There are quite number of theories and phenomena used to describe the relationship between absorbance and the content of the sample. Each phenomenon depends on the specific problem at hand. Recently, the uses of the optical sensors have shown great contributions in industrial applications of an elemental analysis in the areas of food processing, pharmaceutical and mineral processing. Even though the method of analysis is not the same in each case, the principles behind all the measurements are similar because they are based on DRS (Lewis *et al*, 2007). These types of sensors have the advantage of needing no external calibrations for sample variations encountered in the plant (Schneider, 1998). The discussion of the sensors will centre on chemically modified optical sensors and optical fibre sensors, as will be given in the next two sections that follow.

2.1.2.2 Chemically Modified Optical Sensor

The distinguishing feature of a chemically modified optical sensor (CMOS) is that a thin film of active chemical reagent is usually bonded or coated onto the sensor surface to selectively enhance specific properties of the sensor (Carla *et al*, 2009). The reagent that is incorporated or immobilised in the sensor increases the chemical, electrochemical, and transport features of the sensor in a chemically designed way. A chemically modified sensor poses the advantages such as high selectivity, high sensitivity, very low detection limits, and provides linear response for an analyte under study (Bari *et al*, 2009 and Buke *et al*, 2009).

Paula *et al*, (2004) conducted the study for the determination of copper ions using a sol-gel optical sensor. The experimental set up was arranged in such a way that a sample could be continuously circulated in the flow system and detected by the sensor. The method employed in this study was found to be highly selective for copper because of the stable complex formed with a complexing agent. When the sensor was applied to real samples, the sensor gave the results similar to that of inductively coupled plasma mass spectrometry (ICP-MS). However, Paula *et al*, (2004) stated that the sensor showed degradation in the performance, and thus the accuracy was greatly decreased in those applications. This lead to regeneration of the sensor by using special regenerating reagents like picolinic.

The regeneration of CMOS has been common practice in the application of these sensors. Pons *et al*, (2005) mentioned that complexing agents used to improve the short life-time of

the sensors were very expensive and they added value to the operating costs of the plant. In a search for a method that can avoid sensor regeneration, Bari *et al.*, (2009) developed a method that utilises the sol-gel silica sensor incorporated with cyanex to separate copper, nickel and zinc ions within a one sample solution. Atomic absorption spectrometry (AAS) was used to detect and determine the wavelength of each element from the spectra and recoveries above 97 % were obtained for all metals. Despite the high recovery percentages seen, the method suffers from longer analysis time because different acid strengths must be used to achieve a good separation and other operating conditions must be varied.

From literature searched, most studies done have been applied on a laboratory scale using simulated samples or employed with a small volume of real samples (Guell *et al.*, 2007). Even though the CMOS has high selectivity and sensitivity for a particular metal, almost all the methods developed could not be applied on industrial scale since the sensors needed to be regenerated regularly because their repeatability last for a short period, approximately two months (Abbaspour and Moosavi, 2002). One of the developments to compensate for the shortcomings of the CMOS was the use of optical fibre sensors. The optical fibre sensors have proven to work for a longer time, on the scale of years rather than months, without experiencing any mechanical problems (Gaft *et al.*, 2007).

2.1.2.3 Optical Fibre Sensors

The optical fibre sensor coupled to NIR transmittance spectroscopy was employed to determine the binary mixture of ammonia aqueous solution. Zachariassen *et al.*, (2005) studied both the off-line and on-line developments of the sensor at laboratory and industrial scales respectively. The PLS was used to analyse the analytical spectra of the samples in order to derive the model. They found that the calibration model derived from the laboratory analyses did not work well because the samples used seemed to underestimate the amount of interferences expected in a real plant situation. Furthermore, Zachariassen *et al.*, (2005) showed that the sensor performed very well when it came to controlling the ammonia concentration at an acceptable level, even though the effect of temperature was not modelled very well in PLS. The results obtained were accurate and reproducible with the product of high degree of purity.

In mineral processing applications, the use of an optical fibre sensor coupled to visible near infrared (VNIR) spectrophotometer was applied to monitor zinc flotation. Haavisto *et al*, (2008) conducted a study to identify and determine elemental composition of the final grade of the slurry. The elements analysed were zinc, copper and iron. The laboratory tests were done by using the samples collected from the plants and a PLS model was employed to analyse the analytical spectra of the metals. The already existing XRF analyser in the plant was used to update the PLS model, thus improved results for monitoring were obtained. It was further shown that mineral composition has an effect on the spectra of the minerals, that is, smaller size mineral have a better reflectance compared to larger minerals.

Haavisto *et al*, (2008) indicated that the PLS model cannot monitor the process accurately after any process failure. They performed further studies on the zinc flotation plant and suggested a new method called recursive PLS model to compensate for the already mentioned shortcoming (Haavisto and Hyotyneimi, 2009). During the laboratory set up, they found that solid content in the range of 15 - 40 % had no effect on the spectra of the minerals. Furthermore, they found that the recursive PLS model provides more accurate predictions than the non-updated PLS model. The optical fibre sensor in this particular study provided almost continuous control of flotation cells because of improved sampling time on the scale of seconds as compared to traditional XRF analyser which takes up to ten minutes. The model gave poor predictions for the tailings due to low concentration of the minerals in that particular stream.

From the zinc case study, Haavisto and Hyotyneimi, (2009) developed a multichannel VNIR spectrum analyser for the monitoring and control of several slurry lines. They further utilised a recursive PLS model on real plant data and achieved accurate predictions for concentrates and middlings streams whereas tailing were poorly predicted. The high frequency sampling of the VNIR model was important in identifying the cause of oscillation. The XRF analyser aided in the detections of other oscillations observed in the process. Haavisto, (2010) made use of a recursive singular spectrum analysis (SSA) to analyse and isolate the oscillations finding flow rate to be the cause of the oscillation. The recursive SSA method improved the performance of the whole plant due to the fact that rapid oscillation can be easily detected.

In this present work, focus would be on the use of a Blue Cube optical fibre sensor as an online analysis tool in leaching and froth flotation processes in industries. The sensor also

uses the principle of diffused reflectance spectrophotometry, which is the wavelength region of visible near infrared (VNIR) light, to measure the mineral content of the sample. Lottering and Aldrich, (2006) demonstrated that the sensor can be used for the compositional determination of valuable minerals during the separation process of the mineral sands. The sensor provides high accuracy results and shows a promising application in industrial mining since the samples used in the laboratory experiments have a similar composition to those found in real plants.

In addition, de Waal and du Plessis, (2005) used a pilot set-up of an electrostatic separator to study the effect of roller speed, ore temperature, voltage and feed rate on the separation of a heavy mineral sand. The composition of the product stream (non-conducting material) was analysed by a Blue Cube optical fibre sensor. The high accuracy and repeatability of the sensor lead to continuous monitoring of the sand composition. The control system was built and tested for installation in a plant. After several tests, Blue Cube Company developed and installed several on-line instruments for mineral processing applications such as heavy mineral sand mine, flotation and leaching industries. de Waal, (2007) mentioned that all instruments use similar optical components and data processing methods. The calibration procedure is done by relating the mineral spectrum with its known concentration.

In summary, the use of VNIR spectroscopy in mineral processing is a promising technology when it comes to providing solutions to problems encountered in mineral industries, especially the flotation process. The current studies have shown that VNIR spectra and the derived statistical models have high accuracy when used for monitoring and the control of large mineral plants (de Waal, 2007, Haavisto, 2010). Another added benefit is the increased stability in plant operation, as illustrated in Figure 2.2, where the Blue Cube optical fibre sensor is used in a flash flotation process to control the percentage of chromite in the concentrate cell to be within 3-4 %. The improved plant performance results in a higher financial return for the company (Haavisto *et al*, 2008, de Waal and du Plessis, 2005). The Blue Cube optical fibre sensor does not introduce new concepts but rather uses the already existing concept of VNIR spectroscopy. These spectroscopic concepts are used to bridge the gap that exists in industrial and commercial mineral processing applications

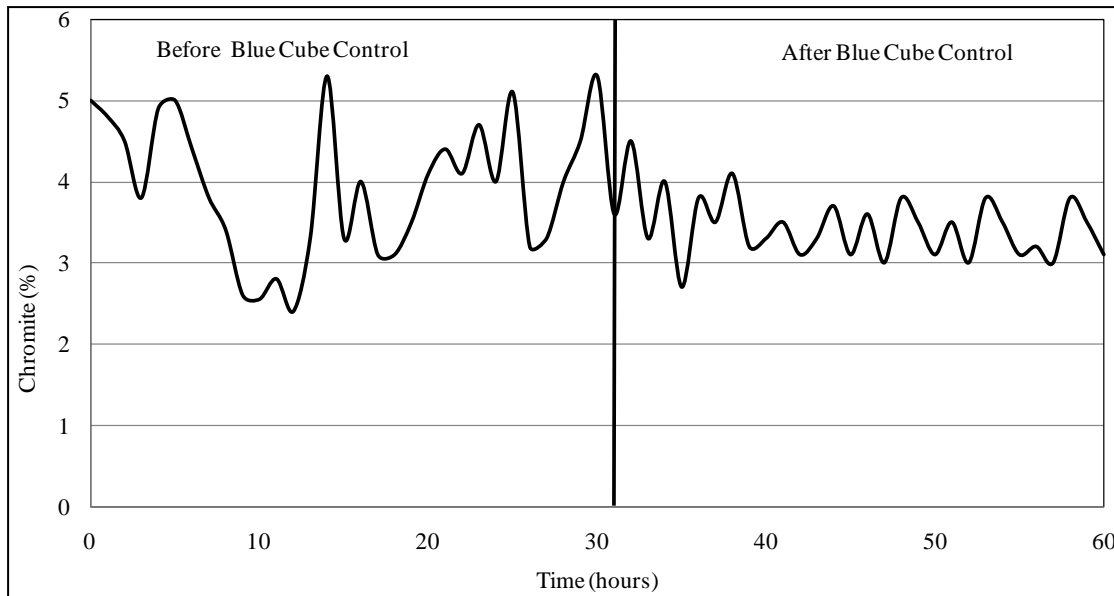


Figure 2.2: Chromite variation before and after implementation of Blue Cube optical sensor

Despite the benefits and increasing number of on-line monitoring techniques in DRS applications, there are still some limitations encountered. The main downside of VNIR reflectance spectroscopy is the large number of external factors affecting the shape of the obtained spectra. The spectroscopy has a large spectrum operating window from 400 – 1000 nm and this can be affected by the lot of interferences. The most influential factors that affect the VNIR spectra include, but are not limited to, particle size, mineral composition and temperature of the sample.

2.2 Factors affecting the performance of Spectroscopy

2.2.1 Particle Size of Mineral

The particle size of the mineral sample has a great effect on the spectral intensities. Michaud *et al.*, (2007) determined the influence of particle size and mineral phase on LIBS signal. In their study, samples (Fe_2O_3 and Fe_3O_4) from an iron ore plant were analysed using a LIBS laboratory analyser. It was further determined that the spectral intensities of the minerals increase with the reduction in particle size of the ore. In a different case study, Haavisto *et al.* (2008) used a VNIR optical sensor to monitor and control different stages of a zinc flotation process. It was observed that the variation in the solids content has effect on the shape of the spectrum. The samples with less solid content were found to have high intensities values. In

general, the possibility of multiple scattering and reflected light occurring decrease as the particles size of the mineral increases.

2.2.2 Mineral Composition

The type of mineral and composition of the sample also have the effect on the absorption properties of mineral of interest. In the VNIR region, each mineral has a specific wavelength where it can absorb radiation however the measured absorption spectra tend to be masked by the interferences. Haavisto *et al*, (2008) found that the samples taken from the tailings section of flotation have lower intensity peaks compared to the ones from concentrate section. It was further observed that tailing samples have less concentration of zinc, thus their absorption ability is decreased. Oestreich *et al*, (1994) found that there is correlation between composition of the flotation froth and colour vector angle. They further proved that different minerals absorb different quantities of light. It is therefore imperative to ensure that during the VNIR measurements, there is little to no interferences of any foreign materials or at least their quantity is known.

2.2.3 Temperature of Sample

Molar absorptivity (ϵ) as given by equation 2.2 in Section 2.1.2.1 is specific and constant for each species in solution and wavelength. This constant is a fundamental molecular property which is directly proportional to temperature (Benalia *et al*, 2006). This means that temperature needs to be kept constant during the VNIR analysis of material at hand. Figure 2.3 illustrates the effect of temperature on absorption spectra of nickel and was redrawn from the explanation given by Yurii *et al*, (2005) and Kumagai *et al*, (2008). From a study performed by Kumagai *et al*, (2008) on the absorption spectra of lithium and magnesium salt, they evaluated the effect of the concentration of salts, temperature and the size of the cations. It was found that the increase in temperature shifts the intensities of maximum absorption peaks to higher wavelengths and absorbance values.

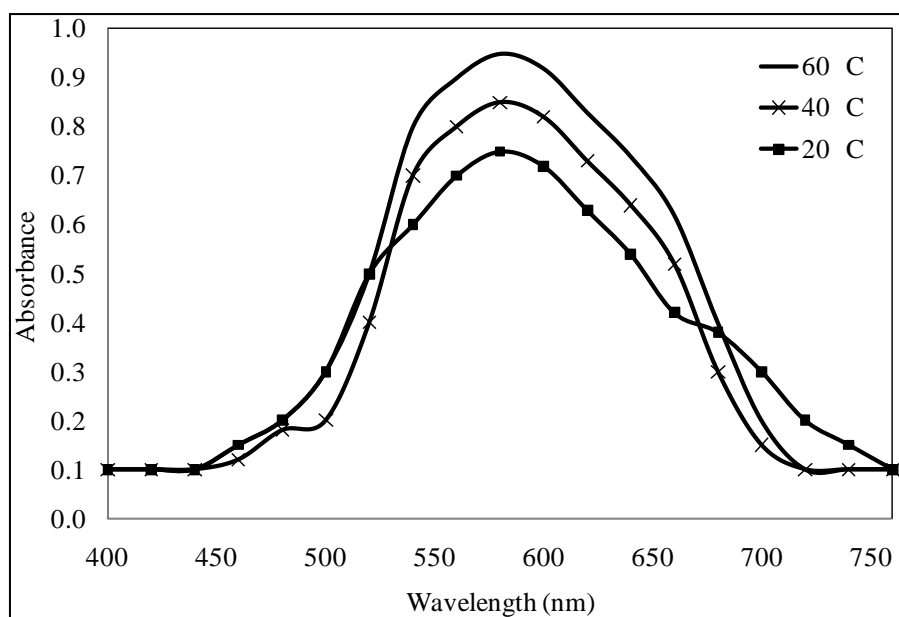


Figure 2.3: UV-VIS absorption of nickel complex and its dependence on temperature (after Kumagai *et al*, (2008)).

CHAPTER 3: CALIBRATION MODEL

The mathematical backgrounds of the ILS and CLS calibration models are presented first, followed by their applications in spectral analysis of the mixtures. The traditional ILS and CLS models use selected wavelengths and the whole spectrum wavelengths respectively. The literature review reveals that both models have similar accuracy when applied to simple mixtures but for the complex mixtures ILS shows improved performance due to its inverse nature of the algorithm. However, the CLS models have the advantage of qualitative nature for relating absorptivities to the individual constituents in the mixture. The chapter further shows that algorithms of the models can be modified to improve their quantitative analyses.

3 REVIEW OF CALIBRATION MODELS

The combination of the diffuse reflectance spectrophotometry (DRS) sensor and multivariate calibration techniques had been proven that it can be used in process monitoring of flotation plant. Haavisto *et al*, (2008) used a PLS model to control the zinc flotation process with the optical spectrum of slurries. In general view multivariate calibration models had been applied successfully in a number of applications including, but not limited to, pharmaceutical, food processing and mineral processing industries. The most used models up to date are PLS, PCR, ILS and CLS whereby the first two have received attention due to their ability to study non-linear systems. However, the last two are mostly also applied for quick analysis and linear systems. The present study will utilise the benefits of ILS and CLS models since the system under this study is thought to be linear due to very dilute concentrations of the metal. Furthermore, there is an added advantage during the modelling because both models depend on Beer-Lambert Law (Haaland *et al*, 2000 and Dinc *et al*, 2003) and the law works very effectively for low concentrations.

3.1 Classical Least Squares Methods

3.1.1 Theory

The classical least squares (CLS) method is usually used to refer to a multivariate least squares technique that utilizes the physical model as the basis of the method. The CLS calibration and prediction algorithms are also based upon an explicit linear additive model, called the Beer-Lambert law, which can yield excellent estimates of the pure component spectra as they exist in the sample matrix. Hence there is significant chemical and spectral information available in the calibration step of the algorithm.

Let us begin the calibration step with the following assumption that states that at each frequency or wavelength, there is linear relationship between the concentration (C) of an absorbing species and its spectral absorbance (A) when a source of light is passed through such species. The Beer-Lambert law relation is defined as follows:

$$A = \epsilon bC \quad (3.1)$$

where ϵ is the absorptivity of the absorbing species and b is the path length that light travels through the solution. Since absorptivity is characteristic for each species and path length is unvarying, then k can be defined as the product ϵb . Then adding random error (e) in the spectrum at each frequency, equation 3.1 can be written as:

$$A = kC + e \quad (3.2)$$

The random error is assumed to be normally distributed with an expectation of zero and variance proportional to T^{-2} where T is the transmittance value of the spectrum at each frequency.

Most of the applications in real samples involve more than one species in the solution, thus the Beer-Lambert law can be represented in the matrix form and the following notation in the equation should be taken into consideration; upper-case bold letters are used for matrices, lower-case bold for vectors and italicised lower-case letters for scalars. Further includes \wedge to

indicate estimated values, ^T to denote a transposed matrix, ⁻¹ for matrix inversion and ⁺ for the pseudoinverse of a matrix. The basic CLS model can be expressed as:

$$\mathbf{A} = \mathbf{K}\mathbf{C} + \mathbf{E}_A \quad (3.3)$$

Where \mathbf{A} is the $p \times n$ matrix of the absorbance spectra from the n samples at the p frequencies,

\mathbf{C} is the $m \times n$ reference concentration matrix containing m components

\mathbf{K} is the $p \times m$ matrix of the m pure-component spectra of all spectrally active components

\mathbf{E}_A is the $p \times n$ matrix of spectral errors in the model

The linear least-squares solution for \mathbf{K} for the model in equation 3.3 from a series of calibration samples with known component concentrations is given as

$$\mathbf{K} = \mathbf{C}^T \mathbf{C}^{-1} \mathbf{C}^T \mathbf{A} \quad (3.4)$$

During the CLS prediction step, the first assumption made is that of a zero baseline which allows the absorbance spectrum of the unknown sample to be expressed as:

$$\mathbf{A}_u = \mathbf{K}\mathbf{C}_u + \mathbf{E}_u \quad (3.5)$$

where \mathbf{A}_u represents the spectral matrix of the unknown samples to be predicted and \mathbf{C}_u is the concentration matrix containing m components in n_u unknown samples. \mathbf{E}_u is the matrix error in unknown spectrum. The concentrations of the unknown samples can be estimated, first by substituting eq. 3.4 into eq. 3.5 and then solving by least squares to yield

$$\mathbf{C}_u = \mathbf{A}_u \mathbf{K}^T (\mathbf{K} \mathbf{K}^T)^{-1} \quad (3.6)$$

3.1.2 Application in Spectral Analysis

Classical least squares (CLS) multivariate modelling has long been used for the qualitative and quantitative analyses of infrared and absorption spectra of aqueous solutions. It has been

shown that CLS methods are very effective and accurate for the analysis of simple well-characterised linear systems or gas phase methods which obey Beer's law and when all components interfering with the spectra of the analyte are known (Griffith, 1996). The development of CLS-based methods had led to improvement in spectral analysis of complex and nonlinear systems.

Haaland *et al*, (1999) used a sol-gel coated sensor for trace detection of organic components (acetone and isopropanol) in aqueous solutions and then applied CLS and partial least squares (PLS) methods to analyse the spectral data. The CLS method yielded poor quantitative results for isopropanol as compared to PLS. On the other hand, the CLS method demonstrated superior qualitative interpretation. In their results, they showed that PLS weight-loading vectors can yield misleading information if the spectral variance of the analyte is too small compared to the total variance.

After the failure of CLS methods in quantifying organic molecules at trace level, Haaland *et al*, (2000) proposed a method to detect and quantify a number of samples containing 12 elements by using inductively coupled plasma atomic emission spectrometers (ICP-AES). The spectral data was analysed by both CLS and PLS methods. The CLS, using a multi-window of the spectra showed improved accuracy, detection limits and quantitative range for elements under investigation and was superior to the PLS method for very low concentrations of the element. This advantage of the CLS method over PLS is contributed to the fact that ICP-AES uses benefits of CLS multivariate methods that rely on explicit additive linear spectral models, since the emission signal from ICP-AES tends to be also additive and linear over a large range.

After the experiments were performed and spectra collected it was discovered that many samples were contaminated by carryover of some of the elements from samples analysed before. The concentration-correction procedure was performed for each element and was incorporated during the CLS calibration but there was no correction for the effect of carryover in the calibration of PLS due to its algorithm. Furthermore, the poor performance of PLS was attributed to a small number of calibration samples. Haaland *et al*, (2000) indicated that CLS method experienced problems with the detection of arsenic when palladium was introduced as interference. This proves that presence of interference affect the quality of the model because both elements have the same emissions at 189 nm. Moreover, it

was thought that at higher concentrations of the elements, CLS methods would give poor prediction due to nonlinearity behaviour of the elements (Skoog *et al.*, 2008).

Since the traditional CLS methods cannot accurately account for the nonlinearities of the system because the explicit equations required to model these effects are not known, Haaland and Melgaard, (2000) developed a new CLS-based algorithm called prediction-augmented classical least squares (PACLS) to compensate for those effects. The PACLS method has the capability of empirically measuring the source of spectral variations not included during CLS calibration and integrating them in the CLS prediction portion of the analysis. The traditional CLS and PACLS methods were used to analyse dilute aqueous solutions of urea, creatinine and NaCl. The squared correlation coefficient (R^2) values of urea from the methods were 0.628 and 0.9960 respectively.

The poor prediction results demonstrated by the CLS method in the work of Haaland and Melgaard, (2000) explain why CLS has not been used in the presence of interfering analyte concentrations that are not available for calibration purposes. The PACLS has shown the ability to accommodate the presence of unmodelled components in the prediction samples. Since the empirically derived spectral shapes might have errors, the PACLS method will suffer degradation in sensitivity analysis. This means that the effect of error on the predictions must be thoroughly studied. In addition, PACLS requires that all spectral components be included as concentrations during calibration and thus is too restrictive in many real industrial applications (Haaland and Melgaard, 2001).

A new hybrid algorithm that has features of CLS, PACLS and PLS has been developed for quantitative analysis of dilute aqueous solutions. The new hybrid method (PACLS/PLS) takes the advantage of the qualitative interpretation of CLS, the special capabilities of PACLS outlined above and retains the flexibility of PLS (Haaland and Melgaard, 2001). PLS has gained widespread use due to its flexibility to define a calibration model even when all the spectrally active components are not known (Mutihac and Mutihac, 2008). The hybrid PACLS/PLS and ordinary PLS were applied to spectral data and it was pointed out that the hybrid method outperform the predictive ability of ordinary PLS when new sources of spectra variation were introduced.

Haaland and Melgaard, (2001) claimed that the hybrid algorithm would achieve a better transfer of multivariate models between various spectrometers, which was impossible with current methods at that time. They further demonstrated that better results were accomplished when recalibrating the PLS algorithm rather than updating the PACLS algorithm during the prediction step. Furthermore it was observed that recalibration of the cross-validated model takes a long time for computationally purposes. If this hybrid method can be used in real industrial applications, then process monitoring and control will be ineffective since the updating of prediction data will be slower than the occurrence of the source of errors.

Since the hybrid PACLS method needs recalibration so that the model can be updated, another algorithm called concentration residuals augmented classical least squares (CRACLS) was developed to allivate problem of recalibration. The CRACLS method retains improved qualitative benefits of CLS, yet it has the flexibility of PLS because it repeatedly augments the calibration matrix of reference concentrations with concentration residuals estimated during the CLS prediction step (Melgaard *et al*, 2002). The PLS and combination of CRACLS with PACLS methods were applied to spectral data of dilute aqueous solutions of glucose, urea and ethanol.

Melgaard *et al*, (2002) indicated that CRACLS/PACLS provided the prediction results comparable to PLS for validated samples studied when there was instrument drift. However, CRACLS was rapidly updated during prediction without the need for time consuming cross-validated recalibration. Moreover, CRACLS was updated only using spectral information, while PLS required both spectral and concentration information during recalibration. Finally, similar prediction results were obtained with CRACLS when using all concentrations simultaneously or using the concentration of each component at a time.

The research team of Haaland and co-workers at Sandia National Laboratories in New Mexico have performed exceedingly valuable work concerning the development of CLS-based methods. They improved the traditional CLS method from its qualitative nature to a mature stage able to perform quantitative analysis for both linear and nonlinear systems. The augmented classical least squares (ACLS) methods developed showed great promise compared to PLS and principal component regression (PCR). Sometimes ACLS outperforms them. Steady progress has been made where the CLS-based methods were applied to dilute aqueous solutions on laboratory scale.

3.2 Inverse Least Squares Methods

3.2.1 Theory

The inverse least squares (ILS) method is used to refer to the multivariate least squares technique that is based on the inverse of Beer-Lambert's law. The ILS method eliminates the drawback of the classical least squares (CLS) method which requires the inclusion of all interfering species and their concentrations in the model. In the ILS method, the calibration and prediction algorithms are built upon the concentrations of the analytes which are modelled as a function of absorbance measurements (Ozdemir, 2008).

Lets begin the calibration algorithm of ILS method by first rearranging the Beer-Lambert law as given by an equation 3.1 to yield the following expression:

$$c = \frac{A}{\epsilon b} \quad (3.7)$$

where all the parameters are the same as defined in the CLS calibration algorithm. Once more, the path length and absorptivity will be held constant and their reciprocal ($1/\epsilon b$) will be replaced by P . Random error will also be added to give the following mathematical expression:

$$C = PA + e \quad (3.8)$$

In many real world problems, the number of components usually appears to be more than one and hence the number of absorbance points included in the model increases. Equation 3.8 can be more concise if it is represented in the matrix form. The notations and symbols used in the CLS method matrices still apply here.

$$\mathbf{C} = \mathbf{PA} + \mathbf{E}_C \quad (3.9)$$

Where \mathbf{C} and \mathbf{A} are the same as explained in equation 3.3

\mathbf{P} is the $m \times p$ matrix of the unknown calibration coefficients relating the components concentrations to the spectral intensities

\mathbf{E}_C is the $m \times n$ matrix errors in the concentrations not fitted by the model

When a set of calibration samples have been made with known concentrations of each sample, and their absorbance spectra has been measured and recorded, the reciprocals of the linear coefficients of absorptivities, or \mathbf{P} matrix, can be determined as:

$$\mathbf{P} = \mathbf{CA}^{-1} \quad (3.10)$$

The linear least-squares solution for \mathbf{P} , in the model equation 3.10, from a series of calibration samples with known component concentrations is given with \mathbf{P} as the estimated calibration coefficients.

$$\mathbf{P} = \mathbf{CA}^T \mathbf{AA}^T^{-1} \quad (3.11)$$

During the prediction step of the ILS method, the unknown concentrations are obtained simply by direct multiplication of the unknown spectrum (\mathbf{A}_u) by the \mathbf{P} matrix determined from equation 3.11.

$$\mathbf{C}_u = \mathbf{PA}_u \quad (3.12)$$

where \mathbf{C}_u is the estimated concentration of a component of interest in an unknown mixture.

The ILS method is more robust than the CLS method because it is not restricted by the fact that the concentrations of all components must be known. Furthermore, it is not limited by the component interactions since the interactions can be treated as impurities. Thus the ILS method can analyse more complex systems as compared to CLS method.

Despite the mentioned advantages of ILS, there are two major shortcomings of the method. First, the number of wavelengths in the calibration spectra cannot be more than the number of calibration samples. Therefore the model cannot be improved by increasing the number of wavelengths at which the absorbances are measured. Secondly, Ozdemir, (2003) stated that the selection of suitable wavelengths at which the absorbances have to be measured is a

cumbersome restriction in ILS method. The wavelength selection strategies, such as stepwise wavelength selection, must be sorted out to provide the best fit for the model.

3.2.2 Application in Spectral Analysis

The inverse least squares (ILS) methods have been used for both qualitative and quantitative analysis of infrared spectra of different substances. It has been shown that the ILS method is more effective for quantitative than qualitative analysis of spectral data. The quantitative nature of ILS can be improved by modification or extension of calibration and prediction algorithms of the traditional ILS method (Paradkar and Williams, 1997). The ILS method has become a popular method for simultaneous chemical analysis and is being studied extensively in a number of different fields, such as petroleum, pharmaceutical and food industries.

Haaland and Thomas, (1988) used four multivariate calibration models (PLS, PCR, CLS and ILS) to perform the quantitative and qualitative analysis of spectral data of the simulated samples. The system that was analysed was a three-component mixture where the sum of the number of molar percentage was 100 % in all 16 samples prepared. The CLS method was found to have the best qualitative results whereas ILS has the poorest. However, the ILS method demonstrated a higher prediction ability quantitatively as compared to the CLS method since it was not only able to estimate the analyte concentrations but also provided the chemical and physical properties of the samples from the infrared spectra.

The inverse nature of the ILS model has made it applicable in many applications. For example, Blanco *et al*, (1999) used the technique to determine the active organic compound and solvent used in nasal spray. The calibration and validation steps of the model were done using the synthetic samples that were prepared by statistically designed experiments, namely factorial design. The resulting model was tested and applied to manufacturing samples, and the samples were predicted with high accuracy with correlation variation values of less than 2.00 %. In the study, they further showed that particles in the suspension affected the spectra of the sample of interest.

Since the ILS method requires selection of wavelength region, Blanco *et al.*, (1999) used the manual selection (MS) and automatic forward stepwise selection (AFSS) procedures. It was found that MS performs better than the AFSS method based on their relative standard errors. Using high-performance liquid chromatography (HPLC) on manufacturing samples, as a reference method, the results indicated that MS gives slightly better predictions and shorter analysis times as compared to HPLC. Later in the analysis, the ILS model was modified by incorporating correction terms in the calibration equation to eliminate the effect of interferences.

The modified form of the traditional ILS method that can result in an effective prediction for unknown samples was proposed by Ozdemir, (2008). This genetic ILS model (GILS) was used to study the diesel fuel parameters whereby the boiling point, total aromatics, viscosity, density, cetane number and freezing point were determined. Large numbers of samples, over 100, were used for the calibration and prediction steps of the model. The near infrared (NIR) spectra were used as the input data. The model used a genetic algorithm for wavelength selection since it can reduce data sets for modelling purposes.

Before a genetic model can be applied to test samples it should be validated by a half-validation procedure since it can reduce over-fitting and computation time (Ozdemir, 2008). The GILS method has a strong prediction ability for most diesel fuel parameters excluding freezing point and cetane number that have standard errors of prediction greater than 10 % and R^2 values less than 0.900. Even though Ozdemir, (2008) concluded that the GILS method was very successful for selecting and extracting valuable information to develop the accurate model from such a large number of calibration samples, the problem with the presented method is that it is very tedious because each parameter of diesel fuel has its own calibration and prediction model.

The use of ILS and its modified forms has gained importance in spectral analysis of pharmaceutical products. The main two reasons being, they can resolve overlapping spectra of the mixtures and do not need any pre-treatment procedures prior to the analysis as compared to other conventional methods, like HPLC (Dinc *et al.*, 2003). Dinc and Ustundag, (2003), carried out a study to investigate the accuracy of the CLS, ILS, PLS and PCR models for the quantification of binary mixtures. The mixture design was used to prepare calibration

samples. On the basis of F-test results, it was found that there was no statistical difference between the models and the results of the models were further supported by HPLC analysis.

From the literature reviewed, most of the researchers have shown that the ILS model performs better than the CLS model. Although a study by Dinc and Ustundag, (2003) had found that a similar accuracy was obtained for both methods. This may be attributed to the nature of the mixture under investigation. For example, a simple mixture can be predicted with high accuracy and precision since there is limited interactions between the components of mixture (Cirovic, 1998). Nagaraj *et al*, (2007) performed a case study to quantify mixtures of pharmaceutical products using the CLS, ILS, PLS and PCR models. The correlation coefficient values in the prediction steps for CLS and ILS models were 0.947 and 0.997 respectively. Another advantage of ILS shown in this study is that it can be combined with a derivate technique to give better and more reliable results.

The application of ILS models in spectral analysis of both UV and NIR spectra data have become useful tools in many processing areas. In almost all applications, the techniques are found to be promising routine analysis tools since their analyses are faster and more reliable compared to conventional methods like HPLC and gas chromatography (GC). Even in cases where the ILS model underperforms, it can be modified to increase its prediction ability (Ozdemir, 2008). Lastly, they have maintained high accuracy in both simulated and commercial samples.

Despite such promising progress, the CLS and ILS models were only applied to dilute aqueous solutions on laboratory scale using very small volumes of samples. The question that remains is what will happen if the same methods are applied on large industrial scale where other factors with differing magnitude, such as plant disturbances (flow rates, pressure and temperature), take place frequently. Table 3.1 shows a comparison of the prediction ability of the CLS and ILS models based on spectral analysis. The “good” and “poor” in the table indicates the performance measure of each model in respect to the specific application shown.

Table 3.1: Comparison of CLS and ILS in terms of spectral analysis

Model	Qualitative Analysis		Quantitative Analysis	
	Simple Mixture	Complex Mixture	Simple Mixture	Complex Mixture
CLS	Good	Good	Good	Poor
ILS	Good	Poor	Good	Good

CHAPTER 4: EXPERIMENTAL WORK

The chapter starts with the review of the experimental design, namely the simplex-centroid mixture design, and further illustrates that statistically designed experiments do reveal hidden and valuable information about the interactions between the constituents of the mixture with few experiments. After the experiments had been designed, the procedure for the samples' preparation was comprehensively laid out based on the plant conditions. Next, the description of a laboratory set-up of a Blue Cube optical fibre sensor instrument is explained in details. Finally, the method for data collection of raw spectra and software programs used for data analysis are presented and their usage description is briefly explained.

4 EXPERIMENTAL WORK

The previously discussed multivariate calibration models in the last chapter require a suitable selection of the calibration samples. The selection is necessary because of the collinearity effect that affects the mathematical computation of the algorithms. Experimental design is usually used to partially overcome the problem of this effect because a few number of samples that covers a larger domain can be chosen. This fact was also supported by Cirovic, (1998) where it was found that the increase in number of parameters' levels during the design reduces absolute error for prediction. It was also pointed out that a calibration set should have the same or at least very similar nature, as that of the samples to be predicted (Haaland *et al*, 2000). Thus the experiments must be properly designed for an effectiveness of the calibration models.

4.1 Review on Experimental Design

4.1.1 Motivation for Experimental Design

In most cases experimental work is done by changing levels of one factor at a time in an unsystematic way in order to try and find the optimum conditions of complex systems, such as mixtures of components. However, as shown by Fisher (1925), changing one separate factor at a time (COST) does not give any information about the position of the optimum in the common case where there are interactions between factors. Therefore the COST approach yields an optimum far from the true value.

There are multiple problems associated with the COST approach as explained and discussed by Fisher, (1925) which are summarised below:

1. Does not lead to real optimum conditions of the experiments
2. Inefficient, unnecessary many runs
3. Provides no information about what happens when factors are varied simultaneously
4. Provides less information about the variability of the response

In order to overcome the problems that are encountered in the COST approach method, statistical experimental design, also known as design of experiments, must be employed. This is the methodology of how to conduct and plan the experiments in order to extract the maximum amount of information in the fewest number of runs (Christine and Montgomery, 2008). There are several designs available to date, specifically factorial, composite and mixture designs, and each depends on the type of research problem and the knowledge of the researcher toward the design. Here are basic steps normally considered when performing a design (Leardi, 2009):

1. The purpose of the experiments – this defines the goals one wants to achieve from the experiments, especially the relevance of the information to be extracted. This first step determines the type of design to be used e.g Composite, mixture etc.
2. Examine the factors that can have the effects – the selection of the factors must be based on scientific knowledge of the subject at hand and not on the personal preference of the researcher.

3. Plan the experiments – once important factors are identified, their levels must be set and the knowledge of the process under investigation plays another important role here. Normally screening experiments are done to check the levels for actual experiments.
4. Run the experiments – this is the most essential part of the design since the results obtained are going to be used to build the regression model. The experiments must be carried out carefully to avoid personal and instrumental errors.
5. Data analysis – this last step converts all the raw data from the experiments into useful information for determining which factors affect the process at hand. In most scenarios regression models and surface response graphs are used for that purpose but the latter was found to be more effective in determining the interactions between the factors.

In most cases, it is found that the outcome of the experiments yield irrelevant information for the description of the system being studied hence the researcher needs to go to step 3 to redefine the level of factors or eliminate some factors from the design (Leardi, 2009). Then the remaining steps can be repeated. There are quite a number of applications where the experimental designs are effectively utilised to study the laboratory and industrial systems and thus, reducing the cost of time and resources in those situations.

The importance of the experimental design can be seen from a study of Alfantazi and Valic, (2003) whereby they realised that factorial experimental design can be effectively utilised to determine the effects that affect the process. A linear relationship regression model was built and the main effect and the interactions were found to be statistically significant based on probability values (P-values) less than 0.05. The results from the design show a good agreement when compared to the experimental results with a R^2 value of 0.996.

In general, statistical experimental designs provide a mathematical framework for changing all pertinent factors simultaneously to achieve results that allow the analysis of interaction between the factors. In most cases, the interactions are the driving force in an experiment (Alfantazi and Valic, 2003). In this project, the simplex-centroid mixture design is used to

run the experiments. The background together with the application of the mixture design will be given in the section that follows.

4.1.2 The Concept of Mixture Design

Most of the processes use the addition of two or more components to produce the desired product. Take, for example, the formulation of the paint and extraction solvents. In a mixture experiment, the independent variables are proportions of different components in a mixture. When the mixture components are subject to the constraint that they must sum to one, there are standard mixture designs for fitting standard models, such as simplex-lattice designs and simplex-centroid designs. In mixture experiments, the measured response is assumed to depend only on the relative proportions of the ingredients or components in the mixture and not the quantity of the mixture (Cornell, 1981).

The positive outcome of a mixture design in mineral processing can be seen from a laboratory study performed by van Tonder *et al*, (2010) where they studied the effect of ore blends in platinum processing conditions. A simplex lattice design was employed for all the experiments. The regression model and graphical presentation of the results were used to determine the behaviour of the different ores. From the flotation experiments, the blends of 'poor' ore (salene) and 'good' ores (Townland) show non-linear behaviour (van Tonder *et al*, 2010). From this study, it can be concluded that properly designed experiments can reveal hidden behaviours of certain ore blends.

Another important reason for performing mixture experiments is to evaluate the effect of interactions between the components of a mixture (van Tonder *et al*, 2010). The interaction effects can be divided into three categories depending on the behaviour of each component. These include synergetic, additive and antagonistic effects. The explanation of each effect is illustrated by an example of an extraction process as show in Figure 4.1. In this example, two pure solvents are mixed together to form one blend solvent. The rate of reaction is used as a response to determine the behaviour of each solvent.

Firstly, it is assumed that both solvents A and B produce extraction percentage values of 60 and 35 % respectively. The question that arises is what will happen if 50% of each solvent is

used to make a mixture. In order to answer this question, a mixture experiment must be performed and there are three possible outcomes that can be expected as explained here and also illustrated by Figure 4.1.

1. The solvents can produce the average extraction percentage of the individual values to give 47.5 %. Any combinations of the catalyst will always give the linear behaviour as shown in Figure 4.1 by a straight line and this is known as the additive effect.
2. Another possibility is the situation whereby the solvents produce an extraction percentage higher than the average value of the individual values, in this case, 65 %. This is shown by an upward curvature in Figure 4.1 that illustrates that any combination of the solvents will always give higher values than the averages values; this is known as the synergistic effect.
3. The last option is that the solvents result in a lower extraction percentage than the average value, which in this case it is 31 %. The behaviour is shown by the downward curvature in Figure 4.1 and it is known as an antagonistic effect since any combination of the solvents will always give lower values than the averages.

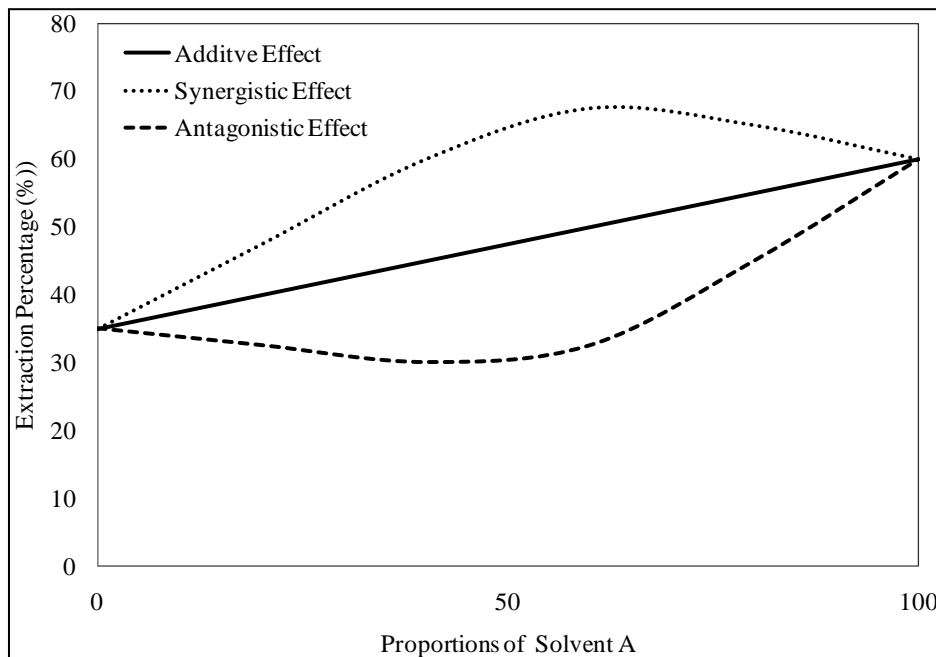


Figure 4.1: Illustration of interactions effect in mixture design

4.1.3 Simplex-centroid design of three components mixture

The simplex-centroid mixture design for this study was designed through the use of Design Expert software from the category of experimental design. The three factors constrained-mixture was generated with three replicates of the centroid point, thus resulting in 12 runs as shown in Table 4.3. The usual assumption made for mixture experiments is that the errors are independent and identically distributed with zero mean and common variance. Another assumption that is made, similar to that in factorial designs, is that the true underlying response surface is continuous over the region being studied.

The design points correspond to all permutations of the pure blends at the vertices, the binary blends along the edge and finally permutations of the blends involving three components are found inside the triangle. The design is augmented with interior points to enhance the information gathered from the interior portion of the design (Statsoft, 2007). When examining Figure 4.2, the fractional percentages of the components in respective mixtures add up to a constant value which is 100%.

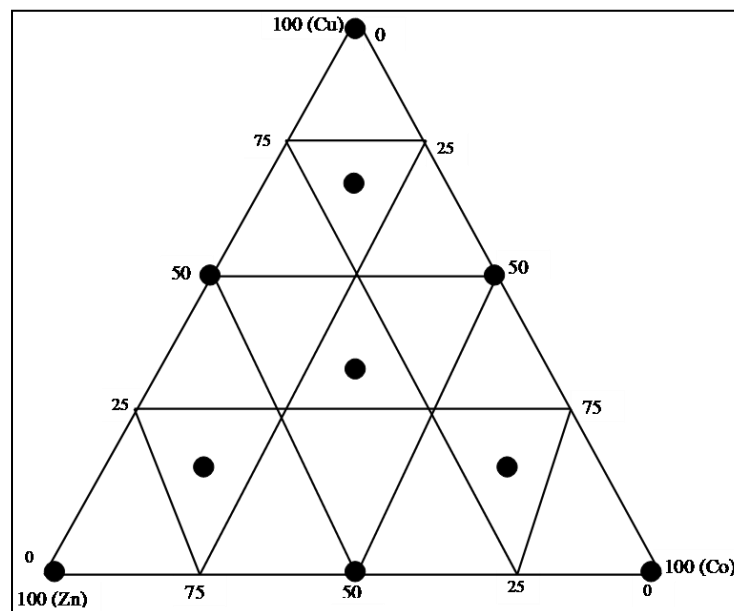


Figure 4.2: Three factor simplex-centroid mixture design

In this design, the aim of the experiment is to model the blending surface response with some form of mathematical formulae as given by equations 4.1, 4.2 and 4.3. Thus a measure of the influence of each component individually and in combination on the response can be

obtained. Below are the formulas for the three components (A, B and C) mixture models. As described by (Statsoft, 2007), an intercept cannot be fit to these reduced mixture models:

Linear model

$$y = \beta_1 x_1 + \beta_2 x_2 + \beta_3 x_3 \quad (4.1)$$

Quadratic model

$$y = \beta_1 x_1 + \beta_2 x_2 + \beta_3 x_3 + \beta_{12} x_1 x_2 + \beta_{13} x_1 x_3 + \beta_{23} x_2 x_3 \quad (4.2)$$

Special cubic model

$$y = \beta_1 x_1 + \beta_2 x_2 + \beta_3 x_3 + \beta_{12} x_1 x_2 + \beta_{13} x_1 x_3 + \beta_{23} x_2 x_3 + \beta_{123} x_1 x_2 x_3 \quad (4.3)$$

Whereby $\beta_1, \beta_2, \beta_3$ are the coefficients for main factors A, B, C respectively and $\beta_{12}, \beta_{13}, \beta_{23}$ are the coefficients for two interaction factors (AB, AC, BC) and finally β_{123} is a coefficient for three interaction factors (ABC). x_1, x_2, x_3 , are the coded values for factors A, B, C respectively and y is a dependent variable value. Only one model will be fitted for this particular experiment. The selection criteria depends not only on the model that gives the best data fit but also on statistical parameters, like P-values and F-values, as will be demonstrated in discussion section. The use of mixture designs can reveal important variables that affect the process (Claeys-Bruno *et al*, 2008). It was also observed that the use of a mixture design can produce high efficiency results.

4.2 Laboratory Samples Preparation

The samples used for the laboratory experiments were prepared like the samples found in the industrial plant at Skorpion zinc flotation where the Blue Cube Hydromet instrument is installed to perform the analyses. The concentration of the metals, as measured by Hydromet at mine, is given in Table 4.1. Further simulation of the samples was done by generating the similar matrix composition by introducing the interferences in the samples. Based on the concentration values from Table 4.1, cobalt, copper and zinc were prepared with maximum

concentrations of 50, 500 and 50000 ppm respectively. This would ensure that the ranges of concentrations, as depicted in the table, were covered.

Table 4.1: The metals' concentrations as found at Skorpion Zinc flotation plant

Metal	Low concentration (ppm)	High concentration (ppm)
Copper	200.0	400.0
Zinc	30000	40000
Cobalt	20.00	40.00

4.2.1 Calibration and Test Samples

The sulphate salts of copper, cobalt and zinc metals were used to make the solutions. The amounts of the salt used for sample preparation are reflected by the values in Table 4.2. Each salt was first dissolved in 100 ml of distilled water and then added to 50 mL of 98% sulphuric acid. The resulting solutions were diluted to 500 mL with distilled water to make the concentrations of 400, 2000 and 100000 ppm for Co, Cu and Zn respectively. High purity sulphate salts were preferred because low levels of purity in the metals' solutions could interfere with the absorption peak of the metals of interest. Therefore, purity plays a very critical role in this investigation. In industrial solutions the interferences present are cadmium and iron metals. The lower concentrations for the calibration and test samples were made by diluting the stock solution with distilled water.

Table 4.2: Preparation of stock solution using sulphuric acid

Substance	Mass (g)	Purity (%)	Source
Copper Sulphate	3.929	99.99	Merck
Zinc Sulphate	219.9	99.50	Saarchem
Cobalt Sulphate	0.954	99.99	Sigma Aldrich
Nickel Sulphate	1.119	99.98	Sigma Aldrich

Since the analyses in this study involve the simultaneous determination of three metals in solution, the calibration set of samples were done using mixture solutions of copper, zinc and cobalt metals. The percentage of the concentrations of each metal, Table 4.3, were generated from a statistical three-component mixture design using Design-Expert software as illustrated in sub-section 4.1.2 of the experimental design. The solutions for the test samples were prepared in a similar manner as the calibration samples, except that the proportions of each metal were chosen randomly so that the total percentages of metals add up to 100 %. The maximum concentrations from which they were prepared are given in Section 4.2. The table showing the samples for the test set is given in Appendix A.

Table 4.3: Sample solutions used for calibration procedure

Run	Standard Order	Percentage of each metal from maximum concentration (%)		
		Zinc	Copper	Cobalt
1	1	16.67	16.67	66.67
2	6	0.00	50.00	50.00
3	9	33.33	33.33	33.33
4	4	50.00	50.00	0.00
5	12	0.00	0.00	100.00
6	11	16.67	66.67	16.67
7	14	0.00	100.00	0.00
8	10	50.00	0.00	50.00
9	1	33.33	33.33	33.33
10	19	66.67	16.67	16.67
11	16	100.00	0.00	0.00
12	2	33.33	33.33	33.33

4.2.2 Samples for Nickel effect

The nickel sulphate ($\text{NiSO}_4 \cdot 6\text{H}_2\text{O}$) salt, weighing 1.119 g, was measured with an analytical balance. The salt was dissolved in distilled water together with 50 ml of 98% of sulphuric acid in a 500 ml volumetric flask to make solutions with concentrations of 1000 ppm. The nickel solution was added to the four different samples. The three component mixture

samples were prepared as shown in Table 4.4. The addition was in increment of 25 ml of 1000 ppm nickel solution. More detail on this procedure is given in sub-section 4.4.2.

Table 4.4: Sample solutions for determination of nickel interference effect

Sample #	Percentage of each metal from maximum concentration (%)		
	Zinc	Copper	Cobalt
1	70.00	0.00	30.00
2	80.00	20.00	0.00
3	0.00	60.00	40.00
4	40.00	30.00	30.00

4.2.3 Samples for Temperature Effect

The samples used to evaluate the effect of temperature on the absorption spectra of metals were prepared as shown in Table 4.5 using the dilution method explained by equation 4.4 in section 4.2.1. The temperature of each sample was varied from 20 °C to 80 °C as will be illustrated in the methodology section under sub-section 4.4.3.

Table 4.5: Sample Solutions for determination of temperature effect

Sample #	Percentage of each metal from maximum concentration (%)		
	Zinc	Copper	Cobalt
1	60.00	10.00	30.00
2	50.00	25.00	25.00
3	20.00	0.00	80.00
4	60.00	40.00	0.00

4.2.4 Blank Samples

Blank samples were prepared in a similar manner as metals solutions, the only difference being that no analyte (copper, zinc and cobalt) was included in the preparation steps. Thus, a volume of 50 mL of 98% sulphuric acid was diluted to 500 mL with distilled water in a

volumetric flask. The acid was added slowly to avoid giving off excess heat as a result of mixing substances. In most cases, the measurement obtained from the blank was subtracted from the solution samples, so that only the response due to respective metals could be determined.

All solutions were prepared daily at the Department of Process Engineering and were stored in plastic bottles before analysis at Blue Cube company. The plastic bottle has the advantage of being not easily corroded by acid as compared to glass sample holders that corrode easily and sometimes they can produce other metals, such as calcium, sodium, which cause interferences to the metals being studied.

4.3 Experimental Set-up

4.3.1 Instrument Description

The instrument used for the analyses has four main essential parts that are used to run the experiments. These are interface, data processor, sample holder and spectrophotometer. The instrument has an optical sensor that uses the principle of diffused reflective spectroscopy to quantify each metal (Lottering and Aldrich, 2006). The spectroscopy has a wavelength region of roughly 350 nm (ultraviolet-visible (UV-Vis)) to 1100 nm (near infrared (NIR)) spectroscopy. Figure 4.3 is the photograph of the overview of the industrial prototype of the Blue Cube optical fibre sensor instrument with the features mentioned above and their functions explained as follows:

The interface is connected to a main switch and it supplies a steady 12 volts to both the data processor and spectrophotometer. The data processor contains the computer processor which processes the data captured from the sample. The spectrophotometer is responsible for providing a light source to the sample. Optical fibres are used for the transmission of light from its source to the sample holder along with transferring the resulting signal from the solution to the data processor for interpretation.

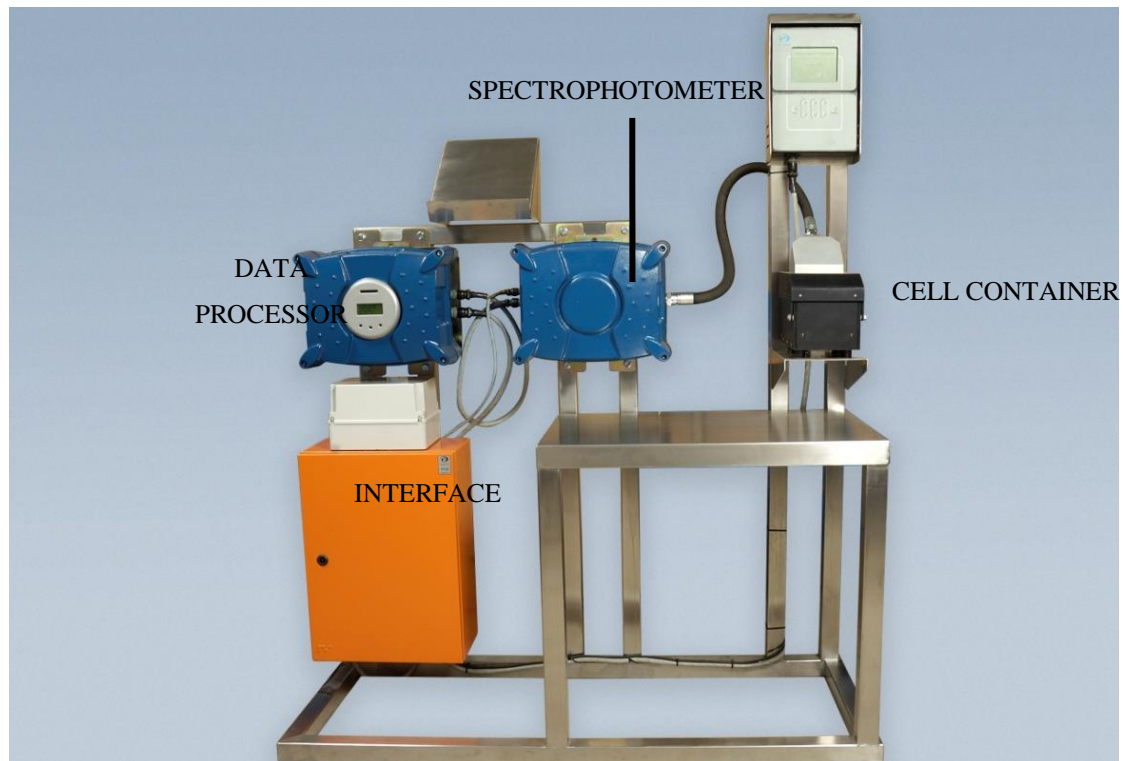


Figure 4.3: Blue Cube optical fibre sensor instrument

Lastly the sample holder contains a measuring cell which holds the solution to be analysed and has a volume capacity of 180 mL. All the parts described above are networked to the personal computer. The computer is used mainly for inputting experimental parameters like light intensity and execution time. In addition, it is suitable for graphically displaying results and the storage of data (spectra).

4.3.2 Internal Calibration of the Instrument

Before any experiment can be run, the internal calibration must be done on the instrument and this is usually done by performing two runs of reference, namely black and light. Black reference is the situation whereby the light is switched-off to correct the baseline and correspond to 100 % absorbance. The light reference involves baseline correction using distilled water but this time the light is switched on and this corresponds to 0 % absorbance. The important factor to be considered during the internal calibration is that the black reference is always performed first so that the light intensity can be stabilised for the

experimental runs. Then the light reference must be performed at least one hour after the black reference simply because the lamp requires that much time to warm up.

4.4 Methodology

4.4.1 Analytical Procedure: Calibration and Test Samples

The instrument does not necessarily require further sample preparation prior to the analysis of metals' solutions. Therefore after the internal calibration of the instrument the standard solutions were run first before any other samples because they have known concentrations which make them easier for comparison with unknown samples. After that, the test metals' sample solutions can be run. The runs of the experiments for each set of samples were performed randomly to accommodate any instrumental error that may be experienced during the measurements, thus the error can be evenly distributed among the samples to be analysed.

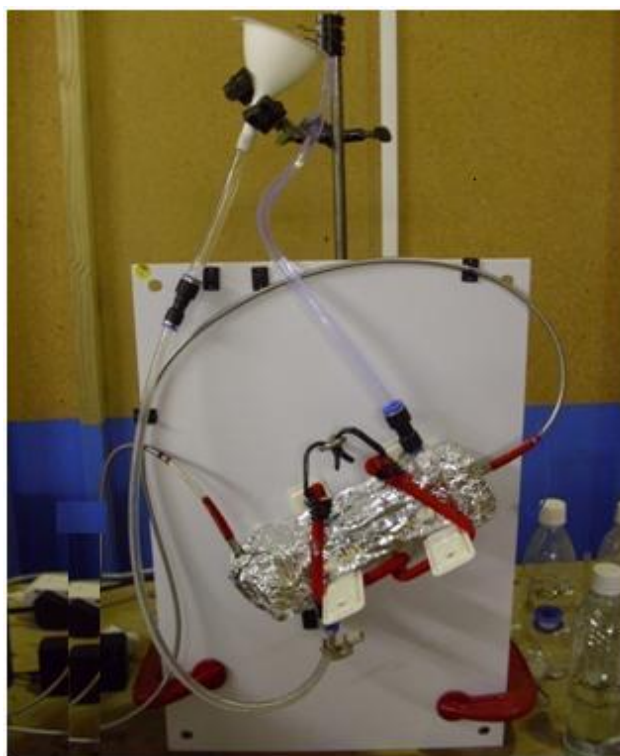


Figure 4.4: Laboratory set-up of Blue Cube instrument showing sample holder

The solution to be analysed was poured into the sample holder through a white funnel until it came out at another outlet end of the holder as shown in Figure 4.4. The plastic clamp was

used to reduce the flow rate of samples by squeezing the inlet tube to the sample holder. The clamp aids in reducing the number of the bubbles in the cell, thus the effect of bubbles on the absorption spectra of the metals is also reduced. Furthermore, the solution inside the measuring cell was allowed to stabilise for 30 seconds before analysis was done. The start button on a remote control was pressed to start capturing the data and three scans, or repeats, were done for each sample for a period of six minutes.

After each measurement, the funnel was detached from the stand to discard the solution into the waste container. The flow is in the reverse direction of the flow as illustrated in Figure 4.5. The system switches off automatically after collecting the data from each scan. The important factor to consider is the cleanliness of the instrument through the entire experimental procedure. In between the runs of the samples, the system was washed twice with deionised water to remove interferences from the previous sample and finally rinsed with the sample to be analysed to improve the accuracy of that particular measurement. Once the instrument had been calibrated, the results of the other samples were obtained from the small display screen on the data processor after each scan.



Figure 4.5: Blue Cube laboratory set-up during the drainage of used solution

4.4.2 Effect of Nickel

In order to study the effect of nickel on the absorption spectra of the metals of interest, the prepared samples of four-component mixture solutions were spiked with a nickel solution in the increment volume of 5 ml starting from 5 ml to 20 ml. The concentration of nickel that was used in the experiments was 500 ppm. The mixing was done within the sample bottles originally used to contain only metals of interest. The analysis procedure was similar to that of calibration and test samples explained in section 4.4.1.1. The experimental set-up used for the calibration and test samples was also used for the evaluation of an effect of nickel and temperature and it is illustrated by Figure 4.6. The figure shows all the components that constitute a Blue Cube laboratory set-up.

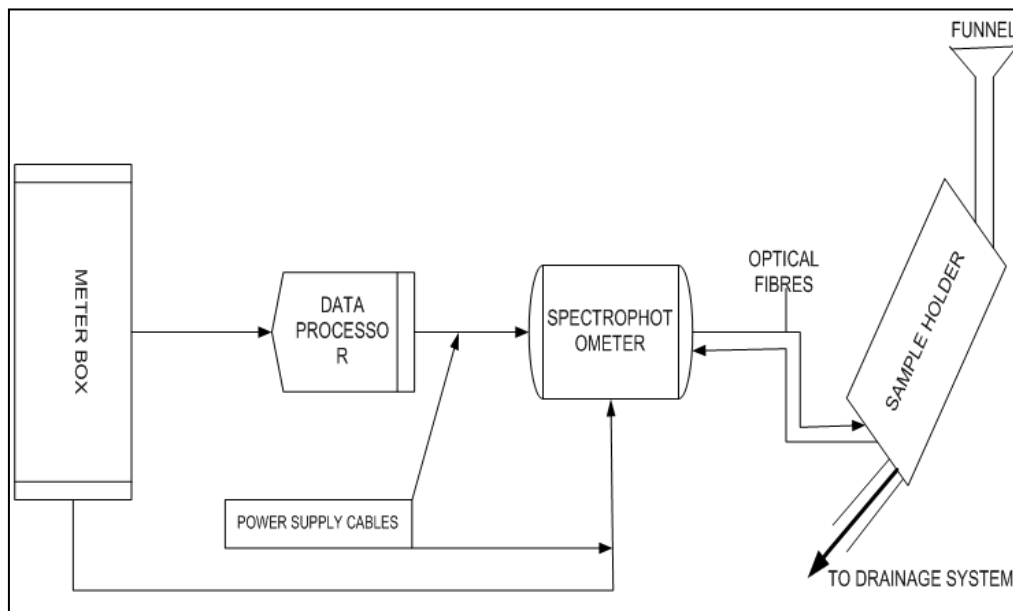


Figure 4.6: Schematic diagram of Blue Cube laboratory set-up

4.4.3 Effect of Temperature on Samples

The effect of temperature on the absorption spectra of the metals of interest was studied by varying the temperature of the samples at the following values: 20°C, 40°C, 60°C and 80°C. The water bath was used to maintain the temperature at each set value and a thermometer was used to take the readings of the samples to confirm the bath temperatures. Samples together with deionised water were allowed to attain the temperature of the bath for a period of one

hour before measurements were taken. The temperature of the solutions could not be increased to 100°C, because the material used for the laboratory set-up could not handle temperatures of that degree. In addition, some leakages were observed at 80°C, showing that the plastic tubes used were loosening up. The measurements and data collection procedures were similar to that of the calibration and test samples except that each solution was not discarded during the temperature increments.

CHAPTER 5: RESULTS AND DISCUSSION

This chapter gives an overview of the results obtained together with discussion. The pre processing method used for conversion of data aided in both quantitative and qualitative analyses. Both CLS and ILS models gave good results for Cu, Co and Zn metals during calibration steps but only Zn metal gave poor prediction results. The derivative spectroscopy which was thought to enhance prediction results of Zn had no effect – rather it gave poor predictions with increasing order of derivative. The increase in temperature of a solution and presence of Ni as an interference affected the prediction ability of both models. Overall, the developed statistical (CLS and ILS) models have similar accuracy as the Blue Cube and PLS models. However, the PLS model shows improved results for Zn metal.

5 RESULTS AND DISCUSSION

The data interpretation in this study will be based on the modelling of ILS and CLS calibration models and a number of software programs will be used for this purpose. Each program will be specific for its own usage to extract the valuable information from the raw data. The results obtained will be compared with the literature already published and some recommendations will be given from there.

Both models developed in this study involve two main steps, namely calibration and prediction. The discussion focuses mainly on the development, validation and evaluation of the models. Throughout the discussion only the ILS model will be discussed since it is assumed that the similar discussion will hold for the CLS model too. Because both models are linear models they should have similar behaviour in data interpretation. However, the exceptions will be given where the CLS model involves a different data manipulation.

5.1 Model Development

The success of any model depends mainly on good formulation and development of its calibration step. A number of factors have to be taken into account in doing that, for example, the number of samples and complexity of the model algorithms. Before the calibration step of the models could be done, the data was first analysed to evaluate the repeatability between individual measurements and also to determine which techniques could be used as a preprocessing step.

5.1.1 Data assessment

The raw data from the Blue Cube optical sensor was given in units of transmittance counts whereby a high transmittance counts value shows that a sample had absorbed less light hence most of the light is transmitted. Figure 5.1 shows the four VNIR spectra of pure copper (500 ppm), cobalt (50 ppm) and zinc (50000 ppm) metals together with their mixture (33 % of each metal) for a given wavelength region of 400 to 1000 nm. Each spectrum is the average of 54 individual measurements performed for that particular sample. Cobalt has the highest light intensity shown by maximum peak around 600 nm in Figure 5.1. The intensity for each sample depends mainly on the type of metal present in the sample solution because 500 ppm of Cu has lower intensity as compared to 50000 ppm of Zn as shown by their spectra in Figure 5.1.

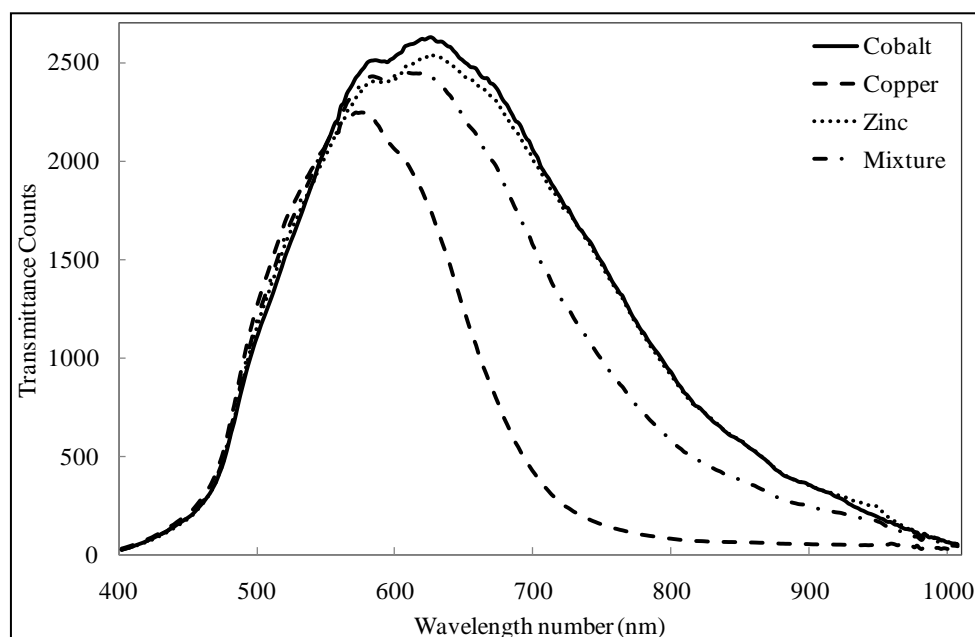


Figure 5.1: Raw spectra of pure Cu, Co, Zn and their mixture

As discussed and shown in Figure 5.1, each individual sample has a different intensity from the other. In addition, there is also a clear distinction in terms of the shapes of their VNIR spectra which further reveal different chemical properties between these metals. From these raw data spectra, it can be deduced that the optical sensor is able to differentiate between the metals in terms of their intensities which are based on their colour. Table 5.1 shows the statistical values of the four spectra show in Figure 5.1 to reflect the repeatability of 54 individual measurements for the whole spectrum range (400 – 1000 nm).

Table 5.1: Repeatability of Individual Measurements from Raw Data

Metal	Intensity Values (counts)		
	Maximum	Mean	Standard Deviation (%)
Copper	2262.72	600.105	0.5518
Cobalt	2680.63	1130.14	0.5723
Zinc	2587.16	1110.85	0.8858
Mixture	2489.99	830.432	0.7553

The percentage standard deviation (% STDV) was used for ease of comparison of the metals since they have different intensity values. The guideline used for a statistically acceptable value of % STDV is any value less than 2.5% and the results in Table 5.1 showed that there was a good repeatability between the individual measurements of each sample being analysed since the % STDV values for these samples were below 1%. Cu metal showed a lowest value among all the metals intensity values, thus indicating a good response of the sensor towards this metal, as will be demonstrated in the further discussion.

5.1.1.1 Measurements Consistency

Another technique to check the consistency of individual measurements is to make a hypothetical cut through the VNIR spectra of Figure 5.1 at wavelength of 760 nm and then plot the values in a stair-case graph as shown in Figure 5.2. The results for all the calibration and test samples are included in the analyses. The horizontal lines in Figure 5.2 represent the values for each run made within each sample being measured and each run consisted of 54

measurements or scans. The vertical lines in the same figure indicate the intensity values of the samples. The measurements shown with a red colour line are from test samples and they seemed to contain some noise in their values shown by the uneven horizontal lines. This problem of noise effect was eliminated by filtering the signal before doing further analysis. The third order smoothing filter that uses a Savitzky-Golay algorithm from MATLAB software was employed to reduce the noise level.

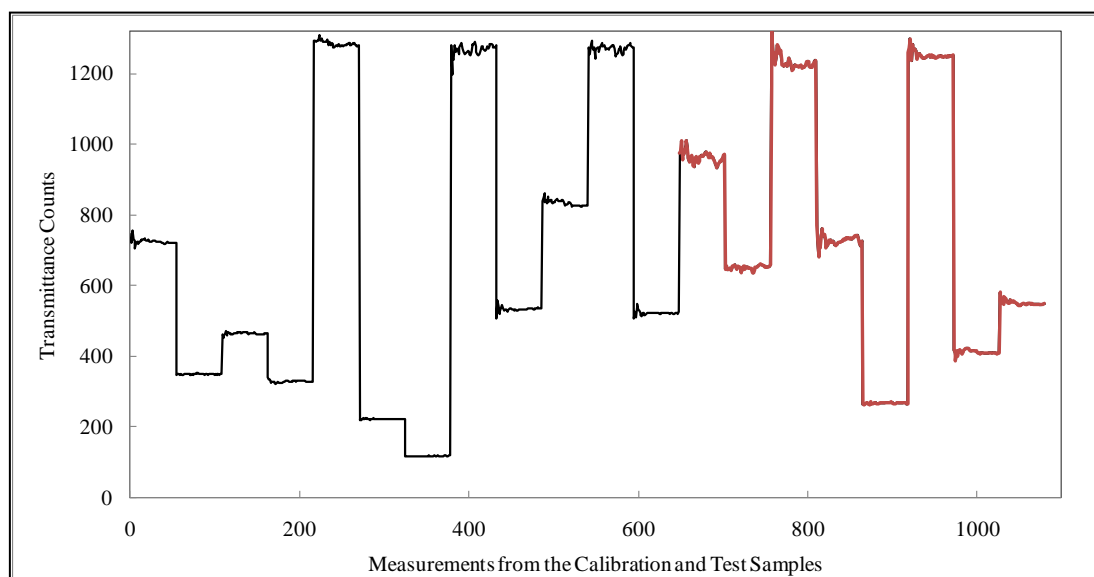


Figure 5.2: Consistency of measurements during calibration and prediction steps

5.1.1.2 Comparison of Calibration and Test data

In order to have a model that can be effectively used for prediction of unknown samples, both calibration and test data must fall within the same concentration range for each metal. In the study for monitoring the concentration of ammonia, Zachariassen *et al*, (2005) underestimated the amount of interferences when preparing laboratory calibration samples – hence the PLS model developed was inaccurate when applied in industrial scale for prediction of unknown samples. Their case study had shown that a difference in composition of the calibration and prediction samples could lead to a poor model.

The similarity between the calibration and test data will be evaluated based on the intensity values for all the samples that were obtained from the instrument. The two procedures namely, Sammon mapping and Kernel density were employed to determine the difference

between the two data sets. The first procedure is based on the working range within which the calibration and test data sets must fall so that similarity can be done as will be illustrated in detail in Figure 5.3 and second procedure evaluates if the samples from both two data sets behave in a similar manner throughout the whole wavelength region of the spectrum and this will be discussed and shown in more depth from Figure 5.4.

Figure 5.3 shows a three-dimensional scatter plot of the results of Sammon projections from both calibration and test data sets. The Sammon mapping algorithm from the MATLAB software program was used to map high-dimensional space data (spectra raw data) to lower dimensionality space data (extracted three features data). The algorithm preserves the structure in both data space sets by ensuring the distance between the two points in original space ($d_{o,s}$) is similar to the distance in the projection space data ($d_{p,s}$). Sammon, (1969) stated that the main aim of the algorithm is to minimise the error between $d_{o,s}$ and $d_{p,s}$ by using a function called Sammon's stress.

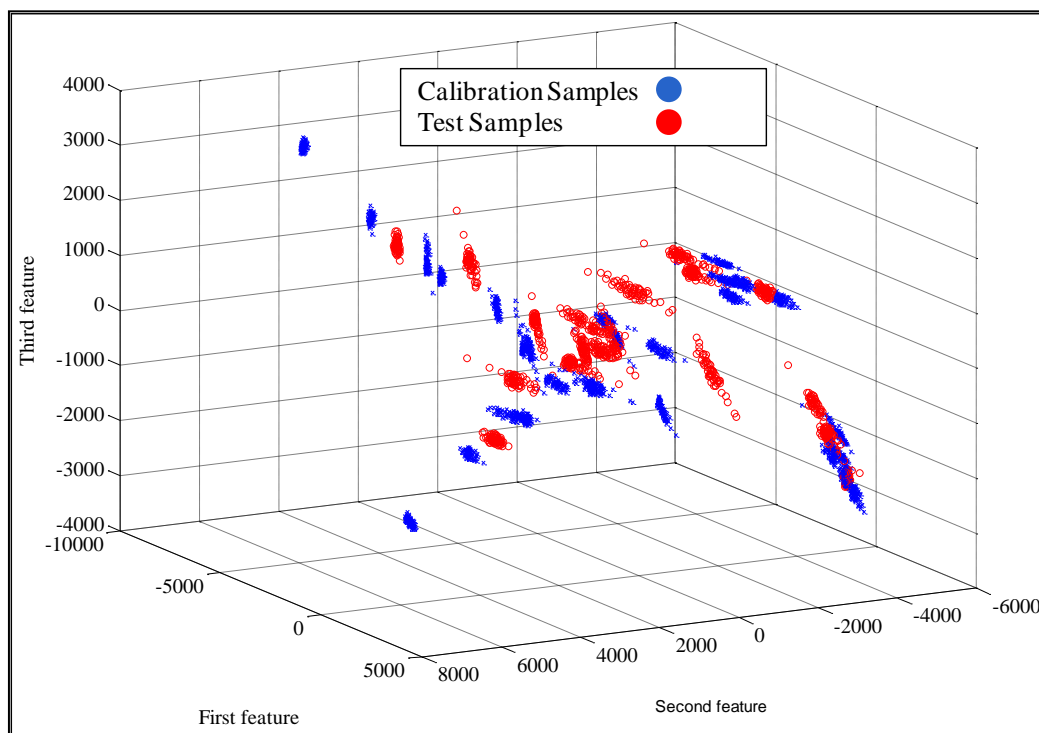


Figure 5.3: Sammon mapping for the calibration and test data

Both calibration and test data fell within the same space as given by Figure 5.3. This figure clearly shows that there is a well defined similarity among the samples of the two data sets since the measurements are close to one another. Furthermore, the calibration set has covered

a much larger range than the test set hence a test set can be predicted very accurately by the models. The value of the stress of mapping was computed to be 3.363×10^{-5} and the value indicated that there is an insignificant difference between the higher and lower space data sets; hence the mapping procedure was considered to be very accurate.

In a general view, the previously discussed result showed a high degree of similarity between the two data sets. Thus to determine the similarities of the individual samples from both calibration and test data sets, the intensity value for each sample was plotted against the wavelength numbers. Figure 5.4, (A) and (B) show the kernel densities of the scaled transmittance values for both calibration data and test data, respectively. The data were scaled by using a standardisation method and the method has aided in the easier comparison of both data sets.

The yellow colour in both sub figures indicates the area where most of the data points lie. It can be noted that the colour follows the same pattern in both sub figures throughout the whole wavelength region and most of the points are found to be saturated around the wavelength of 500 nm. However, in a calibration set the colour is more intense due to a larger number of samples used as compared to the test set. The results from the sub figures show that both calibration and test data sets are similar throughout the whole wavelength region which was used in the experimental analyses. Based on sammon mapping and kernel density methods, it could be concluded that there is no difference between the individual samples of both data sets.

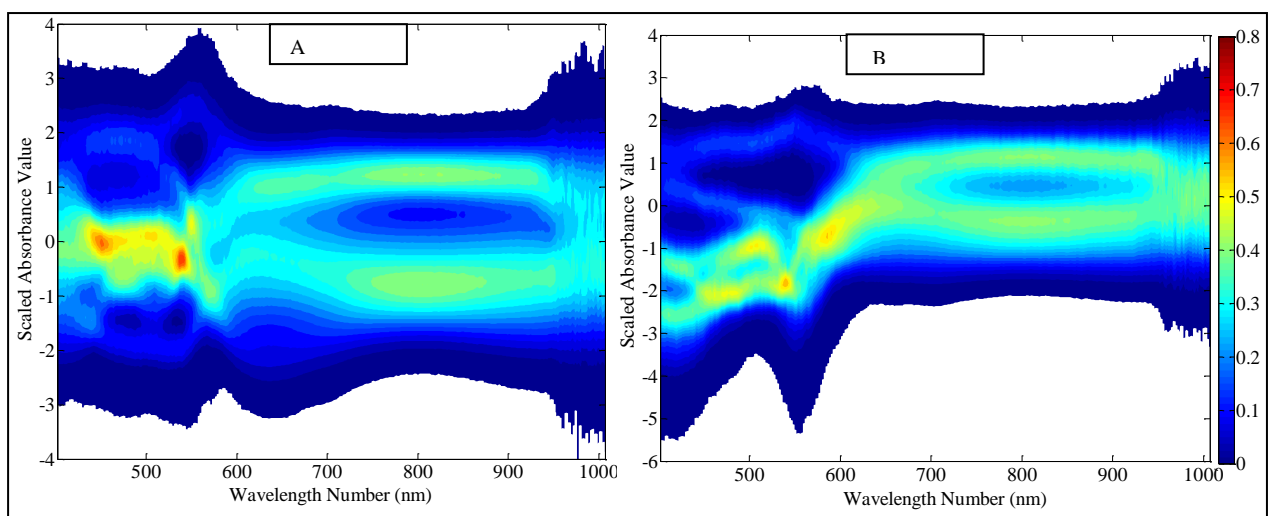


Figure 5.4: Comparison of calibration (A) and test data (B) for each wavelength number

5.1.2 Preprocessing Step

A high degree of similarity between the calibration and test data sets within both the working concentration range and throughout the wavelength region clearly indicates that formulation of the models can be done. However, both data sets must be preprocessed before model formulation. The dimensionality of the data can be reduced by the preprocessing methods. There are quite a number of preprocessing techniques that can be used, and mostly, they depend on the calibration models to be used and the knowledge of the problem at hand. Haavisto *et al.*, (2008) stated that a preprocessing step used in a PLS model did not only have an advantage of reducing the intensity of computational load but it also did not affect the performance of the model.

Most of the studies had used mean-centred spectra to preprocess the data and it was found that the intensity of each component in the mixture can be clearly identified (Haaland *et al.*, 1999). In this study the raw data was converted to absorbance values by using the principles of Beer-Lambert law which states that absorbance of any given component is directly proportional to its concentration. The absorbance of a metal of interest in the solution is approximated by a given formula from equation 5.1.

$$A = \log \frac{I_{\text{solvent}}}{I_{\text{solution}}} \quad (5.1)$$

where I_{solvent} is the intensity of the light that passes through the solvent only. In this case, a blank sample as described in section 4.2.4 was used. I_{solution} is the intensity of light obtained from a sample composed with solvent (blank) and an analyte of interest. The approximation holds for all the samples used in the study because of their dilute concentrations that follow the principles of Beer-Lambert law as stated above.

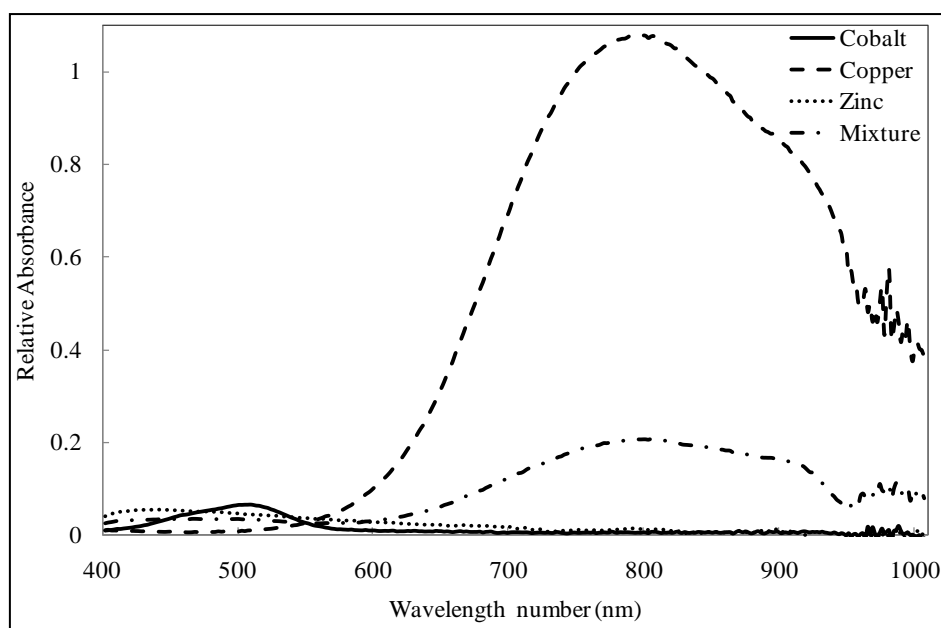


Figure 5.5: Absorption spectra of pure Cu, Co and Zn together with their mixture

The raw data of all the VNIR spectra were transformed into absorbance values and Figure 5.5 shows the absorption spectra of pure Cu, Co and Zn metals together with their mixture. The wavelength region between 950 and 1000 nm is affected by a lot of noise possibly due to instrument drift and this region was discarded for a further data analysis. The transformation has aided by showing clearly maximum peak of each metal and it can be observed that Cu absorbed maximum light at around wavelength region of 800 nm. Since Cu metal has the highest maximum absorption peak among the metals, a preliminary conclusion at this point could be that a quantitative analysis of copper in the mixture will be relatively easy to carry out as compared to other metals.

The maximum absorption peaks for cobalt and zinc could not be visible from Figure 5.5, thus the wavelength region between 400 nm and 560 nm was enlarged to illustrate their peaks. The resulting spectra are shown in Figure 5.6 whereby Co and Zn exhibit maximum absorption peaks at wavelength of 510 and 430 nm respectively. The peak for Zn is not as sharp as that of Co because of weak interactions that exist between the radiation light and Zn ions.

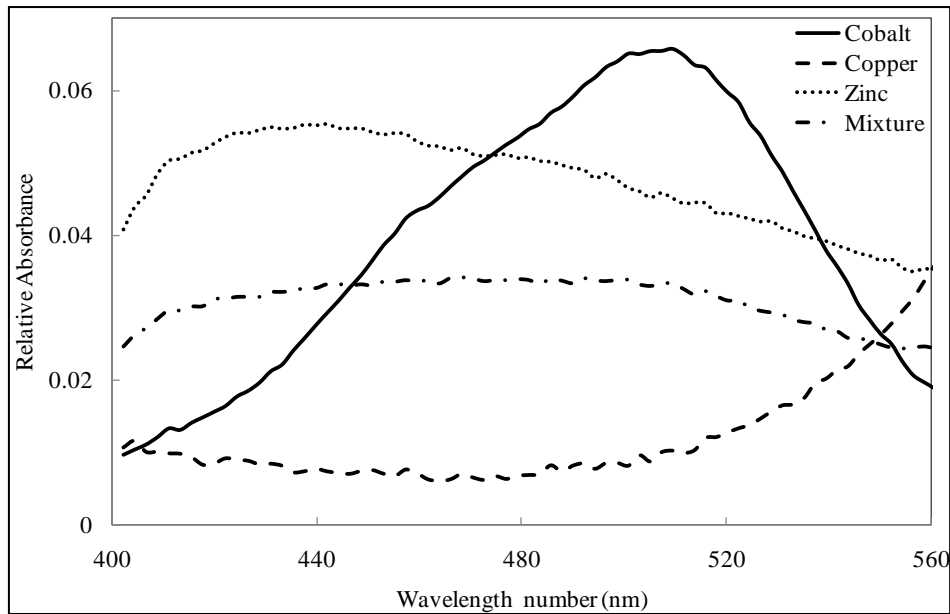


Figure 5.6: Absorption spectra showing maximum peaks of pure Zn and Co

Furthermore, the maximum absorption peaks observed from the spectra in Figure 5.5 and 5.6 aided in qualitative analysis of the metals since each metal has a maximum peak at the specific wavelength number. The transformation of spectra into absorbance values added an advantage to a wavelength selection procedure to be used in the calibration and prediction steps of the models. When using the raw spectra for modelling purposes, as shown in Figure 5.1, it was impossible to select the wavelength region for each metal since the spectra had totally overlapped and masked each other.

5.1.3 Calibration Step

The traditional inverse least squares method involves the selection of wavelength number whereas the traditional classical least squares method uses the whole spectrum of wavelength region to build the calibration part of the models. However, in this case the CLS model was modified by incorporating selected wavelength numbers in its algorithm. Manual selection method was used to select the wavelength numbers for both models whereby the initial wavelength number corresponds to the maximum absorption peak of each metal.

There are some factors that had to be considered when performing the wavelength selection method for these models:

1. ILS model – the number of selected wavelengths cannot exceed the number of calibration samples. This is a big restriction in the calibration step of model since the larger the number of wavelengths, the better prediction can be obtained. The selection process became very tedious and sometimes impossible.
2. CLS model – in this case, the selected wavelength number does not depend on the number of calibration samples. However, it should be considered that too many values selected result in an over fitting of the model and poor prediction. In both models a great care must be taken during the selection procedure.

Table 5.2: Selected wavelength region for each individual metal

Metal	Wavelength region (nm)	
	ILS model	CLS model
Copper	796 – 802	796 – 802
Cobalt	509 – 514	509 – 514
Zinc	435 – 440	438 – 449

Table 5.2 shows the wavelength region that was selected and used to perform the calibration steps of both ILS and CLS model. After the selection, the algorithm for the calibration step was formulated from the statistical toolbox in MATLAB software program. The proportionality constant (P-matrix) to be used in the prediction step of the models was calculated from the measured absorbance of the calibration samples and their concentration values as given by equation 5.2, whereby **C** and **A** are the concentration and absorbance matrix of calibration samples respectively:

$$P = CA^T AA^T^{-1} \quad (5.2)$$

The calibration steps of the models were evaluated based on the correlation coefficient (R^2) between the actual and their predicted values, and percentage root mean squared error (% RMSE) values given by equation 5.3 and 5.4 respectively. Before each statistical parameter was computed, the actual values of the metals in solutions and predicted values from the models were rescaled to 0 – 100 %. The rescaling procedure had added advantage that the calibration and prediction performance of the models can be easily compared among the

metals since now RMSE values will be in dimensionless units (%) of both the calibration and prediction ranges.

$$R^2 = \sum \frac{Y_{pred} - Y_{mean}}{Y_{theor} - Y_{mean}}^2 \quad (5.3)$$

$$RMSE = \frac{\sqrt{\sum Y_{pred} - Y_{theor}}^2}{n} \quad (5.4)$$

where Y_{pred} is a value predicted by the model and Y_{theor} is a theoretical value given by a design for calibration samples. Lastly, Y_{mean} is a mean value of n number of measurements being performed for a particular metal. All the values were expressed in percentages.

The good accuracy and precision of the model is determined by the R^2 values close to 1.00 and % RMSE values less than 10. Table 5.3 show results from the ILS and CLS models after their calibration algorithms had been computed. It is evident that the results of the CLS model are not as good as that of ILS model and also that one statistical parameter cannot be used alone to determine the precision of the models. For instance, the high R^2 value does not necessary reflect that the theoretical and predicted values are high degree of correlation but other parameters like P-value and F-value must be calculated to reach a conclusion about the quality of the model.

Table 5.3: Results from the calibration steps of ILS and CLS model

Metal	R^2 Value		RMSE Value (%)	
	ILS model	CLS model	ILS model	CLS model
Copper	0.9956	0.9978	1.9048	2.7545
Cobalt	0.9947	0.9488	2.1070	7.0215
Zinc	0.9984	0.9174	3.1447	10.056

From Table 5.3, zinc has a slightly higher % RMSE value compared to copper and cobalt results, however all the values for the metals fall within the acceptable limit of 10%. The accuracy and precision of the calibration steps of both models were found to be satisfactory on the basis of % RMSE and R^2 values, thus the models can be used for the prediction of the

unknown samples. This can be further examined from the scatter plots in Figure 5.7, 5.8 and 5.9. A solid line in each scatter plot shows the linear regression fit between the measured and model values, whereas the dotted lines show 95 % confidence interval limits for an estimation of good fit for the ILS model. For all the figures, the majority of the data points fall within the interval limit, thus reflecting good accuracy for the model. The results shown here and onwards are only for the ILS model, the calibration graphs of all the metals for the CLS model are given in Appendix B.1. The fitted equations for the linear regression lines are also shown on the graphs.

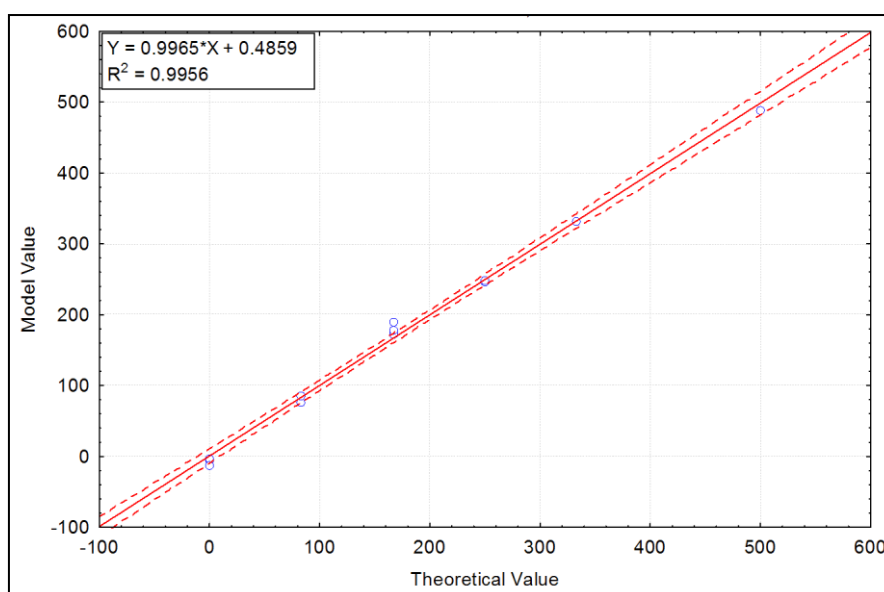


Figure 5.7: Calibration graph for the Cu metal using ILS model

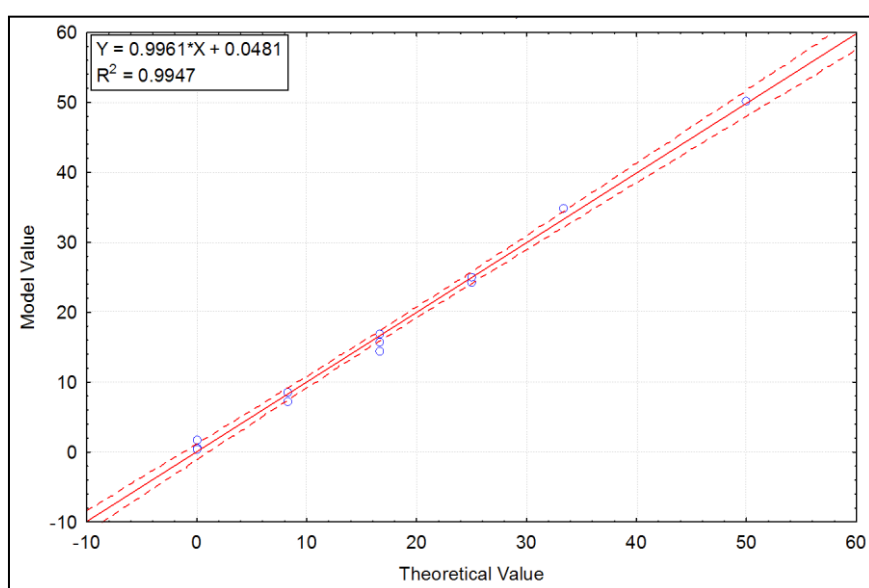


Figure 5.8: Calibration graph for the Co metal using ILS model

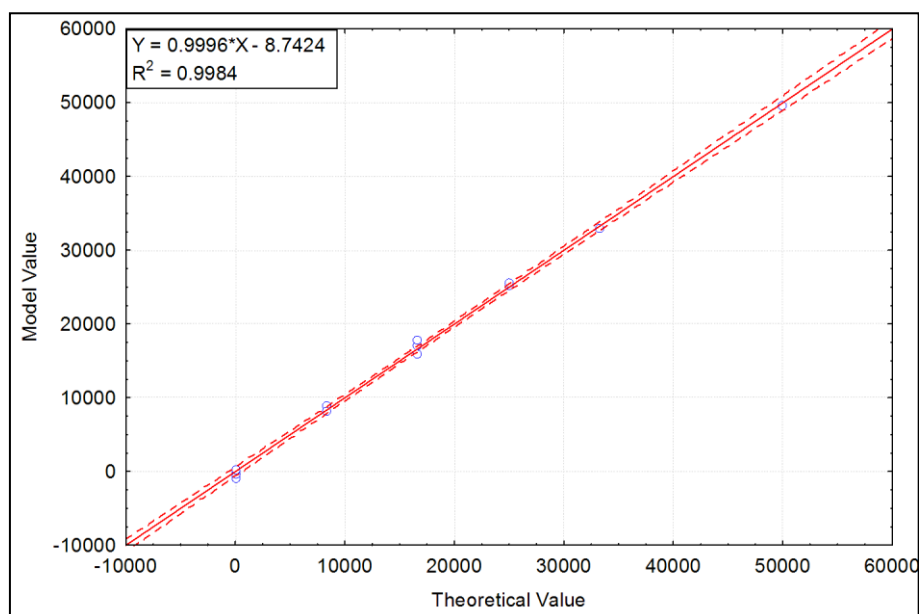


Figure 5.9: Calibration graph for the Zn metal using ILS model

5.1.4 Influence of number of calibration samples

Before the overall evaluation of the ILS model can be done in terms of the prediction ability, it was worthwhile to examine the effect of the number of calibration samples on the prediction ability of the model. Cirovic, (1998) stated that the few number of samples than the components in a mixture leads to unstable mathematical results, for example, it becomes quite impossible to solve for the P-matrix as given by equation 5.2. On the other hand when there is large number of calibration samples, the model can be over fitted hence prediction will become poor.

Moreover, there is also the effect of collinearity in the spectra with a large calibration data. Collinearity effect occurs due the fact that absorbance values of the spectra simultaneously increase and decrease as the concentrations of components in a mixture change. Hence the concentration values of the test samples to be predicted are highly correlated. Again, in this case, the mathematical solutions with each component in a mixture become very unstable.

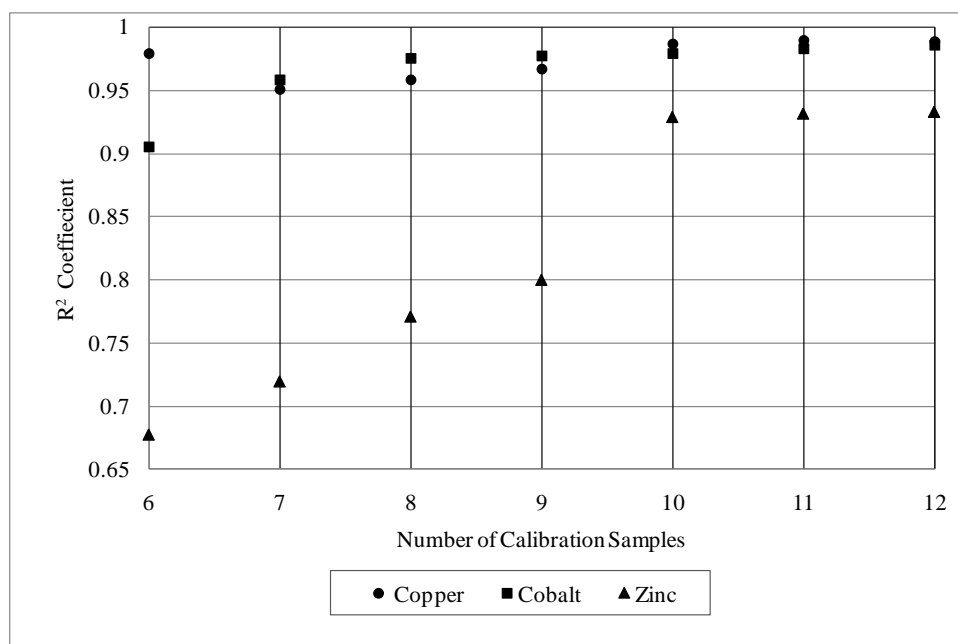


Figure 5.10: The effect of calibration samples on prediction ability of ILS model

Figure 5.10 shows the results for the effect of number of calibration samples on the prediction ability of the ILS model. The quality of the model was evaluated based on R^2 value for each metal. For the tested number of calibration samples, the prediction ability of the model for Zn metal seemed to increase with the number of samples in the calibration step. The prediction results of Zn improve when using ten samples in the calibration step of the model. The prediction ability of the ILS model for Cu and Co metals appeared to be independently related to a number of calibration samples used for developing the model. Both metals have the R^2 values of greater than 0.900 for all different number of samples, as shown by Figure 5.13. The worse prediction of Zn is contributed to its low absorbance in mixture solutions as shown in Figure 5.5 and will be explained in the prediction step of the model.

5.2 Model Validation

In order to apply the formulated ILS model for prediction of the unknown samples, the adequacy of this model must be determined. The assumption used to evaluate the adequacy of the model is that the errors are constant, normally and independently distributed with mean zero. However, in practice, this assumption will usually not hold exactly because of the uncontrollable factors (Leardi, 2009). The adequacy of a model can be easily investigated by

the examination of residuals. If a model is adequate, the residuals should be structureless; that is, they should show no obvious patterns (Montgomery and Runger, 2002).

5.2.1 Residual Plots

A normal probability plot of residuals was used in this study to evaluate the validation of the ILS model. If the underlying error distribution in the fitted data is normal, the points of a plot will resemble a straight line. Montgomery and Runger, (2002) mentioned that in visualising the straight line of the data points, more emphasis should be placed on the central values of the plot than on the extremes. The experimental conditions which may differ from time to time could mainly be contributed to the deviation of the extreme values. From Figure 5.11, the residual values for each measurement lie on the straight line, indicating that the error distribution within the measurements is approximately normal. This means that the normal probability plot of residuals was very satisfactory and consequently used as a measure for the validation of the ILS model. The figure was used to validate the results of calibration step of the ILS model.

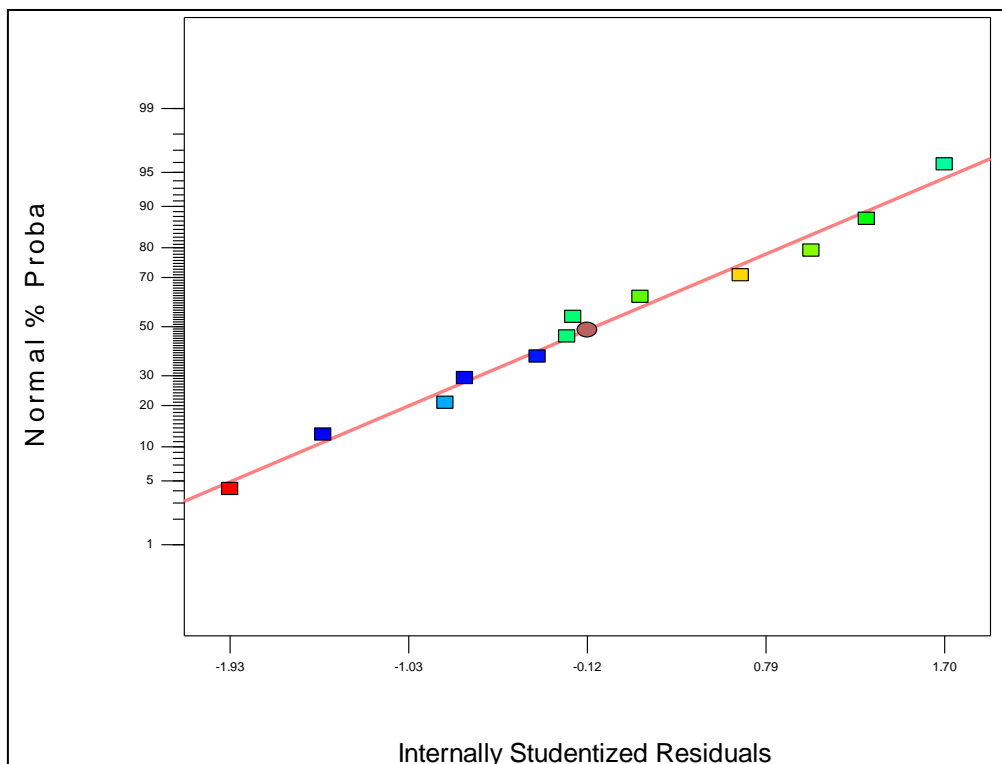


Figure 5.11: Normality plot of the studentised residuals of calibration samples

5.2.2 Influence of mixture component on calibration step

On the basis of residual plot, the previous section had proved that the ILS model was valid. Thus the ILS model can be used for the prediction purposes. However, due to different heights of maximum peaks of the absorption spectra of Cu, Co and Zn metals, it was necessary to investigate which metal in the mixture solutions affect the quality of calibration step of the ILS model. The regression models, given by Table 5.5, were developed to combine the results of all the metals. The absorbance value for each calibration sample, shown in Table 5.4, was calculated by taking the average of absorbance values at the maximum peaks of each metal present in a mixture for that particular sample. The absorbance values were used to develop these regression models.

Table 5.4: Absorbance response from the calibration samples

Run order	Standard			Absorbance
	order	Zinc	Copper	
1	1	16.67	16.67	0.1182
2	6	0.00	50.00	0.1779
3	9	33.33	33.33	0.1533
4	4	50.00	50.00	0.1875
5	12	0.00	0.00	0.0354
6	11	16.67	66.67	0.2255
7	14	0.00	100.00	0.2761
8	10	50.00	0.00	0.0375
9	1	33.33	33.33	0.1285
10	19	66.67	16.67	0.0758
11	16	100.00	0.00	0.0408
12	2	33.33	33.33	0.1291

The pseudo-coded values for each calibration sample together with its absorbance from Table 5.4 were processed by Design Expert software using a simplex centroid mixture analysis tool for a mathematical or regression model to be fitted. In order to determine which model will best fit the data, the sequential model sum of squares and model statistics calculations were

carried out before the regression model could finally be fitted. Two criteria were employed to select a model that has a high accuracy in explaining the data given in Table 5.4.

Firstly, the selection of the best model is to choose a highest order polynomial model where the additional terms are significant and a model is not aliased, as given from Design Expert Software, version 7.1.6 software. Another guideline from Design Expert software is also to choose a model which maximises both adjusted R^2 and predicted R^2 values. Both of these guidelines are adhered to by the linear model as shown in Table 5.5 with both R^2 values greater than 0.900. Moreover, the P-value of the linear model is less than 0.05 showing the model was found to be statistically significant within 95 % confidence interval limits of the fitted calibration data. The F-value is used to test the null hypothesis that a regression model being proposed fits the data well. The large F-value indicates that a model explains a variance in the data very accurately. The linear model also satisfied this criterion of the F-test.

Table 5.5: Sequential fit and statistics of the models

Model Type	Sum of Squares	F value	Adjusted R^2	Predicted R^2	P-value
Linear	0.0625	107.8800	0.9511	0.9036	<0.0001
Quadratic	0.0012	1.6350	0.9596	0.7413	0.2781
Special Cubic	0.0000	0.0215	0.9517	0.4903	0.8892
Cubic	0.0009	2.7117	0.9714	0.0454	0.2125

From the previous discussed points of Table 5.5 above, it is evident that the linear model had fitted data very accurately as compared to other models. The derived linear regression model is given as follows:

$$Y = 0.2987x_1 + 0.05249x_2 + 0.04516x_3 \quad (5.5)$$

Where Y is the response (absorbance) and, x_1 , x_2 and x_3 are pseudo-coded values for Cu, Co and Zn metals respectively.

From equation 5.5, it can be noted that all the regression coefficients are positive reflecting that the metals have synergetic effects on the absorbance values of the mixture solutions. The magnitude of the regression coefficient values indicates the contribution of each metal towards the measured absorbance. Copper has the greatest effect on the absorbance value of a given mixture solution. The fitted linear regression model clearly shows that there are no interactions among the individual metals. The absence of the interactions was further supported by a contour plot illustrated in Figure 5.12.

The contour lines in Figure 5.12 are straight and parallel to one another indicating that there is a linear combination within the metals towards their contribution to the measured absorbance values. The presence of interactions, if any, will be indicated by the upward and downward curved lines for synergetic and antagonistic effects respectively. The effects depend on the behaviour of the individual metals in a mixture (van Tonder *et al*, (2010)).

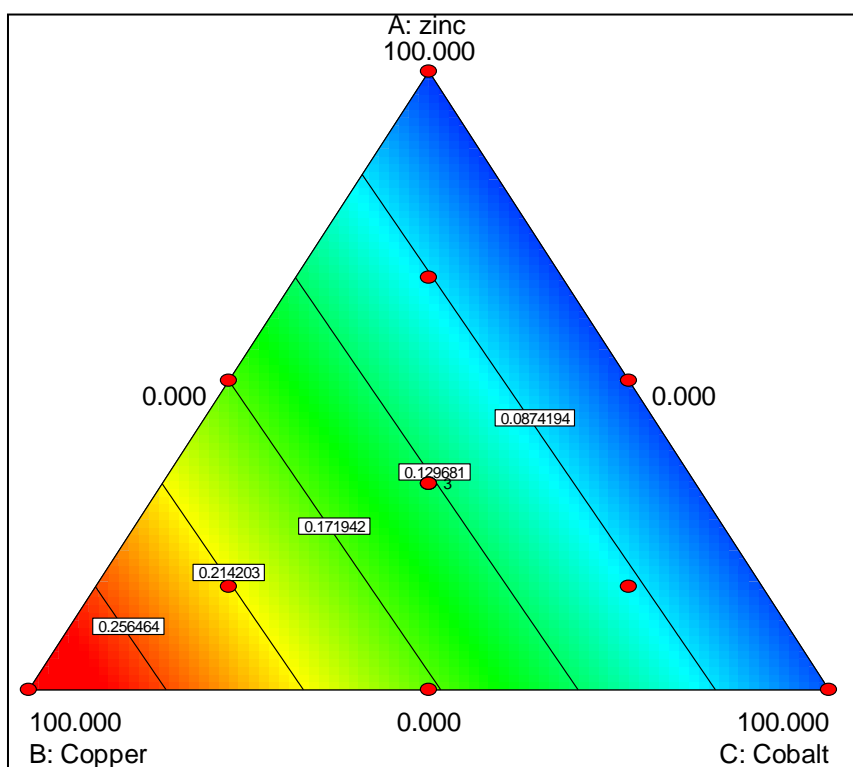


Figure 5.12: Absorbance contour plot for the components of the linear mixture model

When examining Figure 5.12, from 100% Co and 100% Zn solutions towards 100 % Cu solutions, the absorbance values increase. This indicates that Cu has a major contribution for a quality calibration step of the ILS model since the model was developed from the absorbance values. In terms of contribution to the absorbance values, Cu is followed by Co

and then Zn. The least contribution of Zn metal towards the measured absorbance can also be seen from the colours of the solutions in Figure 5.13.

Figure 5.13 shows the stock solutions of the pure three metals used in this study and the solution of Cu and Co are colourful whereas that of Zn is colourless. Thus, the Zn solution has a very low ability to absorb light as compared to other metals. The Blue Cube optical fibre sensor used in the study measures the intensity or transmittance of each solution hence all the solutions containing zinc will be expected to decrease the efficiency or quality of the calibration step of the models. In conclusion, the contribution of the metals towards the measured absorbance decreases in the following order: $\text{Cu} > \text{Co} > \text{Zn}$.



Figure 5.13: Stock solution for pure Cu, Zn and Co metals

5.3 Testing of the model; Prediction Step

After the model had been developed and validated from the calibration step, it was used for prediction of the unknown samples. These test samples have the same concentration range as the calibration samples as shown by Figure 5.3. The same wavelength region selected in the calibration step was also used in this step. The computation of the algorithm for the prediction step of the ILS model was done using the statistical toolbox in MATLAB software program. The concentration of the unknown samples (C_u) was calculated from measured

absorbance of these unknown samples (A_u) and the proportionality constant (P) that was obtained from calibration step using equation 5.2. The relationship between these three parameters is given by an equation 5.6 as follows:

$$C_u = PA_u \quad (5.6)$$

The previous discussion as given by Figure 5.10 had shown that more than ten calibration samples gave accurate prediction ability of the ILS model. Several statistical parameters were used to evaluate the prediction ability of the ILS model; namely R^2 , and % RMSE values. However, one of the most important tools in statistical analysis is a visualisation of the results. This can give a clear indication of the behaviour of the factors investigated in the specific study. The scatter plots for Cu, Co and Zn metals are shown in Figure 5.14, 5.15 and 5.16 respectively. The scatter plots generated by STATISTICA software program show the correlation between experimental and model values. The 95 % confidence interval limits for a fitted regression line were also plotted on the same graphs and indicated by curved dotted lines. The fitted equations for the linear regression lines are also shown on the graphs.

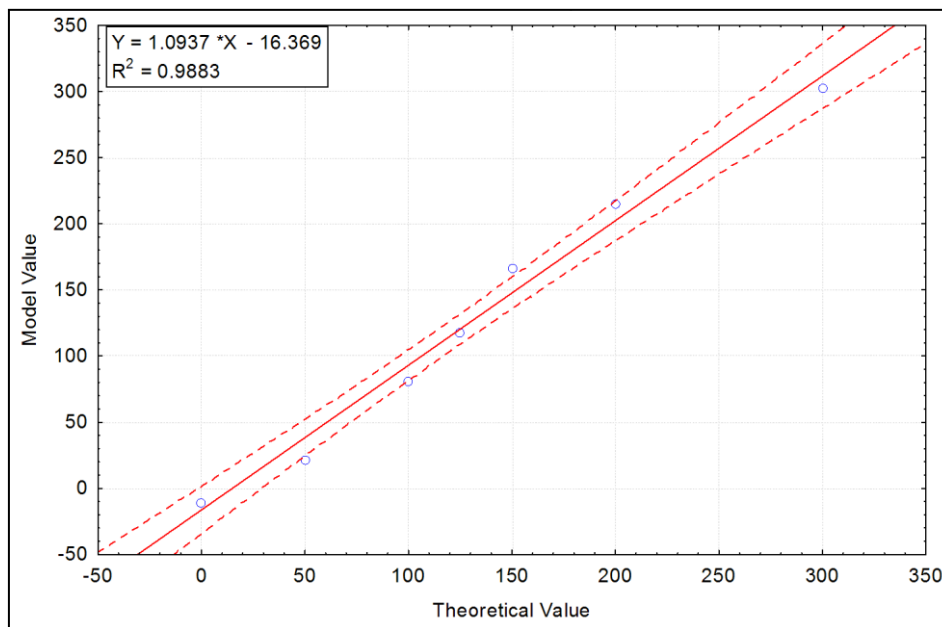


Figure 5.14: Graph for the prediction of Cu metal using ILS model

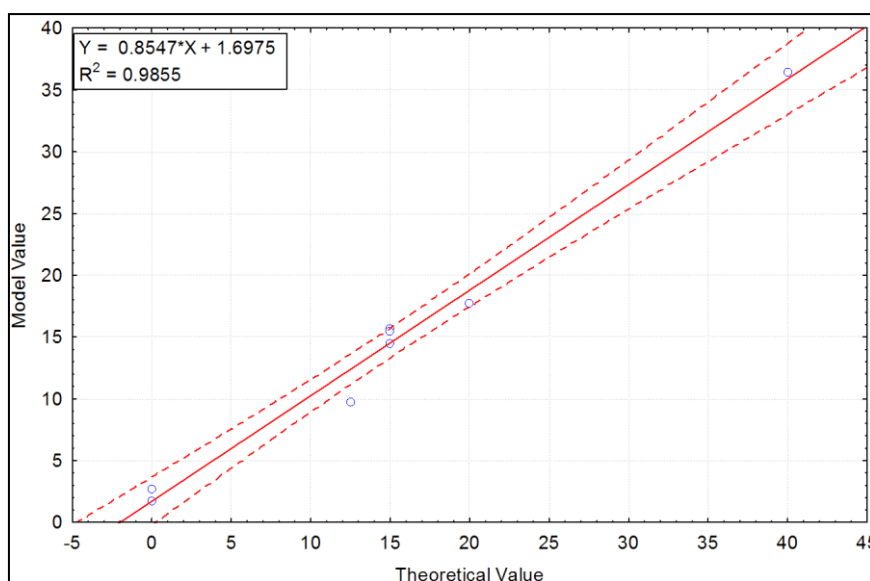


Figure 5.15: Graph for the prediction of Co metal using ILS model

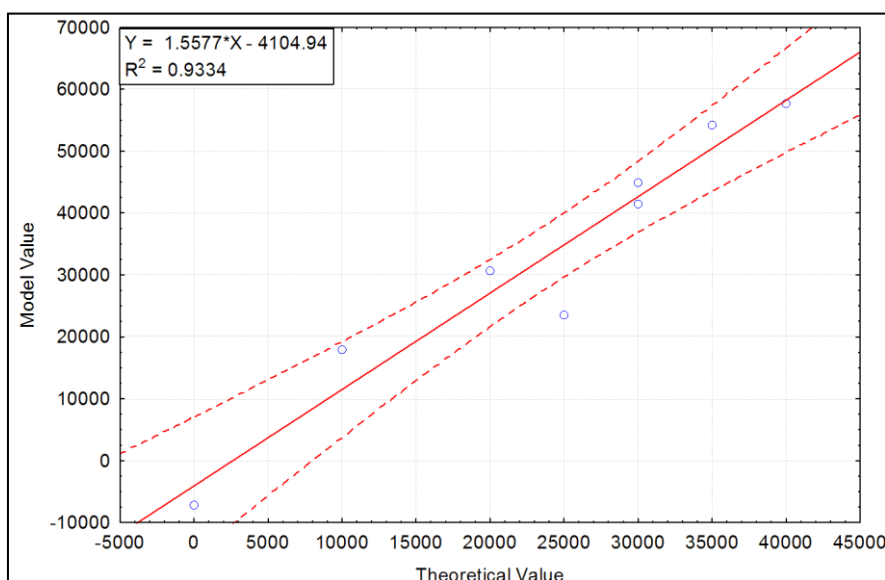


Figure 5.16: Graph for the prediction of Zn metal using ILS model

When analysing the scatter plots, there are two most important factors to take into consideration. Firstly, the width of the confidence interval limits and lastly the number of data points that falls outside the interval limits. Figures 5.14 and 5.15 have narrow width of confidence interval limit indicating that the error associated with the prediction of Cu and Co within 95 % confidence interval is statistically insignificant. The scatter plot of Zn has wider confidence interval limit as shown by Figure 5.16. If this figure has a similar interval like other metals, most of the data points will fall outside the 95% limit. This reflects that the regression line does not fit the data very accurately. However, the deviation of the data points could be considered to be statistically acceptable based on the fact that the ILS algorithm is a

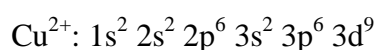
linear model. The prediction graphs of all the metals for the CLS model are given in Appendix B.2. The statistical results for evaluation of the ILS and CLS models are given in Table 5.6.

Table 5.6: Results from the prediction steps of ILS and CLS model

Metal	R ² Values		RMSE Values (%)	
	ILS model	CLS model	ILS model	CLS model
Copper	0.9883	0.9910	2.9057	2.2654
Cobalt	0.9855	0.9441	4.2743	11.315
Zinc	0.9334	0.8995	14.010	21.282

The performance of the CLS model for the prediction of the unknown samples is worse than results of the ILS model, as indicated by larger % RMSE values for all the metals in Table 5.6. The poor results of the CLS model could be explained by the fact that the K-matrix obtained from the calibration is inverted during the computation of the prediction step algorithm. Thus the mathematical solution of algorithm becomes unstable. Both the ILS and CLS models gave poor results for prediction of zinc as compared to the other metals. Once again, the worse prediction of Zn is attributed to its low absorbance in the mixture solutions that is caused by the colourless solution of pure Zn metal as was shown by Figure 5.5.

The poor results for the Zn metal could be explained in terms of transitions that exist within the metal. The transitions are caused mainly by the presence of electrons in the atoms and the ligands present in the solution. The distribution of electrons within the metal plays important role in absorption of a radiation light. The metal exists as the ions in the aqueous solution and all the transition metal ions in water solutions are complex ions. If no ligands appear to be present, the water molecules in solution will act as ligands by attaching to the metal ion, $[\text{Zn}(\text{H}_2\text{O})_6]^{2+}$. The ligands field causes the d-orbitals to split, as shown in figure 5.17. In octahedral geometry, the most common type of complex, two levels will be formed: t_{2g} and e_g. An electron can absorb a photon and transition from the lower energy t_{2g} level to the higher energy e_g level will take place. The electron configurations or distributions for the cations of the three metals are illustrated below.



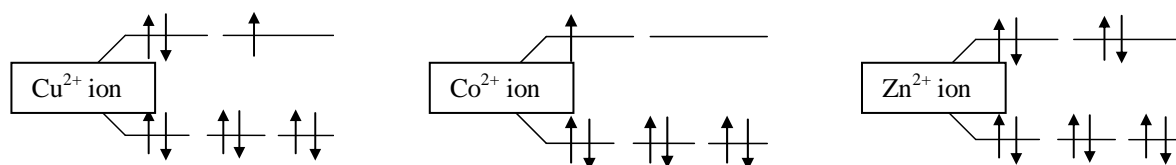
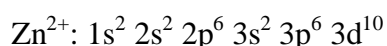
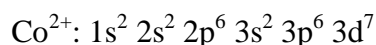


Figure 5.17: Electron Configuration of in the outer d-orbital of Cu, Co and Zn ions.

The ions from these metals use 3 d-orbital shells for the transitions process. The transitions that occur within each ion depend on the energy required of an electron to move from one orbital to another. The energy level diagrams shown in Figure 5.17 indicate the outer orbital shells of each metal involved during the transition process. The arrows represent the electrons that are filled in the orbitals according to a spin rule. Skoog *et al.*, (2008) indicated that the electrons are filled starting with low energy state level orbital sub-shells. Furthermore, the filling of electrons depends on the magnitude of crystal field splitting energy of the ligand.

From Figure 5.17, Cu and Co ions have unfilled orbitals to interact with the negative charge from the ligands present in the aqueous medium. There is possibility of a transfer of electrons within their 3 d-orbital of the ions. On the other hand, Zn has a fully filled 3d-orbital shell; hence it has different characteristics from both Cu and Co metals. With this regard, there is no transfer of electrons from and to the d-orbital shell of Zn ion. In this case, there are no d – d transitions that can occur, and thus no visible light is absorbed and the solution appears colourless. The behaviour of Zn ions make it to have a low intensity in the mixture which had resulted in poor prediction results by both the ILS and CLS models. The poor prediction of zinc could be enhanced by using the derivative forms of the absorbance spectra as will be explained in detail in a Section 5.4.

5.4 Derivative Spectroscopy

Derivative spectroscopy has been used in many applications of spectroscopy like in the near infrared spectra, ultraviolet-visible absorption spectra and flame emission spectra. The derivative methods had shown a number of advantages over the last decade in analytical spectroscopy. Firstly, they have been used for spectral discrimination whereby similar spectra of different constituents were easily identified. Secondly, they have been employed for resolution of spectra that overlapped with one another, so that their peaks could be determined by their wavelength (De Luca *et al*, 2009). Lastly, they have been used for elimination of insignificant background from the main spectra of interest (Demetriades-Shah *et al*, 1990). In their applications, derivative techniques are used more frequently for quantitative purposes than qualitative analysis.

5.4.1 Mathematical background

The spectral analyses using a derivative spectroscopy require the peaks of the analyte to be easily identified. There are number of techniques available for generating derivative spectroscopy and the two most common are electronic and mathematical techniques. The electronic techniques are easy to apply since most of the instruments come with a function that generates the derivative spectra. However, the derivative, in such case, is with respect to time not the wavelength hence they suffer in qualitative analysis. On the other hand mathematical technique had advantage that the derivative process can be easily monitored. The techniques are optimised by selecting only the portions of spectra to be used in the data analyses (Demetriades-Shah *et al*, 1990). In the present study, the first and high orders of mathematical derivative spectroscopy are utilised to enhance the maximum absorption peak of zinc. The enhancement will aid in improved prediction results of Zn metal.

The assumption which was made for zero-order absorbance spectra that they obey the Beer's law still holds for the derivative spectra. The assumption is mostly used when performing quantitative analysis of spectral data. The first and high order derivative spectra are given by equation 5.7 and 5.8 respectively. They are based on the linear relationship between concentration and absorbance of each sample. The superscript n in equation 5.8 indicates the nth order of derivative.

$$\frac{dA}{d\lambda} = \frac{d\varepsilon}{d\lambda} bc \quad (5.7)$$

$$\frac{d^n A}{d\lambda^n} = \frac{d^n \varepsilon}{d\lambda^n} bc \quad (5.8)$$

The mathematical techniques had been applied to a number of situations to study the behaviour of components of the mixture. Abbaspour and Mirzajani, (2005) used zero and first derivative spectral data to develop the PCR and PLS models to study the ternary mixtures of the synthetic pharmaceutical products. From their results, they found that first order derivative has no effect on the prediction ability of PCR models. However, PLS model when combined with first order derivative give better results when compared to other models. There was also a good agreement found when the model was applied to real samples.

In another case study, De Luca *et al*, (2009) mentioned that third order derivative spectroscopy had improved the prediction ability of low content component in a mixture. They used PCR and PLS models to analyse spectral data for zero to fourth order derivative spectroscopy. The simulated samples of ternary mixture were used for the calibration purposes. The combination of simplex centroid mixture design and third order derivative spectroscopy was established to resolve the overlapping peaks of the components of a mixture. Hence, the quantification analysis of each component was relatively easy to perform. The performance of both models was increased by using a wavelength selection procedure that extracted the useful information for model formulation (De Luca *et al*, 2009).

In this present study, the mathematical derivative spectra were computed as follows; first derivative spectroscopy was calculated by taking the difference of two successive absorbance values throughout the wavelength of the spectrum region. Then the high order derivative spectra were calculated by applying the computation of the first derivative in the successive steps until to the fourth order. The computation for the first order spectra was done in MATLAB software program using equation 5.9.

$$A_{Deri} = \frac{(A_{\lambda+\Delta\lambda} - A_{\lambda})}{\Delta\lambda} \quad (5.9)$$

where A_{deri} is the calculated derivative absorbance and $\Delta\lambda$ is the difference between two successive wavelengths.

The major problem associated with the computation of the derivative spectroscopy is that the derived spectra have a lot of noise. Thus, the signal-to-noise ratio decreases with increasing order of the derivative. Cirovic, (1998) showed that the presence of noise in both calibration and test data affect the performance of the model being developed. The noise in this study was reduced by using a Savitzky-Golay smoothing filter from signal processing toolbox in MATLAB software program. The filter uses a third order polynomial function to fit the smoothed data.

Another challenge encountered in the derivative spectroscopy is the selection of wavelength region to be used to develop the model. A manual selection method explained and used for the zero order spectroscopy in Section 5.1.3 was also employed. However, in this case, the selection procedure becomes tedious since the derivative spectra have both positive and negative peaks. Furthermore, the number of peaks increases with order of derivative spectroscopy. It was noted that as the order of derivative spectroscopy increases, the selection procedure becomes very time consuming and sometimes impossible.

5.4.2 Data Manipulation

The algorithms of all the orders of derivative spectroscopy together with the algorithm of the smoothing filter were incorporated in the ILS model. During the computation of each derivative spectrum, both the first and last data measurements are lost. The order of polynomial function used for smoothing the noisy data was optimised and third order filter was selected. The selection of filter was based on the order that does not distort the shape of the derivative spectra but the order that give a good approximation of the derivative spectra. The wavelength regions selected for each order of derivative are given in Table 5.7. A few numbers of wavelengths were selected for the high order of derivative. The results of derivative spectra are given in Figure 5.18 that follows.

Table 5.7: Selection of wavelength region from derivate spectra for ILS model

Derivative order	Wavelength region (nm)		
	Copper	Cobalt	Zinc
First	685 – 687	457 – 459	455
Second	640 – 642	559 – 561	457 -459
Third	597 – 599	531	426 – 429
Fourth	729	501	429 – 431

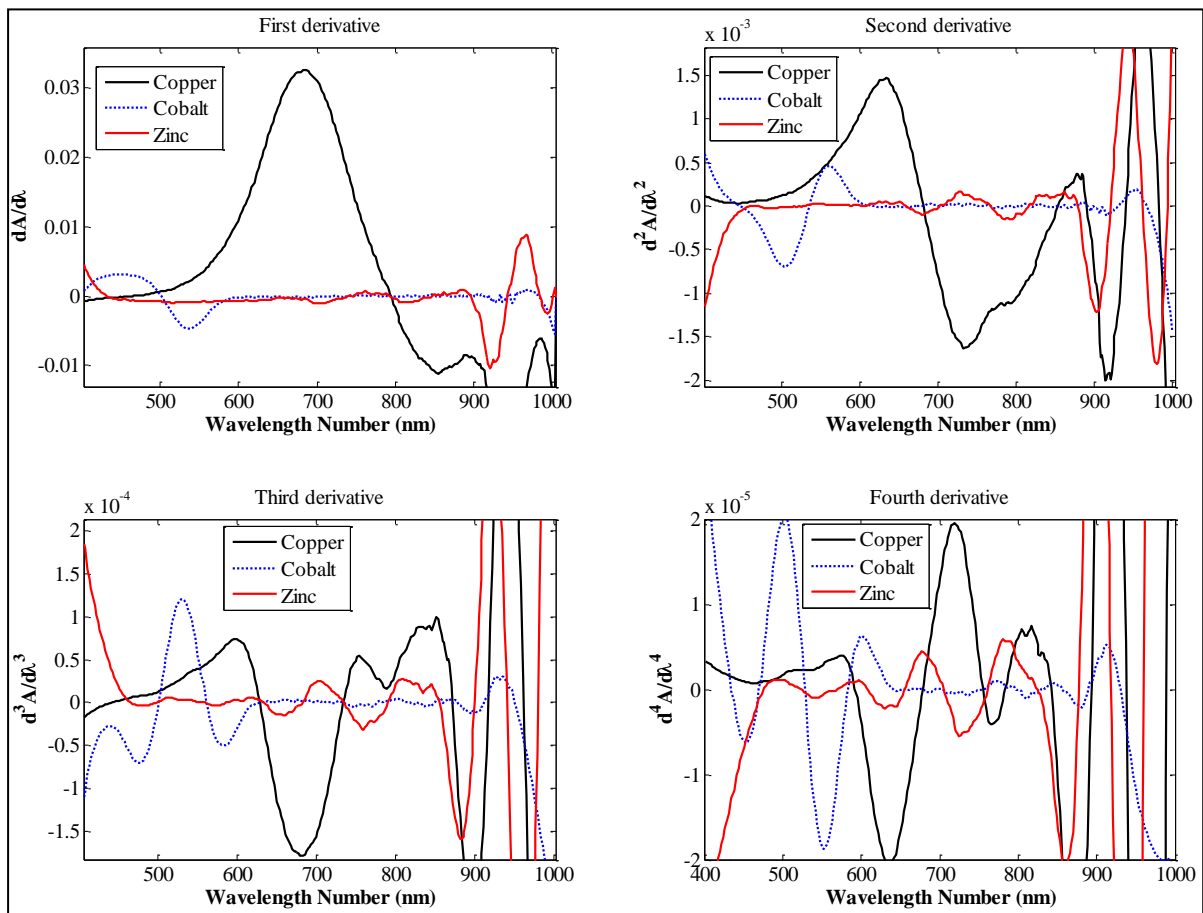


Figure 5.18: First, second, third and fourth derivative spectroscopy of Cu, Co and Zn metals

From Figure 5.18, the number of maximum absorption peaks for each metal increases with the order of derivative spectroscopy and there are also negative peaks observed for each spectrum. A high number of oscillations in each spectrum occur at the higher wavelengths. These features of the spectra had resulted in difficulties for selecting the region to be used during the modelling purposes. Due to the closely positive maximum peaks in the third and

fourth order derivative spectroscopy, only one wavelength, as shown in Table 5.7, was selected for the calibration step of the ILS model.

5.4.3 Optimisation of the Model

After a careful manual selection of the wavelength region for each metal, the algorithm for each order of derivative was developed and computed using a MATLAB software program as previously discussed. The quality of the derivative spectroscopy models was evaluated based on both R^2 and % RMSE values. Figure 5.19 shows the results for R^2 values of all the metals for different orders of derivative. When using all the orders of the derivative spectroscopy, the prediction values for Zn metal are lower as compared to a normal or zero order absorbance spectroscopy.

The maximum absorption peak of Zn from zero absorbance spectroscopy given by Figure 5.6 is not as sharp as compared to other metals. Hence taking a derivative of a Zn spectrum, the peak becomes almost flat as shown in Figure 5.18 and consequently there is no clearly observed peak in the derivative form of absorbance. Thus the prediction results of Zn become very poor as reflected by the lower R^2 values in Figure 5.19. On the other hand, there is positive effect on the prediction results for Cu and Co metals when derivative spectroscopy is applied. The maximum peaks of both Cu and Co are easily identified as shown by Figure 5.18.

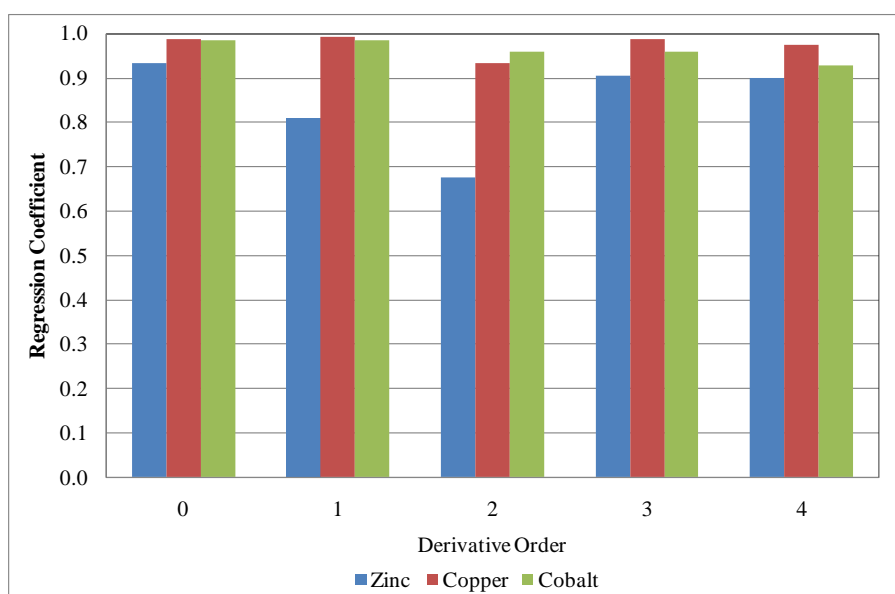


Figure 5.19: Evaluation performance of derivative spectroscopy

The % RMSE values for the metals, as shown by Figure C.1 in the appendix section, increase with the order of derivative spectroscopy. This indicates that the error of prediction is large with higher orders. The increased number of the maximum peaks had resulted inappropriate selection of the wavelengths. Among the orders of derivative spectroscopy used in the study, only the third order gave the better results close to that of a zero absorbance spectroscopy. In conclusion, the results show that all the orders of the derivative spectroscopy gave worse prediction values as compared to the zero absorbance spectroscopy. Thus in this study, the derivative spectroscopy cannot be used to enhance the prediction results of Zn metal as it was suggested earlier in the section.

5.5 Robustness of the Model

The developed model was further tested for its ability to determine the concentrations of the Cu, Co and Zn metals in the presence of interferences. The interferences on the prediction of the ILS model that were evaluated in this study are the temperature and nickel. The reasons stated below explain why each factor was evaluated:

1. *Temperature*: usually in the industrial applications, the temperature of the feed stream of the hydrometallurgical solution differs at each specific time with operating conditions of a plant. Hence, it was considered to determine within which temperature range the ILS model calibrated at room temperature can still produce a good performance in terms of the prediction ability.
2. *Nickel*: in most cases, an ore used in real plant condition comes with a lot of gangue and other valuable minerals. An ore used in most zinc mines is zinc sulphide which is associated with minerals like copper, nickel and cadmium in different proportions. The model was tested for the effect of nickel on absorption spectra of metals of interest.

5.5.1 Effect of Temperature

The solutions containing Cu, Co and Zn metals were set at different temperatures. The same ILS model calibrated with solutions at room temperature was used to predict the

concentrations of these solutions. The effect of temperature on the absorption spectra of the metals was tested using a zero absorbance spectroscopy. In addition, the relationship between the temperature and P matrix of the ILS model would be determined and discussed in Section 5.5.1.3.

5.5.1.1 Model Predictive ability

The results for the effect of temperature on prediction ability of the ILS model for copper, cobalt and zinc metals are shown in Figure 5.20, 5.21 and 5.22 respectively. The temperature values of the four samples were varied from a room temperature of 20 °C up to 80 °C in the increment of 20 °C as indicated in the figures. From Figure 5.20, it is observed that temperature has a minor effect on the predicted values for Cu metal with %RMSE value less than 10. Hence the precision of the ILS model was found to be fairly accurate for this particular metal.

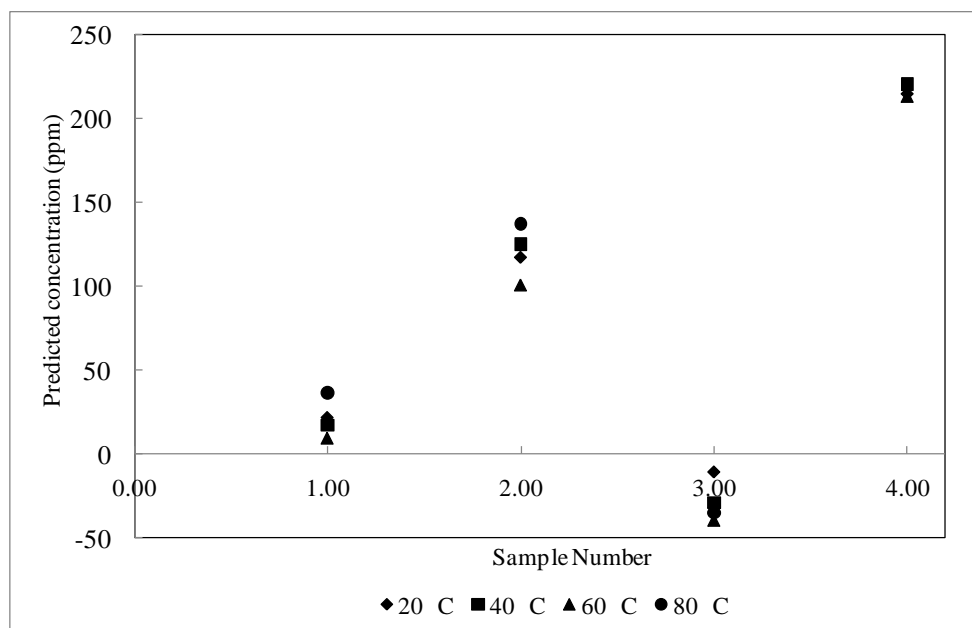


Figure 5.20: Prediction ability of ILS model for copper metal at various temperatures

Furthermore, the predicted values for Co and Zn metals were found to be affected by different temperature values that were used. The prediction results of Zn metal was affected most, as could be seen by a large dispersion of its measurements in Figure 5.22. Among the samples investigated under this study, sample 4 was found to be less affected by temperature

variation. Sample 4 was composed of 200 ppm of Cu, 0 ppm of Co and 30000 ppm of Zn and this sample has the highest amount of Cu among other samples.

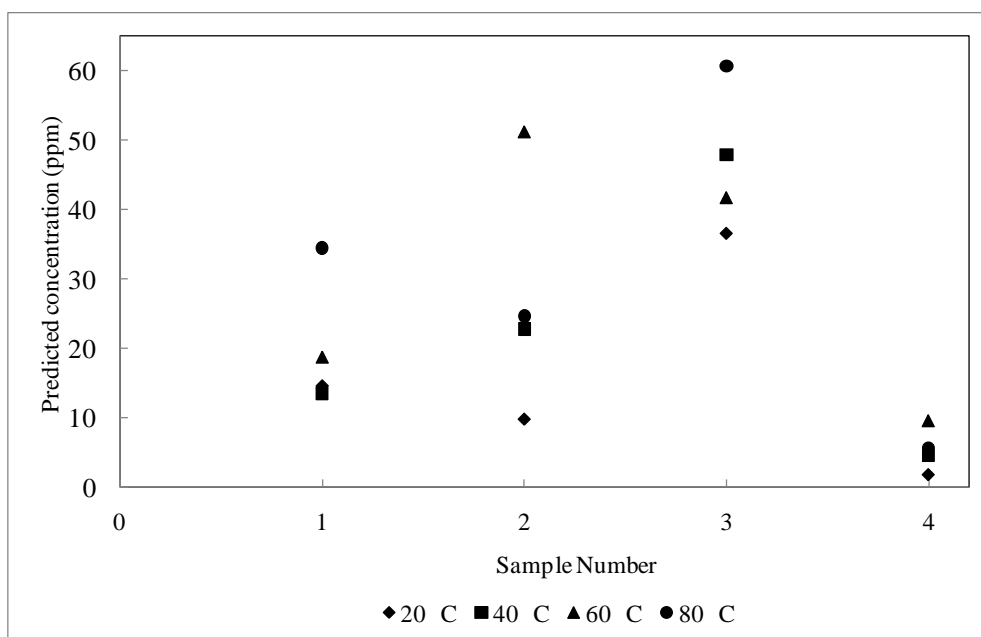


Figure 5.21: Prediction ability of ILS model for cobalt metal at various temperatures

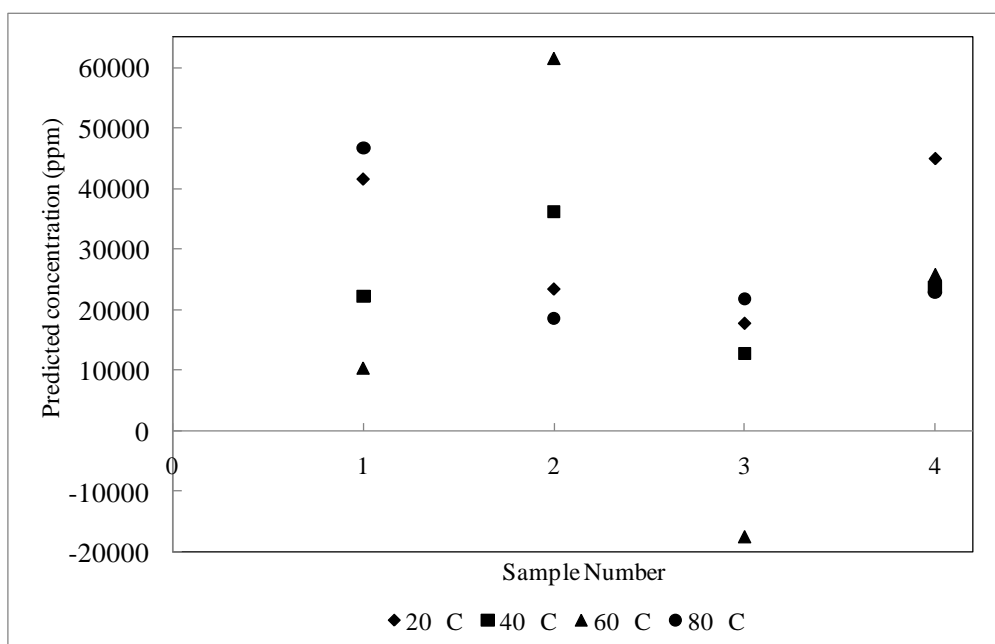


Figure 5.22: Prediction ability of ILS model for zinc metal at various temperatures

In order to determine whether there is a variation among the individual measurements within each sample for all metals, the percentage root mean squared error (% RMSE) values were

computed and their results were tabulated in Table 5.8. The guideline used was that the % RMSE values should be less than 10 % so that the prediction ability of the ILS model could be considered to be accurate. According to the % RMSE values from the same table, only sample 4 can be predicted fairly accurately by the model for all the metals. Cu metal shows better results with the entire % RMSE values less than 10%, thus indicating a little effect of temperature.

Moreover, there is no general trend that can be observed between the prediction ability of the model and individual metal in the mixture of the samples. The variation of the prediction results among samples could be explained by the fact that each sample has a different metal composition. Each metal has its own transitions which are affected differently by temperature. A detailed explanation of these transitions is given in Section 5.5.1.2.

Table 5.8: Precision of ILS model for Cu, Co and Zn at various temperatures

Metal	Sample 1	Sample 2	Sample 3	Sample 4
	% RMSE	% RMSE	% RMSE	% RMSE
Copper	6.1105	2.8093	6.1445	6.2921
Cobalt	19.8258	41.9959	22.5068	11.9807
Zinc	29.3844	38.7900	31.1521	18.2108

5.5.1.2 Influence on Spectra

The results presented in Figure 5.23 show the absorption spectra of the mixture of Cu, Co and Zn metals at different temperature values. The composition of the mixture was 50 ppm of Cu, 15 ppm of Co and 30000 ppm of Zn, given in Table 5.8 as sample 1. The results obtained were consistent and similar to those found by Kumagai *et al*, (2008) studying the effect of temperature on salts of lithium (Li) and magnesium (Mg). They observed that the increase in temperature shifted the Li and Mg spectra to higher absorbance values. In this study, also the intensities of the absorption spectra increase with temperature as clearly seen in the wavelength range of 700 – 1000 nm.

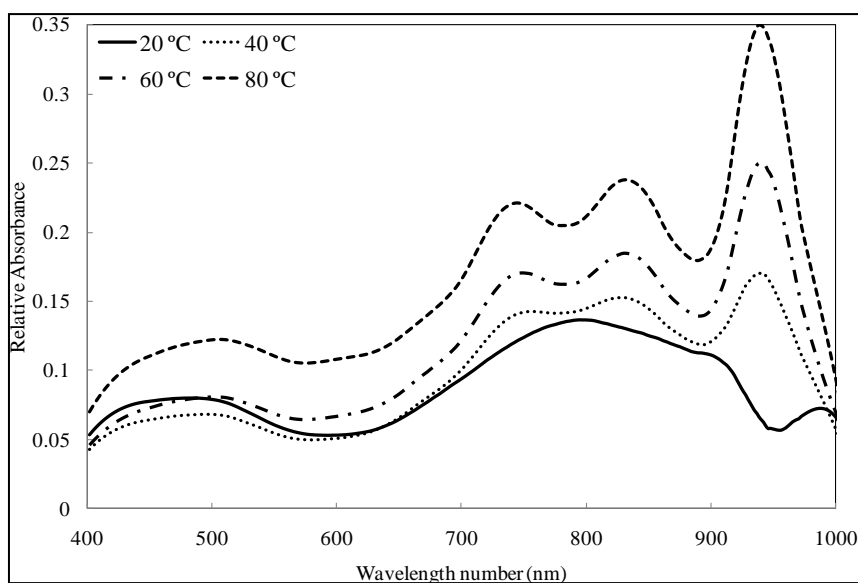


Figure 5.23: Influence of temperature on absorption spectra of the metals

However, for the wavelength range of 400 – 600 nm in Figure 5.23, the results for temperature 40 °C and 60 °C are lower than the result at room temperature (20 °C). This could maybe due to either the heat loss from the samples or the type of the metal in the mixture. The other three samples showed similar results to that of sample 1. In another samples analysed, it was further observed that when the temperature is increased, the maximum absorption peak of each metal shifted to the higher wavelengths. The shift could be attributed to the Jahn-Teller distortion effect experienced by the complex ions (Jones, 2001). This distortion destroys the symmetry of the complex and thus electronic energy levels are also affected.

From Figure 5.23, as the temperature increases, the region of the spectra due to Cu metal result in two maximum absorption peaks at around 800 nm. The two peaks are more pronounced with an increase in temperature. These peaks could be attributed to the presence of water molecules in the solutions. This observation maybe supported by the more intense peaks in Figure 5.23 which occurs at the wavelength of 950 nm. However, these three peaks could also be result of the reaction of copper metal when it is heated. By measuring the intensities of the absorption spectra of the solution in the absence of copper metal, it will be verified which substance is responsible for the peaks. The absorption spectra of the solution at different temperatures are given in Figure 5.24. The solution of a mixture was composed of 40 ppm of Co and 10000 ppm of Zn.

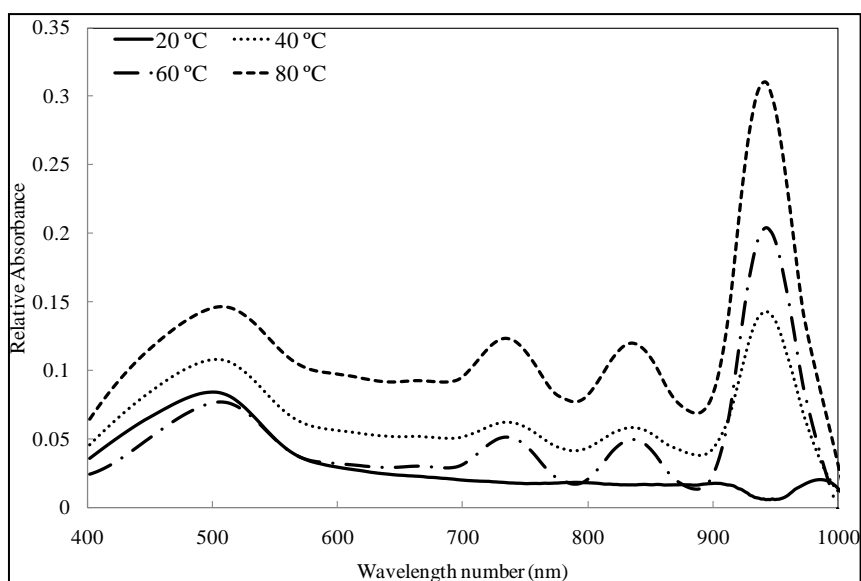


Figure 5.24: Effect of water on the absorption spectra of Co and Zn metals

The peaks in the wavelength region between 700 and 1000 nm, from Figure 5.24 are similar to the peaks seen in Figure 5.23. The absence of Cu peaks at room temperature from Figure 5.24 clearly shows that the peaks observed at higher temperature are due to water molecules not to the copper metal. At higher temperatures, water changes its state from liquid to vapour and water vapour shows several maximum absorbance peaks in the near infrared (NIR) region. In most cases, the relative absorbance values are due to vibrational transitions of the water molecule. Vibrational transitions are caused by the energy change that occurs between the bonds that hold the molecule together (Skoog *et al*, 2008). The wavelength region from 700 – 1000 nm is the NIR region and the vibrational transitions become more pronounced in this region as illustrated by the highest peaks at around 950 nm. Water vapour exhibit higher peaks than the metal of interest in this study because its absorbance values are contributed by both electronic (absorption) and vibrational transitions.

Cu, Co and Zn metals exhibit mainly electronic (absorption) transitions when their solutions are measured at the higher temperatures. The influence of temperature on absorption spectra of the metals could be explained in terms of electronic transitions using the phenomena of collision theory and electronic transitions. The collision theory states that when the temperature of the solution is increased, the rate of collision of the molecules within the solution also increases. In this study, as the temperature is increased, the rate at which the radiation source from the sensor interacts with the ions is also increased. Then, the assumption would be that the electrons within the ions will have more excitation energy to

move to higher energy levels as shown in Figure 5.25. Hence the intensities of the absorption spectra will shift to higher values.

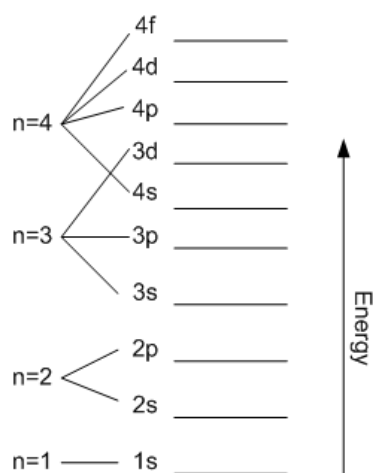


Figure 5.25: Energy levels for orbitals of an atom

5.5.2 Effect of Contaminants

The presence of interferences in the solution to be analysed affect the absorption spectra of the metal of interest. Haavisto and Kaartinen, (2009) studied the maximum absorption spectra of the zinc solutions from different stages of flotation. They showed that the spectra of the dilute and impure solutions occur at a lower wavelength as compared to that of pure concentrated solutions. In this study, the effect of nickel (Ni) on spectra of Cu, Co and Zn metal was examined on four samples.

5.5.2.1 Model Predictive ability

The prediction values of the Cu, Co and Zn metals in the presence of Ni are given by Figure 5.26, 5.27 and 5.29 respectively. The nickel solution was used for the experiments in the increment of 50 ppm from 0 ppm to 200 ppm as indicated in the figures. The zero order absorbance spectra were used to evaluate the effect of nickel to the solutions. The prediction ability of ILS model for Cu and Co metals decreases with increasing concentration of nickel as reflected by Figure 5.26 and 5.27 respectively. The lower predicted values for Cu and Co metals could be due to the strong interactions exhibited by absorption spectra of Ni over these

two metals. This is evident from Figure 5.28 and the detailed explanation of the interactions followed from the same figure.

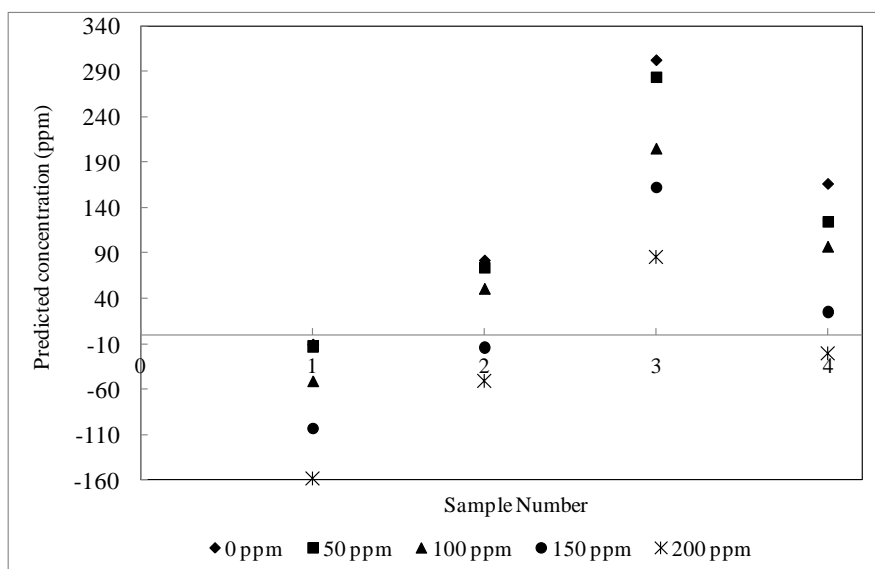


Figure 5.26: Prediction ability of ILS model for copper metal in presence of nickel

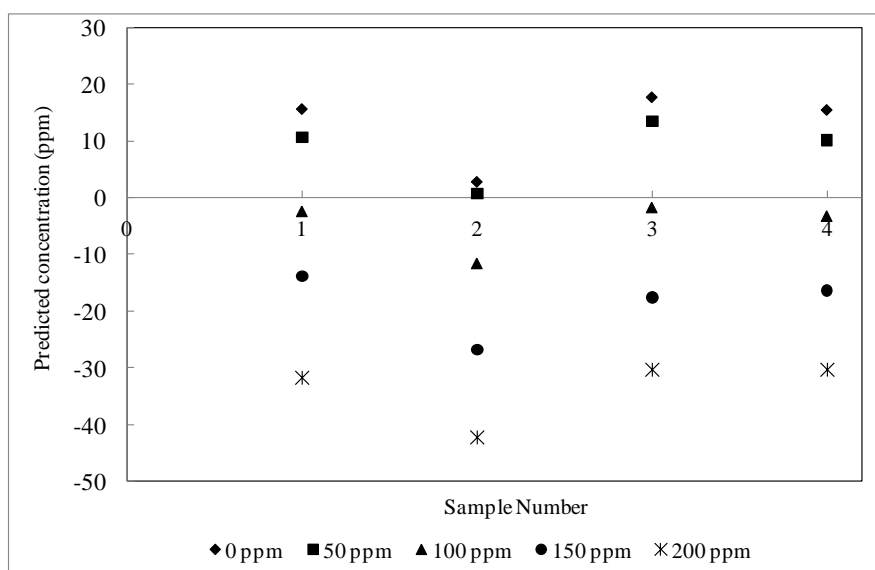


Figure 5.27: Prediction ability of ILS model for cobalt metal in presence of nickel

Figure 5.28 illustrated the absorption spectra of a solution of Cu, Co and Zn metals in the presence of nickel. The solution was composed of 300 ppm of Cu and 20 ppm of Co. The presence of Ni in the solution shifts the maximum absorption spectra of Cu to lower absorbance values. In the wavelength range of 400 – 750 nm, the absorption spectra of the solution increase with the increase in the concentration of nickel until it reaches the inflection point around 750 nm as shown in the figure. After the inflection point the absorption spectra

decrease with the increase in the concentration of nickel. The region after the inflection point is where the maximum absorption peak of Cu occurs.

From Figure 5.28, it can be observed that nickel has negative effect on the predicted values of Cu as previously shown in Figure 5.23. The Co metal has the maximum absorption peak occur at 520 nm. The spectra around that wavelength cannot be effectively distinguished from one another. Thus, the only assumption that could be made for the poor results of Co is that the presence of nickel in that region suppressed the maximum absorption peak of the Co metal. Furthermore, the suppression could be thought to be more distinct with an increase in concentration of Ni.

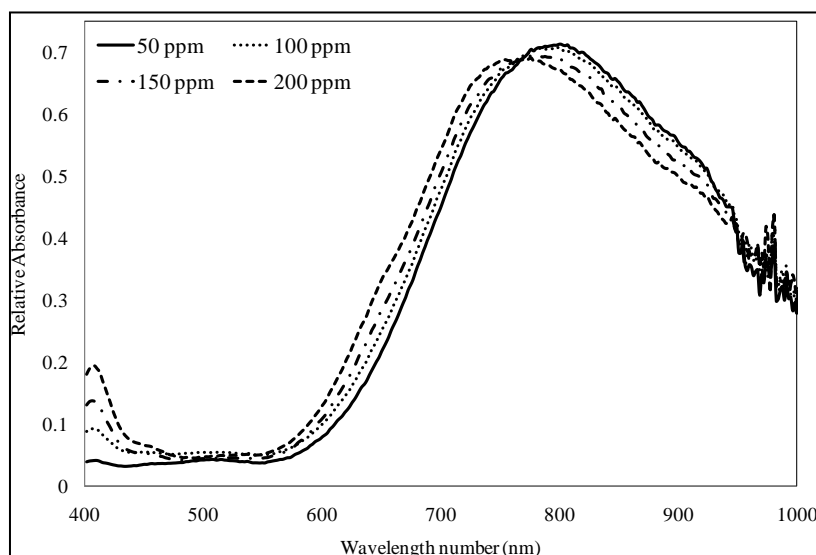


Figure 5.28: Absorption spectra of solution of Cu and Co in the presence of nickel

The prediction values for the Zn metal computed by the ILS model are given in Figure 5.29 for all the four samples analysed. The results for Zn metal showed no defined relationship between the concentration of nickel and the predicted values of the model. Sample 2, 3 and 4 showed that increase in concentration of Ni increases the prediction values for Zn metal while sample 1 showed conflicting results. From these arguments, the conclusion was that the concentration of Ni increases the predicted values for Zn metal. This conclusion was also supported by the absorption peak at around 410 nm in Figure 5.28. The peak is due to the presence Ni metal in the solution.

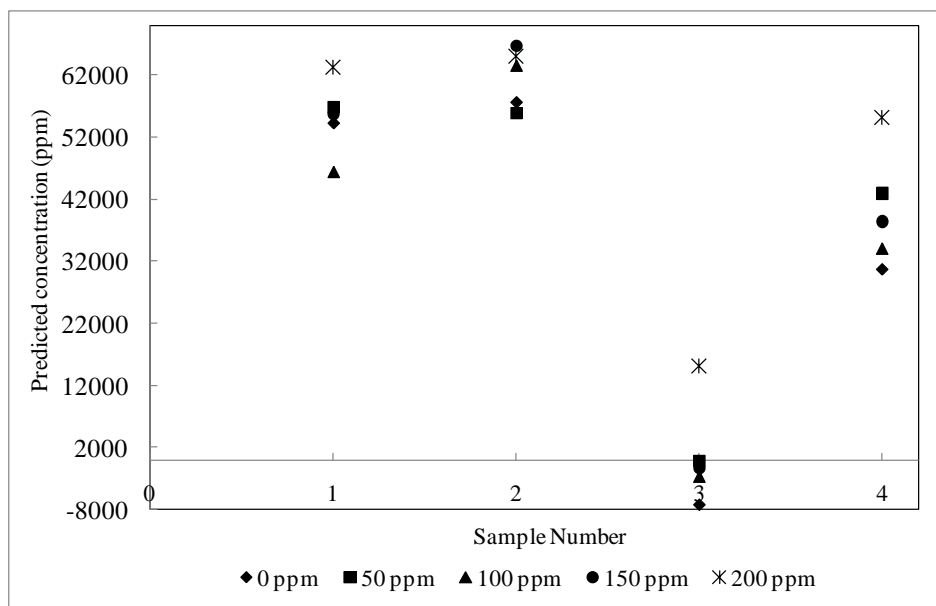


Figure 5.29: Prediction ability of ILS model for zinc metal in presence of nickel

5.5.2.2 Influence on Spectra

The previous section had determined the effect of Ni based on the predicted values of the ILS model. In this case, the effect of nickel based on the absorption spectra of Cu, Co and Zn metals was examined. The spectra of the pure Cu, Co, Zn and Ni solutions were plotted together and given by Figure 5.30. Ni metal is characterised by two maximum absorption peaks, the sharp and broad peaks, which occur around 410 nm and 720 nm, respectively. Skoog *et al.*, (2008) also reported two absorption peaks for aqueous solution of nickel metal at both 400 nm and 700 nm. They further stated that the position of the peaks depends on the oxidation state of Ni and a ligand bonded to it.

The positions of the two peaks of Ni are very close to maximum absorption peaks of Cu and Zn metals; hence a poor quantitative analysis of these metals is expected to occur in the presence of Ni. The maximum absorption peak of Zn is fully masked by the peak of Ni at wavelength of 400 nm as shown by Figure 5.30. The resolution technique or procedure must be applied for quantitative analysis of Zn in the presence of Ni.

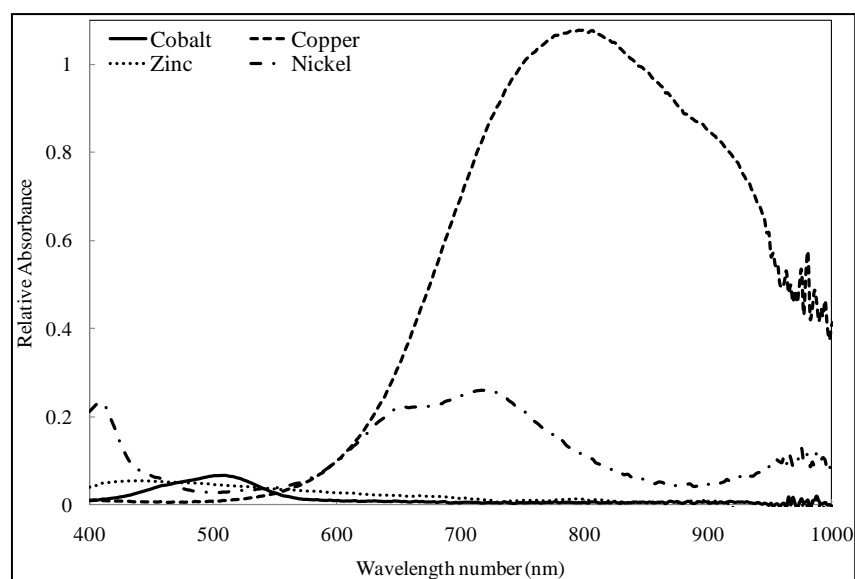


Figure 5.30: Absorption spectra of pure Cu, Co, Zn and Ni metals

In general, the presence of Ni in the solutions decreases the absorbance values of the Cu and Co metals whereas it increases the absorbance values of the Zn metal. The effect of Ni on these metals is explained clearly by using Beer's law which states that absorbance of a metal is directly proportional to its concentration. In this case, it would be expected that an effect of Ni should be linear with the addition of its volume. Figure 5.31 further proved that the nickel obeys the Beer's law since the relative absorbance values at both maximum peaks increase with concentration of Ni solution. The peak at 720 nm becomes very identifiable with the increase in concentration.

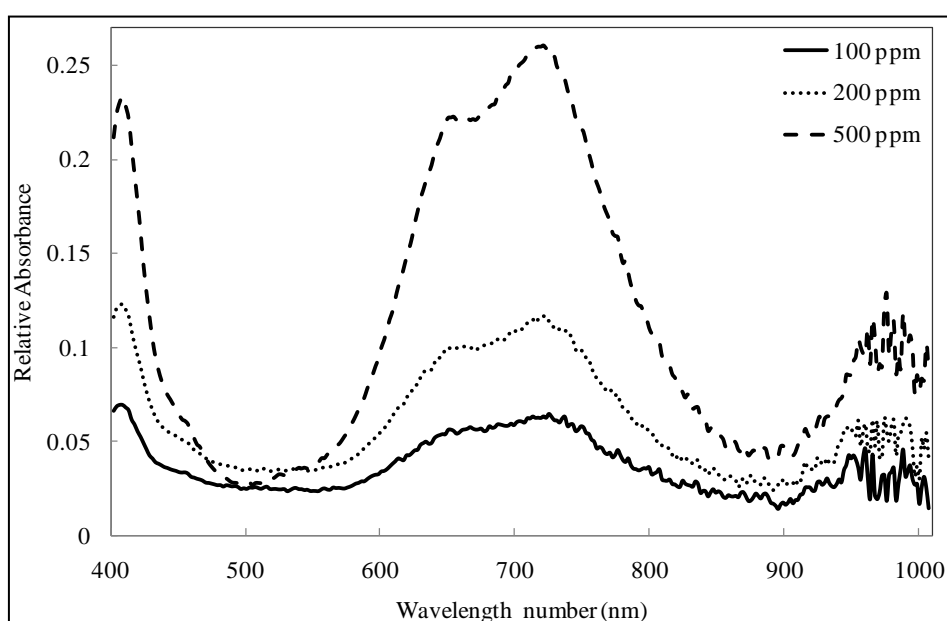


Figure 5.31: Absorption spectra of nickel in increasing concentration

In summary, the developed models were found to give poor results in the presences of disturbance during the measurements of absorption spectra of the Cu, Co and Zn metals. The model calibrated at room temperature cannot handle effectively the solutions with higher temperatures. The presence of Ni as the interference in the solutions makes the model to be unstable. Since Ni was not included in the calibration step of the model, the model gave the poor predictions for the Cu, Co and Zn metals. Zachariassen *et al*, (2005) performed a PLS model based on NIR spectra and they found that the temperature was not modelled accurately in the calibration part of the model. They compensate the effect of the temperature by including a third PLS component in the calibration step. Finally, this study had also proved that calibration part of the model must be updated when a new disturbances is encountered.

5.6 Potential Applicability of the developed Models

In order to evaluate the potential applicability of the developed statistical models, the ILS and CLS models, their prediction ability results were compared with a Blue Cube model and PLS model. The Blue Cube Company had already installed its instrument at Skorpion zinc mine and the instrument uses a statistical model to quantify the aqueous solution of the metals. It was worthwhile to perform a comparison with already existing and implemented model in the industrial plant. All the statistical models were further compared to an analytical technique, atomic absorption spectroscopy, as discussed in Section 5.6.2.

5.6.1 Blue Cube Model

The similarity between the developed models and Blue Cube model was based on the prediction ability of each model when the experimental analyses were performed with the test samples. The accuracy values of the models were calculated based on the theoretical values of the samples. A comparison was done in two ways; first by evaluating the behaviour of the models for prediction of the individual metal and lastly by using both t- and F-tests to determine if there is a statistical difference between all the models. Figure 5.32, 5.33 and 5.34 show the multiple line plots of all the runs for the test samples for the quantification of the Cu, Co and Zn metals respectively. The prediction abilities of the models for quantification of copper metal were found to be similar to one another as shown by Figure 5.32.

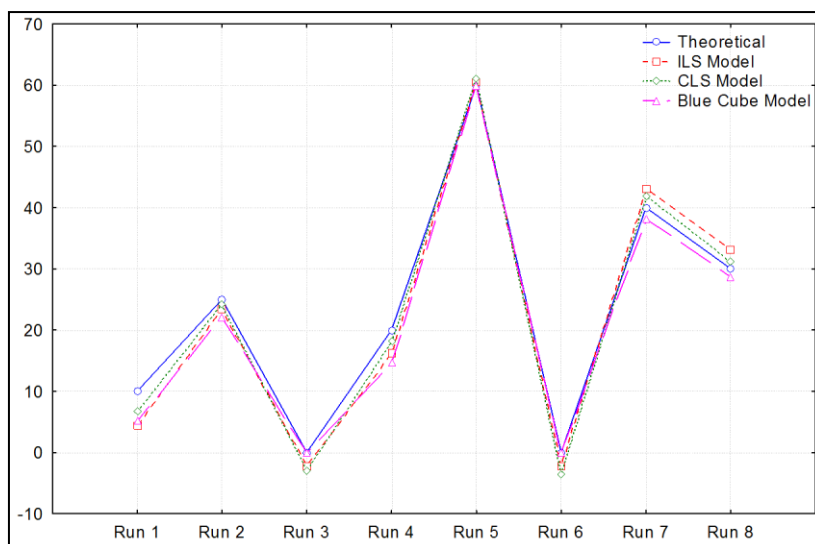


Figure 5.32: Comparison of developed models and Blue Cube for a Cu metal

The prediction abilities of the models for Co metal seemed to be lower than that of Cu and runs 2, 4 and 7 gave worse results compared to other runs as shown by Figure 5.33. These three runs were having a low content of Co in the solutions. For the case of the Zn metal, as illustrated by Figure 5.34, both the ILS and CLS models have almost similar accuracy values that were worse as compared to the results of Blue Cube model. For all the runs being performed, the accuracy of the Blue Cube model is similar throughout all the prediction results of the metals. This is because the Blue Cube model has prediction values like that of theoretical data set.

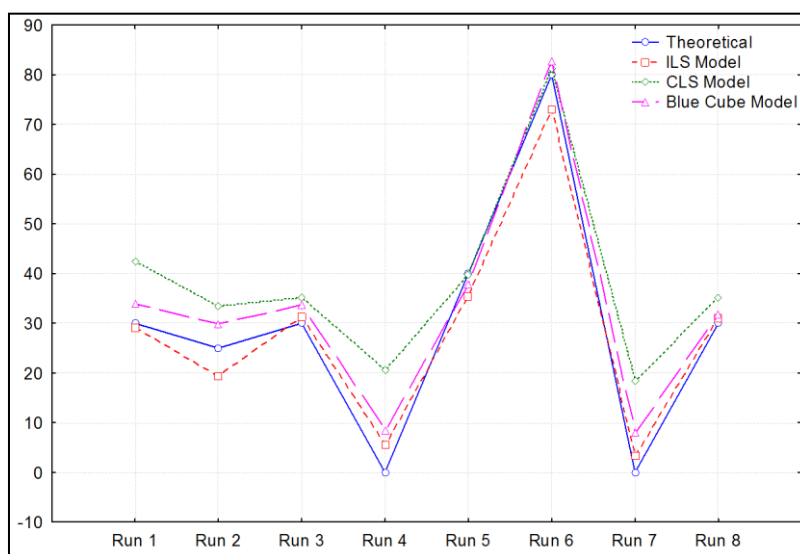


Figure 5.33: Comparison of developed models and Blue Cube for a Co metal

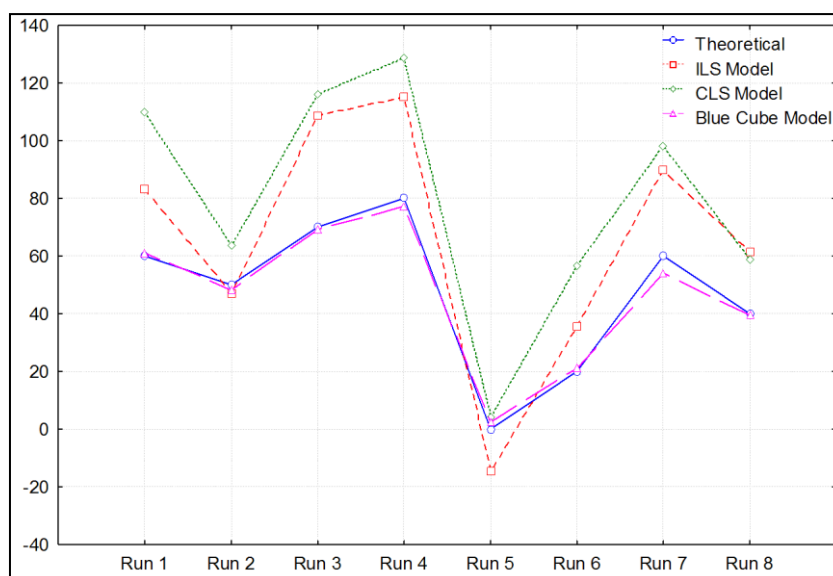


Figure 5.34: Comparison of developed models and Blue Cube for a Zn metal

The accuracy results of the ILS and CLS models differ from one metal to the other. Moreover, the accuracy among the metals decreases in the following: Cu > Co > Zn. The results for Zn metal, as shown by Figure 5.34, was questionable, hence the analysis of variance (ANOVA) test was performed to determine if there is any statistical difference among the models within 95 % confidence interval limit. The ANOVA results of Cu, Co and Zn metals are shown in the Table 5.9 and 5.10.

Table 5.9: Summary statistics for the comparison of the models

Groups	Copper		Cobalt		Zinc	
	Average	Variance	Average	Variance	Average	Variance
Actual	23.125	420.982	29.375	631.696	47.500	707.143
ILS model	22.018	509.568	28.502	468.257	65.780	1838.281
CLS model	22.075	504.548	38.313	373.393	79.439	1698.837
Blue Cube model	21.047	434.650	33.272	536.038	46.517	622.038

The summary of the statistics computed for all the models and the theoretical data is shown in Table 5.9. Both the ILS and CLS models show the larger average and variance values for Cu and Zn as compared to a theoretical data set. The developed methods (ILS and CLS) and the Blue Cube model show a similar variance for only Cu and Co metals. However, the ILS and CLS models gave much larger variance results for prediction of Zn metal. The variance value

explains the precision of the individual measurements in a particular set of data. The results that are presented here show that the Blue Cube model performs better than the developed models in this study. The extent of an improved performance of Blue Cube model can be evaluated by ANOVA test.

The main of purpose of the ANOVA was to test whether the Blue Cube model performs better than other models at 5% significance level. The null hypothesis tested by F-value is to determine whether there is any difference in the means of the models for the prediction of the metals. The calculated F-values for all the metals are smaller than the critical F-value as shown in Table 5.10. Moreover, the P-values for the metals are greater than the significance level (0.05) for all the models. The P-value indicates the probability of finding how close is the calculated F-value from zero. The high P-value for Cu shows that all the models have similar accuracy and precision for quantification analysis of this metal. On the basis of the F-value and P-values, it is clear that there is no significant difference among the means of the models. Thus the accuracy and precision results of all the models are similar within the 95% confidence interval limits.

Table 5.10: Results of ANOVA test for comparison of the models

Metal	F-value	P-value	F-crit*
Copper	0.0123	0.9980	2.9467
Cobalt	0.3188	0.8116	2.9467
Zinc	1.6422	0.2021	2.9467

*the critical F-value is calculated at 0.05 significance level.

In order to determine whether there are any differences among the individual means of the models, but specifically which pairs of means are significantly different, the multiple comparison tests were performed. The tests were computed using a multcompare function in MATLAB software program and the results were given by Table 5.11. This function overcomes the drawback of multiple t-tests by reducing the probability of making at least one incorrect conclusion among the pairs. The results in the table below show a 95% confidence interval for the difference of the means within each pair. All the intervals contain 0, so it was concluded that there is insignificant difference among the theoretical data, ILS, CLS and Blue

Cube models. The accuracy of all the models is found to be satisfactory as compared to the theoretical data.

Table 5.11: Multiple comparisons of pair of the models and theoretical data

Group [#]	Copper		Cobalt		Zinc	
	Lower 95% C.I	Upper 95% C.I	Lower 95% C.I	Upper 95% C.I	Lower 95% C.I	Upper 95% C.I
1 2	-28.4084	30.6217	-29.7240	31.4707	-65.8962	29.3354
1 3	-28.4655	30.5647	-39.5350	21.6597	-79.5550	15.6765
1 4	-27.4369	31.5932	-34.4944	26.7003	-46.6330	48.5985
2 3	-29.5721	29.4580	-40.4083	20.7863	-61.2747	33.9569
2 4	-28.5436	30.4865	-35.3677	25.8270	-28.3527	66.8789
3 4	-28.4865	30.5436	-25.5567	35.6380	-14.6938	80.5378

[#] 1 = Theoretical, 2 = ILS Model, 3= CLS Model, 4 = Blue Cube Model

5.6.2 Partial Least Squares Model

The developed models in this study were further compared to partial least squares (PLS) model. The PLS models had quite a number of applications in industries like food processing, pharmaceutical and mineral processing. These models are suitable for large processes with hundreds to thousands of controllable variables. In addition, the PLS models can analyse large data with noisy, collinear and incomplete variable (Wold *et al*, 2001).

5.6.2.1 Background of the PLS Model

Cirovic, (1998) evaluated the effect of a mixture design on the prediction ability of the PLS model. Simulated samples were used for both the calibration and prediction steps of the model. The solutions were prepared from the Plackett-Burman design and different concentration levels were evaluated. The PLS model was validated using a new validation sets. The results obtained from the study revealed that a large number of constituents in the mixture gave poor prediction for the model. Simulations with added noise affect the

performance of the PLS model; however the effect of noise was negligible with less number of constituents in the mixture.

In the study for minerals fingerprinting, Alvey *et al*, (2010) used a laser-induced breakdown spectroscopy (LIBS) together with PLS model for real-time geochemical analysis of the garnet ore. The main objective of their study was to classify the samples based on the composition and origin of the ore. They utilised PLS discriminant analysis (PLSDA) technique to analyse the LIBS spectra of the samples. The wavelengths of main elements and impurities were used for compositional and locational classification, respectively. The best latent variables of the PLSDA technique were estimated by cross-validation method. Alvey *et al*, (2010) determined that about 94.7 % and 55.0 % of the tested samples were classified correctly based on composition and origin, respectively. The low percentage for origin classification was related to few number of samples used in the training algorithm of the PLSDA model. Their study had proved that a combination of statistical signal processing and chemometric techniques can be used for rapid real-time analysis and discrimination of minerals.

In the quantification study of serpentite in nickel laterite ore, Basile *et al*, (2010) used PLS model for prediction of the unknown samples. PCA was employed for classification of synthetic mixtures used for calibration purpose. The mixtures were prepared in relation to the composition of natural ore using the experimental design. The IR spectra data was used for model development and validation. It was further determined that PLS model have high accuracy with R^2 and % RMSE values of 0.97 and 1.97, respectively. Basile *et al*, (2010) showed that the model gave poor results for prediction of natural ores because of a different composition of the natural ore.

Haavisto *et al*, (2008) employed the PLS model to control and monitor the copper flotation plant. The measurements were based on the VNIR spectra of Cu, Fe and Zn. The percentage of each element was kept within its acceptable limit, thus the plant stability was improved. The PLS model gave inaccurate results when the plant conditions were altered. In an attempt to correct that situation Haavisto *et al*, (2008) used a recursive PLS model and it showed improved prediction as compared to non-updated PLS model.

Before a detail data interpretation with the PLS model can be carried out, a brief mathematical background on PLS algorithms is given here. In the calibration step of the PLS model, both the absorbance (**A**) and concentration (**C**) matrices are decomposed into latent variables using equation 5.9 and 5.10, respectively. In both equations **T** and **U** are the scores of the matrices **A** and **C** respectively, whereas **P** and **Q** are the loading matrices of the latent variables. The residual matrices for the absorbance and concentration are given by **E** and **F**.

$$\mathbf{A} = \mathbf{TP}^T + \mathbf{E} \quad (5.9)$$

$$\mathbf{C} = \mathbf{UQ}^T + \mathbf{F} \quad (5.10)$$

The vector scores of both the absorbance and concentration are computed to result into the weight matrices. The **A** and **C** weight matrices are used together to determine the regression coefficient (**B**). The calibration algorithm explains most variation in both **A** and **C** matrix and maximise the linear relation between the two matrices. For the detail calculations the reader is referred to Wold *et al*, (2001). The main purpose of the calibration step of PLS model is to determine the regression coefficient (**B**) that is used in the prediction part of the model as shown in equation 5.11 whereby the subscript *u* indicate unknown or test sample.

$$\mathbf{C}_u = \mathbf{A}_u \times \mathbf{B} \quad (5.11)$$

5.6.2.2 Data Interpretation with PLS model

The PLS model used to analyse the data in this study was generated from Latentix software version 2.00. The software program comes with formulated algorithms for both the calibration and prediction steps of the model. The procedures that are used for obtaining the results for the PLS model are presented in the section that follows. The calibration and test raw data in ILS and CLS models were also used in this model. The model used was PLS1 but it will be referred as PLS through the discussion. All the wavelengths for the spectra were selected for model development and evaluation.

5.6.2.2.1 Model Development

Before the model can be formulated, the raw data was auto scaled, that is, it was first mean-centred and then scaled. These preprocessing steps make all the metals to have similar contribution in the prediction ability of the model. The score and residual plots were used to determine the outliers in the data. The seventh sample, as shown in Figure E.1 in the appendix, was found to have both large residual and hotelling (T^2) values. It was supposed to be discarded from the calibration samples for further analysis, but it was not. The deviation of this sample is attributed to that the sample has 100 % copper and Cu has most intense of all metals which result in higher absorbance values.

The score plot of the samples is shown in Figure 5.35. It can be observed that most information about the concentration is explained in the first principal component which accounts about 80 %. The contribution of two principal components is 90 %. This high percentage shows that there are similar features among the sample, thus the samples can be used for calibration step of the PLS model.

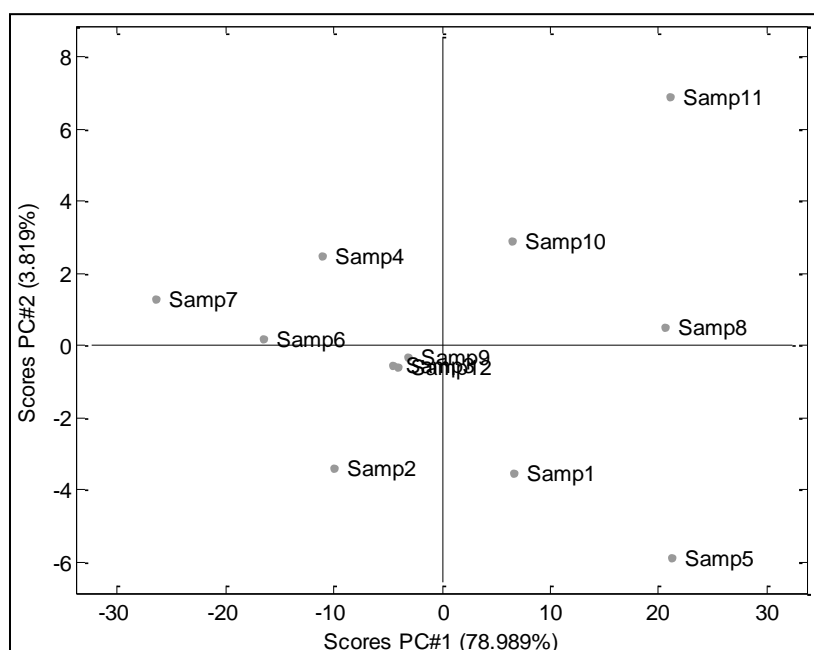


Figure 5.35: Score plot for detection of the outliers

Figure 5.36 shows a graph of explained variance in the concentration data of the metals as a function of PLS component. Copper could be explained effectively by the model because after the first PLS component about 90 % is achieved whereas other metal retain that

percentage when using third PLS component. In overall, the variance in each metal could be explained accurately by fourth PLS component. This observation from Figure 5.36 shows that calibration samples can be used to predict the concentration of the unknown samples. The results from the graphs, as shown by Figures E.2, E.3 and E.4 in the appendix, indicate a high degree of correlation between the actual and predicted values. The R^2 values are greater than 0.990 for all the metals.

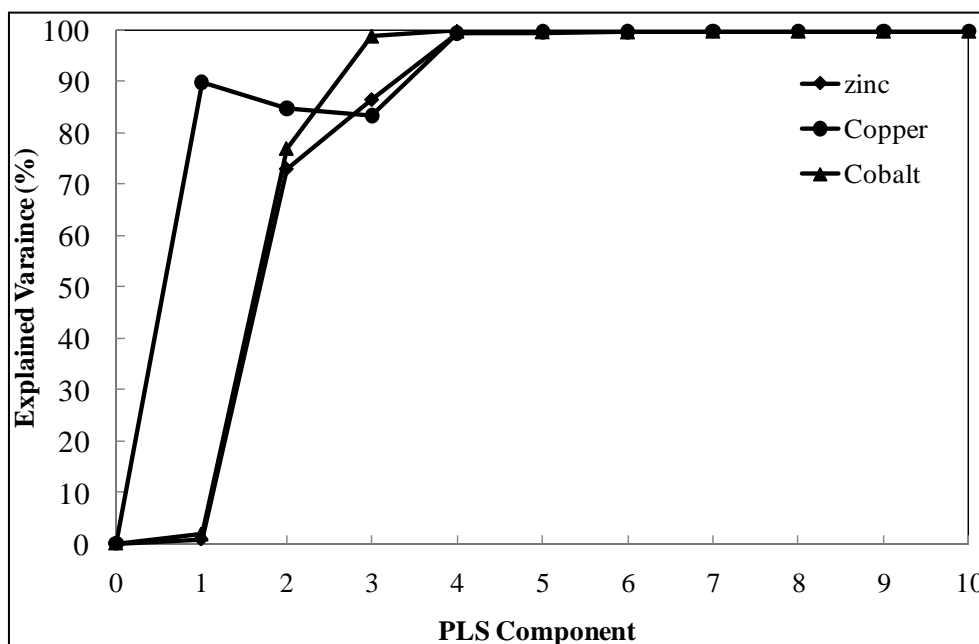


Figure 5.36: The explained variance in the calibration data

5.6.2.2.2 Model Validation

In most cases, the model needs to be validated before it can be used for prediction of the unknown samples. The best validation procedure is to use another sub-set of data to test the formulated model. In this study, the model validation was done using a full cross-validation (CV) procedure because of the absence of real validation set. The leave-one-out sample approach was employed in the validation procedure because of the small number of calibration data. Another advantage of the CV is to determine the number of components for the best PLS model. The component which gives a smallest residual error is chosen for the model development.

The validation residual errors for all the metals, as shown in Figure 5.37, decrease with the increasing number of PLS components. From the fourth PLS component to tenth, the residual errors are minimal and almost equal. The model with four components was chosen for further analysis. Other components greater than the fourth one can be chosen, however they could result in an over fitting of the model, thus a prediction ability of the model will decrease.

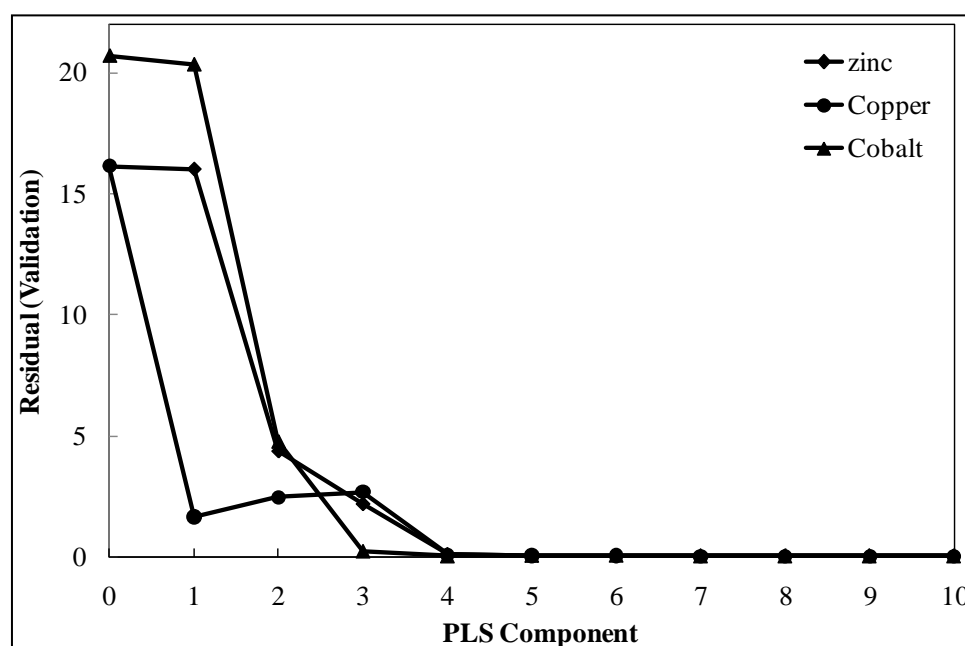


Figure 5.37: Cross- validation method for the PLS model

5.6.2.2.3 Model Prediction

The four component calibrated PLS model was used to determine the metals' concentrations of the unknown samples. The prediction values for all the metals were scaled to percentage values, as shown in Figure 5.38. This comparison enabled the evaluation of the overall prediction ability of the PLS model. Zinc shows slightly low R^2 value and this could be explained by its low relative intensity in the mixture. However, the high R^2 values for all the metals indicate that the PLS model have a good accuracy for predicting the concentrations of their unknown samples.

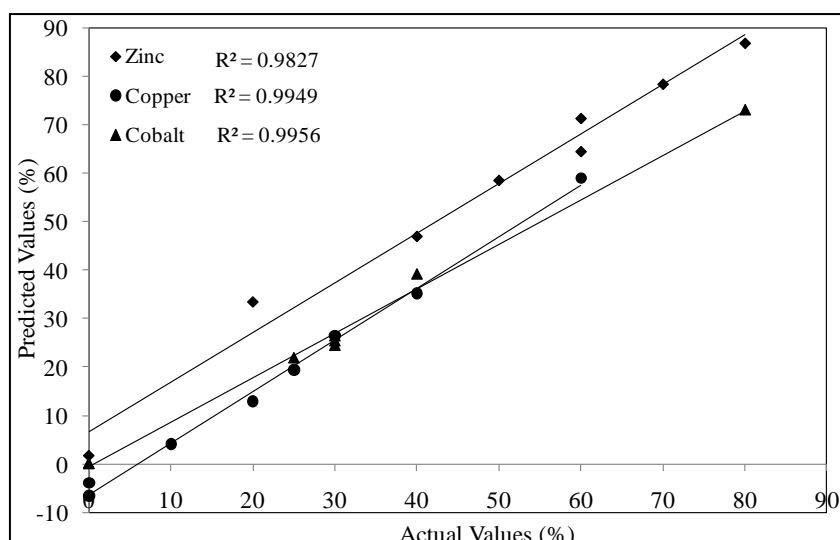


Figure 5.38: Prediction results of the unknown samples

The prediction ability of the PLS model was compared to the ILS and CLS models. The results of all the models are shown in Figure 5.39 as the bar plot. As previously discussed, the high degree quality of the model is based on % RMSE value less than 10. Copper and cobalt can be predicted accurately by the ILS and PLS models with % RMSE less than 5, whereas zinc was predicted accurately by the PLS model only. The pronounced prediction ability of the PLS over the other models is mainly due to the fact that during the PLS calibration step, both concentration and absorbance data are decomposed into latent variables. These variables are uncorrelated in low dimensional data space, thus the prediction results is much increased in PLS model.

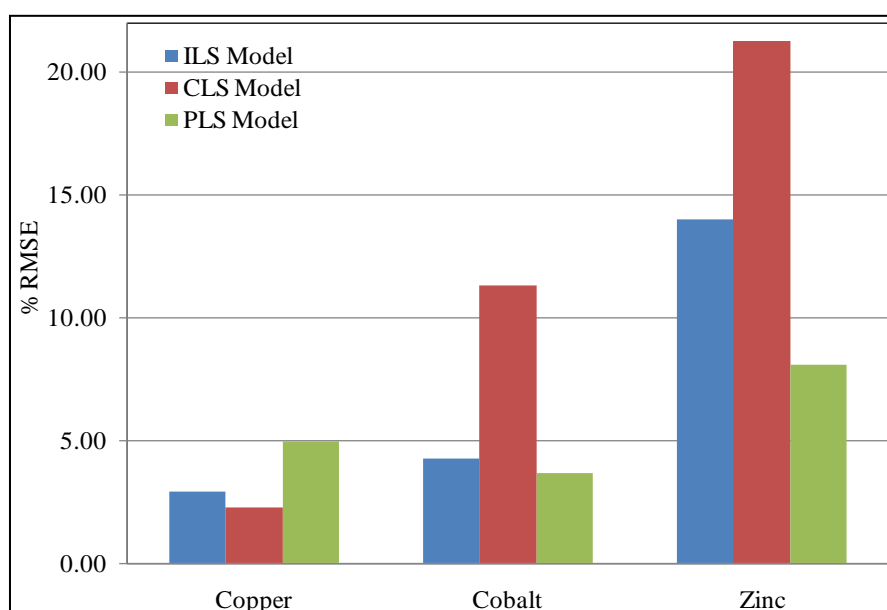


Figure 5.39: Comparison of the ILS, CLS and PLS model

As show in Figure 5.39, the PLS model gave improved prediction results for Zn and this was a major concern for both ILS and CLS models. Multiple comparisons and ANOVA tests were carried out to determine if there is any significant difference between the accuracy of all the models. The mean values of the models were tested at 5 % significance level. The results in Table 5.12 show a 95% confidence interval for the difference of the means within each pair. All the intervals include 0, so it was concluded that there is insignificant difference among the models. P-values also shown in Table 5.12 indicate the probability of finding the mean values of all the models to be same for a specific metal. A high P-value for Cu shows that all the models have a similar accuracy for this metal as compared to Co and Zn metal. The degree of accuracy decreases with lower P-value.

Table 5.12: Statistically comparisons for prediction ability of CLS, ILS and PLS model

Model 1	Model 2	Copper		Cobalt		Zinc	
		-95% C.I	+95% C.I	-95% C.I	+95% C.I	-95% C.I	+95% C.I
CLS	ILS	-34.5508	61.8682	-28.2948	28.4089	-17.3093	36.9313
CLS	PLS	-25.3066	71.1124	-24.6377	32.0660	-13.9102	40.3305
ILS	PLS	-38.9653	57.4537	-24.6948	32.0090	-23.7212	30.5195
P-value		0.9311		0.4571		0.4957	

5.6.3 Atomic Absorption Spectroscopy (AAS)

The previous discussions show that both ILS and CLS models have a comparison similar to that of Blue Cube and PLS models. All the models compared were statistical methods. It was worthwhile to compare the prediction results of the ILS and CLS models with the analytical technique. The test samples were analysed by atomic absorption spectroscopy (AAS) technique. The AAS experiments involve the calibration of each metal at the time. After the calibration, then the test samples are analysed for the Cu, Co and Zn metal in the solutions. The metals are quantified individually from each sample. The calibration curve of the AAS technique is done by highly pure standard solutions for each metal.

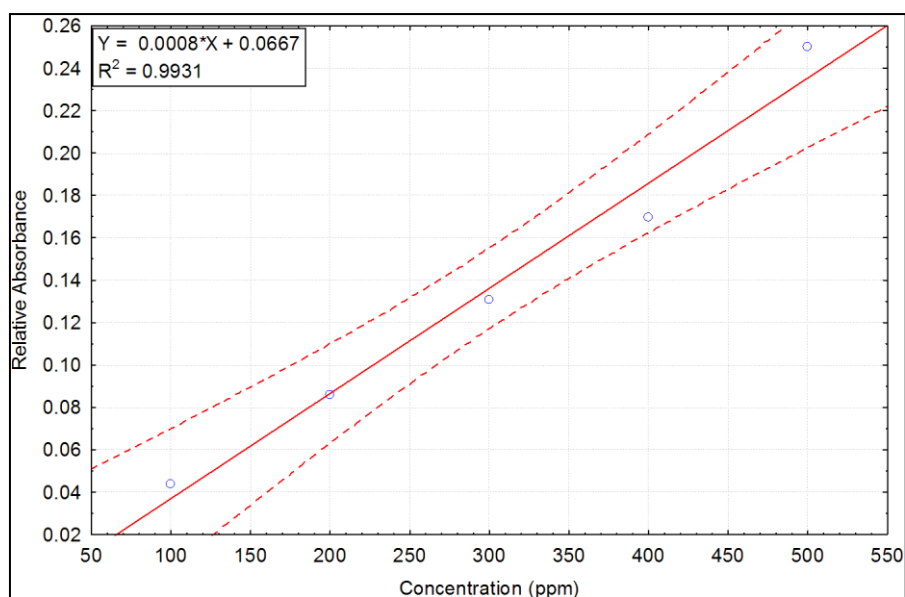


Figure 5.40: Calibration graph of the Cu metal for AAS analysis

Figure 5.40 shows the calibration graph for Cu metal during the AAS experiments. It can be observed that a good relationship was found between the relative absorbance of Cu metal and its concentration. The high R^2 value indicates that the linear regression fit the data accurately. A solid line in the scatter plot shows the linear regression fit between the measured and model values, whereas the dotted lines show 95 % confidence interval limits for an estimation of good fit for the data. The results for the Co and Zn metal are given in Appendix E as Figure E.5 and E.6. Their results are similar to that of Cu metal.

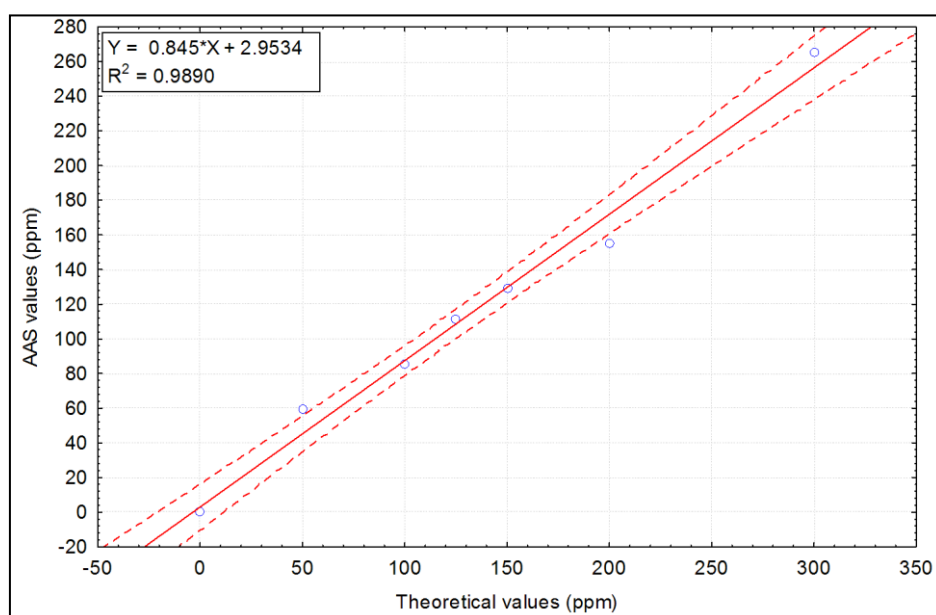


Figure 5.41: Predicted results for copper using the AAS technique

Figure 5.41 shows the predicted results for the analysis of the Cu metal. The high R^2 value of 0.9890 from the regression line shows that the AAS technique can measure the Cu metal very accurately from the solutions. The results that are presented here have the similar accuracy and precision than that of the prediction results of the ILS and CLS models. The AAS experiments confirmed that the results of the ILS and CLS models were accurate.

In summary, this section study had proved that the accuracy and precision of both the ILS and CLS models are comparable with those of the AAS method. However, the advantages of the models are the simultaneous quantification of Cu, Co and Zn metals and the speed of the analysis. The calibration procedure for each metal for the AAS method makes the analysis time to be much longer as compared in the statistical models. Furthermore, the models also showed a more reliable data interpretation than the AAS method.

CHAPTER 6: CONCLUSIONS AND RECOMMENDATIONS

This chapter gives the conclusions and recommendations based on the outcome of the results in the current study. It is shown that the CLS and ILS calibration models cannot predict effectively the samples performed at different experimental conditions. Nonetheless, the accuracy of these models is similar to that of the Blue Cube and PLS models within 95% confidence intervals. The future work is recommended based on the observations made during the experimental analyses and the literature review being studied.

6 CONCLUSIONS AND RECOMMENDATIONS

6.1 Conclusions

Diffuse reflectance spectrophotometry was calibrated successfully with standard solution and the preprocessing technique used to convert the raw data into absorbance values was very useful in both the quantitative and qualitative analyses of the Cu, Co and Zn metals. The height and position of the maximum absorption peaks were utilised respectively for each analysis. The peaks for Cu, Co and Zn metal occur at the wavelengths of 800, 510 and 430 nm respectively.

The CLS and ILS models have similar accuracy for all the metals during the calibration step with R^2 values greater than 0.950. However, the CLS model showed less reliable prediction results for all the metals as compared to the ILS model. In addition, both the ILS and CLS models gave poor predictions for zinc, compared to Cu and Co, with the R^2 values of 0.9334 and 0.8995 respectively. The poor prediction results are due to the low relative intensity of the Zn metal in the mixture. Zinc ions have outer shells that are completely filled with electrons in their d-orbitals; hence rate of transition within the ions is very limited.

The intensity of the absorption spectra of the metals increased with the rise in temperature. The increase in the nickel concentration lowered the predicted values for Cu and Co metal but on the other hand it increased the predicted values for Zn metal. In general, the models developed from a normal room temperature in the absence of contaminants could not handle effectively the effect in the increase of temperature and nickel concentration. The models could only give accurate results up to temperature of 40 °C and 50 ppm of nickel concentration.

The accuracy and precision of these statistical (ILS and CLS) models were determined to be similar to the results of Blue Cube optical fibre sensor within 95% confidence interval limits. The performance between the models and sensor was estimated using the analysis of variance (ANOVA) test. The PLS model shows a similar accuracy when compared to both ILS and CLS models for prediction of copper and cobalt metals. However the PLS model demonstrates improved predictive ability for the determination of zinc metal. The results of all the statistical models were verified and validated by the analytical technique, atomic absorption spectroscopy (AAS) and good comparison was found.

Furthermore, the use of the experimental design revealed that there are no interactions between individual metals in the solution of mixture, i.e. interaction terms in a linear regression model were found to be insignificant at a 95% confidence level. The graphical display of the results, given as the contour plots also revealed a linear relationship among the metals. The linear regression model was given as follows: $Y = 0.2987x_{Cu} + 0.05249x_{Co} + 0.04516x_{Zn}$. Based on coefficients of Cu, Co and Zn metal derived from the regression model, the contribution of the metals was determined to decrease in this order; Cu > Co > Zn.

In an attempt to improve the prediction ability of the models for Zn quantification, first to fourth order of derivative spectroscopy was employed. The third order derivative shows similar results as the zero absorbance spectroscopy but other orders of the derivative spectroscopy gave inaccurate results for all the metals with %RMSE greater than 10. The predictions became very poor due to difficulties involved in selecting the wavelength region for the models. None of the orders of the derivative shows improved prediction results for Zn.

In general, this study demonstrates that the chemometric models (ILS and CLS) developed here can be used for quantification of several metals in real hydrometallurgical solutions, as samples were simulated according to conditions in a zinc plant. However, in order to observe the potential applicability of the study, the models must be further tested and applied on real samples as discussed in Section 6.2 below.

6.2 Recommendations

A manual selection method used to select the wavelength region in this study is very tedious, time consuming and sometimes is quite impossible to be employed in the derivative spectroscopy. Hence other methods like genetic algorithm or neural network must be sorted out. Wiegand *et al.*, (2009) showed that a robust genetic algorithm can effectively perform the variable selection in a PLS model to extract valuable information about the predictors.

The low intensity of Zn metal can be increased by using a complex agent that will chelate the Zn ions in the solutions and thus, enhance the maximum absorption peak of Zn metal. This enhancement procedure will only be applicable to the laboratory samples. When the models are supposed to be used in the industrial applications, the enhancement procedure will add cost to a plant. But this procedure could give indication whether poor predictions results is due to low absorbance in the mixtures solution.

In order to study the influence of temperature and nickel concentration on the absorption measurements of Cu, Co and Zn metals very effectively, a combined factorial-mixture design must be used. The details of such experimental design are explained by Anderson and Whitcomb, (2000). They illustrated the experiments that simultaneously combine mixture components of a solution and process factors of an operation.

Finally, the potential applicability of the study can further evaluated by applying the developed statistical (ILS and CLS) models on spectra data of the real plant solutions. Then assess the performance of the models in terms of the disturbances encountered in a plant operation. However, more experiments needed to be done in the laboratory to evaluate the effect of flow rate.

REFERENCE

- Abbaspour, A. and Mirzajani, R., 2005. Simultaneous determination of phenytoin, barbital and caffeine in pharmaceuticals by absorption (zero-order) UV spectra and first-order derivative spectra--multivariate calibration methods. *Journal of Pharmaceutical and Biomedical Analysis*, 38(3): 420-427.
- Abbaspour, A. and Moosavi, S.M.M., 2002. Chemically modified carbon paste electrode for determination of copper(II) by potentiometric method. *Talanta*, 56(1): 91-96.
- Aldrich, C., Marais, C., Shean, B.J. and Cilliers, J.J., 2010. Online monitoring and control of froth flotation systems with machine vision: A review. *International Journal of Mineral Processing*, 96(1-4): 1-13.
- Alfantazi, A.M. and Valic, D., 2003. A study of copper electrowinning parameters using a statistically designed methodology. *Journal of Applied Electrochemistry*, 33(2): 217-225.
- Alvey, D.C., Morton, K., Hammon, R., Gotfried, J., Remus, J., Collins, L. and Wise, M. 2010. Laser-induced breakdown spectroscopy-based geochemical fingerprinting for the rapid analysis and discrimination of minerals: the example of garnet. *Appl. Opt.*, 49(13): 168-180.
- Anderson, M.J. and Whitcomb, P.J., 2000. Designing Experiments that Combine Mixture Components with Process Factors. *PCI Magazine*: 1- 9.
- Bari, F., Begum, N., Jamaludin, S.B. and Hussin, K., 2009. Extraction and separation of Cu(II), Ni(II) and Zn(II) by sol-gel silica immobilized with Cyanex 272. *Hydrometallurgy*, 96(1-2): 140-147.
- Bartolacci, G., Pelletier, P., Tessier, J., Duchesne, C., Bosse, P-A. and Ournier, 2006. Application of numerical image analysis to process diagnosis and physical parameter measurement in mineral processes- Part I: Flotation control based on froth textural characteristics. *Minerals Engineering*, 19: 734-747.

- Basile, A., Hughes, J., McFarlane, A.J. and Bhargava, S.K., 2010. Development of a model for serpentine quantification in nickel laterite minerals by infrared spectroscopy. *Minerals Engineering*, 23(5): 407-412.
- Benalia, B., Boucetta, A., Lazara, Z., Elblidia, K. and El Assyrya, A., 2006. Temperature effect on spectral and conformational properties of 4-naphthyl-quinoline: UV-visible spectroscopy study. *Journal of Molecular Liquids*, 126: 29-32.
- Biesinger, M.C., Hart, B.R., Polack, R., Kobe, B.A. and Smart, R.S.C., 2007. Analysis of mineral surface chemistry in flotation separation using imaging XPS. *Minerals Engineering*, 20(2): 152-162.
- Blanco, M., Serrano, D. and Bernal, J.L., 1999. UV-spectrophotometric determination of beclomethasone dipropionate and phenylethyl alcohol in a nasal spray by inverse least-squares regression. *Talanta*, 50(3): 527-532.
- Buke, B., Divrikli, U., Soylak, M. and Elci, L., 2009. On-line preconcentration of copper as its pyrocatechol violet complex on Chromosorb 105 for flame atomic absorption spectrometric determinations. *Journal of Hazardous Materials*, 163(2-3): 1298-1302.
- Carla, P.S., Helena, M.C., Luciana, S.R. and José, P.P., 2009. Evaluation of poly(sodium 4-styrenesulfonate) film coating in thin mercury film electrodes for lead determination. *Journal of Electroanalytical Chemistry*, 626: 192-196.
- Christine, M.A. and Montgomery, D.C., 2008. Response Surface Design Evaluation and Comparison. *Journal of Statistical Planning and Inference*, 139: 1-8.
- Cirovic, D.A., 1998. Influence of mixture design on multivariate prediction of PAHs in mixture spectra. *Talanta*, 45(5): 989-1000.
- Claeys-Bruno, M., Lamant, J., Blasco, L., Phan-Tan-Luu, R. and Sergent, M., 2009. Development of a skin care formulation using experimental designs. *Chemometrics and Intelligent Laboratory Systems*, 96(2): 101-107.

- Coghill, P.J., Millen, M.J. and Sowerby, B.D., 2002. On-line measurement of particle size in mineral slurries. *Minerals Engineering*, 15: 83-90.
- Cornell, J.A., 1981. *Experiments with mixtures*. John Wiley & Sons, New York.
- De Luca, M., Oliverio, F., Ioele, G. and Ragno, G., 2009. Multivariate calibration techniques applied to derivative spectroscopy data for the analysis of pharmaceutical mixtures. *Chemometrics and Intelligent Laboratory Systems*, 96(1): 14-21.
- De Waal, P., 2007. Tomorrow's Technology-Out of Africa-Today. *The Journal of the South African Institute of Mining and Metallurgy*: 3,7-8.
- De Waal, P. and Du Plussis, F.E., 2005. Automatic control of a high tension roll separator. *Heavy Minerals 2005, Society for Mining, Metallurgy, and Exploration,, Heavy Minerals Conference Proceedings 2005*: 241-249
- Demetriades-Shah, T.H., Steven, M.D. and Clark, J.A., 1990. High resolution derivative spectra in remote sensing. *Remote Sensing of Environment*, 33(1): 55-64.
- Dinç, E., 2003. Linear regression analysis and its application to the multivariate spectral calibrations for the multiresolution of a ternary mixture of caffeine, paracetamol and metamizol in tablets. *Journal of Pharmaceutical and Biomedical Analysis*, 33(4): 605-615.
- Dinç, E. and Üstündag, Ö., 2003. Spectrophotometric quantitative resolution of hydrochlorothiazide and spironolactone in tablets by chemometric analysis methods. *Il Farmaco*, 58(11): 1151-1161.
- Dinç, E., Yücesoy, C., Palabiyik, I.M., Üstündag, Ö. and Onur, F., 2003. Simultaneous spectrophotometric determination of cyproterone acetate and estradiol valerate in pharmaceutical preparations by ratio spectra derivative and chemometric methods. *Journal of Pharmaceutical and Biomedical Analysis*, 32(3): 539-547.

- Fisher, R.A., 1925. *Statistical Methods for Research Workers*. Oliver and Boyd, London.
- Gaft, M., Sapir-Sofer, I., Modiano, H. and Stana, R., 2007. Laser Induced Breakdown Spectroscopy for Bulk Minerals online Analyses. *Spectrochimica Acta:Part B*, 62: 1496-1498.
- Griffiths, P.R. and de Haseth, J.A., 2007. *Fourier transform infrared spectrometry*. John Wiley & Sons, New Jersey, 207-212 pp.
- Güell, R., Fontàs, C., Salvadó, V. and Anticó, E., 2007. Development of a selective optical sensor for Cr(VI) monitoring in polluted waters. *Analytica Chimica Acta*, 594(2): 162-168.
- Haaland, D.M., Chambers, W.B., Keenan, M.R. and Melgaard, D.K., 2000. Multi-window Classical Least-Squares Multivariate Calibration Methods for Quantitative ICP-AES Analyses. *Applied Spectroscopy*, 54(9): 1291-1302.
- Haaland, D.M., Han, L. and Niemczyk, T.M., 1999. Use of CLS to Understand PLS IR Calibration for Trace Detection of Organic Molecules in Water. *Applied Spectroscopy*, 53(4): 390-395.
- Haaland, D.M. and Melgaard, D.K., 2000. New Prediction-Augmented Classical Least-Squares (PACLS) Methods: Application to Unmodeled Interferents. *Applied Spectroscopy*, 54(9): 1303-1312.
- Haaland, D.M. and Melgaard, D.K., 2001. New Classical Least-Squares/Partial Least-Squares Hybrid Algorithm for Spectral Analyses. *Applied Spectroscopy*, 55(1): 1-8.
- Haaland, D.M. and Thomas, E.V., 1988. Partial least-squares methods for spectral analyses. 1. Relation to other quantitative calibration methods and the extraction of qualitative information. *Analytical Chemistry*, 60(11): 1193 - 1202.
- Haavisto, O., 2010. Detection and analysis of oscillations in a mineral flotation circuit. *Control Engineering Practice*, 18(1): 23-30.

- Haavisto, O. and Hyötyneimi, H., 2009. Recursive multimodel partial least squares estimation of mineral flotation slurry contents using optical fibre reflectance spectra. *Analytica Chimica Acta*, 642: 102-109.
- Haavisto, O. and Kaartinen, J., 2009. Multichannel reflectance spectral assaying of zinc and copper flotation slurries. *International Journal of Mineral Processing*, 93(2): 187-193.
- Haavisto, O., Kaartinen, J. and Hyötyniemi, H., 2008. Optical spectrum based measurement of flotation slurry contents. *International Journal of Mineral Processing*, 88(3-4): 80-88.
- Jones, C., 2001. d-and f-Block Chemistry. Polestar Wheatons Ltd. Royal Society of Chemistry, Cambridge, 97-130 pp.
- Kumagai, Y., Lin, M., Lampre, I., Mostafavi, M., Muroya, Y. and Katsumura, Y., 2008. Temperature effect on the absorption spectrum of the hydrated electron paired with a metallic cation in deuterated water. *Radiation Physics and Chemistry*, 77(10-12): 1198-1202.
- Leardi, R., 2009. Experimental design in chemistry: A tutorial. *Analytica Chimica Acta*, 652(1-2): 161-172.
- Lewis, E., Sheridan, C., O'Farrell, M., King, D. and Flanagan, C., 2007. Principal component analysis and artificial neural network based approach to analysing optical fibre sensors signals. *Sensors and Actuators*, 136: 28-38.
- Lottering, J.M. and Aldrich, C., 2006. Online Measurement of Factors Influencing the Electrostatic Separation of Mineral Sands. *The Journal of the South African Institute of Mining and Metallurgy*, 106: 2.
- Melgaard, D.K., Haaland, D.M. and Wehlburg, C.M., 2002. Concentration Residual Augmented Classical Least Squares (CRACLS): A Multivariate Calibration Method with Advantages over Partial Least Squares. *Appl. Spectrosc.*, 56(5): 615-624.

- Michaud, D., Leclerc, R. and Proulx, É., 2007. Influence of particle size and mineral phase in the analysis of iron ore slurries by Laser-Induced Breakdown Spectroscopy. *Spectrochimica Acta Part B: Atomic Spectroscopy*, 62(12): 1575-1581.
- Montgomery, D.C. and Runger, G.C., 2002. *Applied statistics and probability for engineers*. John Wiley & Sons, Inc., 510 - 523 pp.
- Mutihac, L. and Mutihac, R., 2008. Review: Mining in Chemometrics. *Analytica Chimica Acta*, 612: 1-18.
- Nagaraj, Vipul, K. and Rajshree, M., 2007. Simultaneous Quantitative Resolution of Atorvastatin Calcium and Fenofibrate in Pharmaceutical Preparation by Using Derivative Ratio Spectrophotometry and Chemometric Calibrations. *Analytical Science*, 23: 445 - 451
- Oestreich, J.M., Tolley, W.K. and Rice, D.A., 1994. The development of a color sensor system to measure mineral compositions. *Minerals Engineering*, 8(1-2): 31-39.
- Ozdemir, D., 2008. Near Infrared Spectroscopic Determination of Diesel Fuel Parameters Using Genetic Multivariate Calibration. *Petroleum Science & Technology*, 26(1): 101-113.
- Paradkar, R.P. and Williams, R.R., 1996. Genetic Regression as a Calibration Technique for Solid-Phase Extraction of Dithizone-Metal Chelates. *Applied Spectroscopy*, 50(6): 753-758.
- Paula, C.A., Alberto, N.A. and Montenegro, C.P., 2004. Direct Determination of Copper in Urine using a Sol-gel optical Sensor Coupled to Multicommutated Flow System. *Anal Bioanal Chem*, 380: 108 - 114.
- Pons, C., Forteza, R. and Cerdà, V., 2005. Optical fibre reflectance sensor for the determination and speciation analysis of iron in fresh and seawater samples coupled to a multisyringe flow injection system. *Analytica Chimica Acta*, 528(2): 197-203.

- Remes, A., Saloheimo, K. and Jamsa-Jounela, 2007. Effect of speed and accuracy of on-line elemental analysis on flotation control performance. *Minerals Engineering*, 20: 1055-1066.
- Sammon, J.W., Jr., 1969. A nonlinear mapping for data structure analysis. *IEEE Transactions on Computers*, c-18(5): 401-409.
- Sauter, D. and Ragot, J., 2008. Advanced control methodologies for mining, mineral and metal (MMM) processing industries. *Control Engineering Practice*, 16: 157-158.
- Schneider, A., 1998. Optical Sensor System for the Online Measurement of Carbon in Fly ash. *Sensors and Actuators*, 380: 27-32.
- Skoog, D.A., Holler, F.J. and Crouch, S.R., 2008. *Fundamentals of Analytical Chemistry*. Thomson Brooks/Cole, Canada, Chapter 24 & 26 pp.
- Sowerby, B., 2002. Online Measurement and Control in Sustainable Mineral Processing and Energy Production. *ATSE Focus*, 120: 1.
- Statsoft, 2007. *Design of Experiments with Statistica*. High Performance Statistical Software, Tulsa.
- Van Tonder, E., Deglon, D.A. and Napier-Munn, T.J., 2010. The effect of ore blends on the mineral processing of platinum ores. *Minerals Engineering*, 23(8): 621-626.
- Wiegand, P., Pell, R. and Comas, E., 2009. Simultaneous variable selection and outlier detection using a robust genetic algorithm. *Chemometrics and Intelligent Laboratory Systems*, 98(2): 108-114.
- Wills, B.A., 1997. *Mineral processing technology*, Sixth Edition. Butterworth-Heinemann, Oxford, 258-274 pp.
- Wold, S., Sjöström, M. and Eriksson, L., 2001. PLS-regression: a basic tool of chemometrics. *Chemometrics and Intelligent Laboratory Systems*, 58(2): 109-130.

- Ylinen, R., Miettunen, J., Molander, M. and Siliamaa, E.R., 2000. Vision and model -based control of flotation. In: Future trends in automation in mineral and metal Processing. IFAC MM'2000, 22: 475-480.
- Yurii, B., Galina, G., Laurence, A.N., Teresa, B.F. and Yanan, H., 2005. Phase equilibrium in poly(rA) · poly(rU) complexes with Cd and Mg ions, studied by ultraviolet, infrared, and vibrational circular dichroism spectroscopy. *Biopolymers*, 78(5): 275-286.
- Zachariassen, C.B., Larsen, J., van den Berg, F. and Engelsen, S.B., 2005. Use of NIR spectroscopy and chemometrics for on-line process monitoring of ammonia in Low Methoxylated Amidated pectin production. *Chemometrics and Intelligent laboratory systems*, 76: 149-161.

APPENDIX A: TEST SAMPLES

The individual metals' concentration values for the unknown samples were chosen arbitrary so that the overall percentage of the metals equals to 100 %. The values in Table A.1 were selected and prepared to fall within the concentration range of the calibration samples.

Table A. 1: Composition of the unknown samples

Percentage of each metal from maximum concentration (%)			
RUN	Zn	Cu	Co
1	60.00	10.00	30.00
2	50.00	25.00	25.00
3	70.00	0.00	30.00
4	80.00	20.00	0.00
5	0.00	60.00	40.00
6	20.00	0.00	80.00
7	60.00	40.00	0.00
8	40.00	30.00	30.00

APPENDIX B: PERFORMANCE OF CLS MODEL

B.1 Calibration Step of CLS model

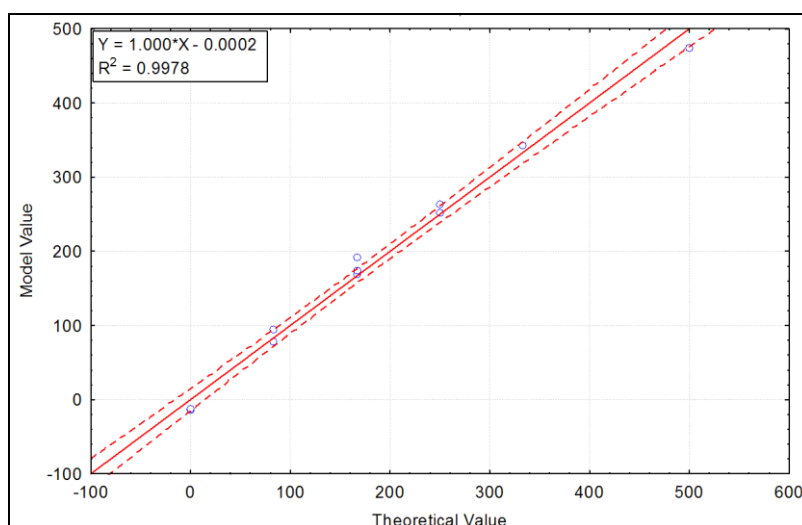


Figure B. 1: Calibration graph for the Cu metal using CLS model

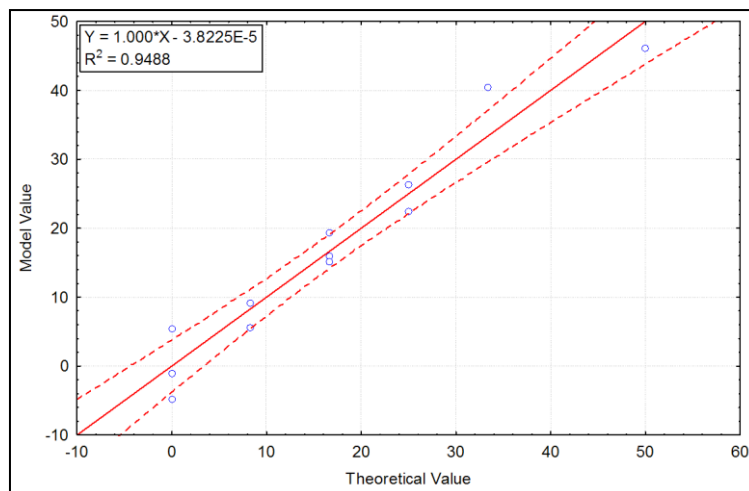


Figure B. 2: Calibration graph for the Co metal using CLS model

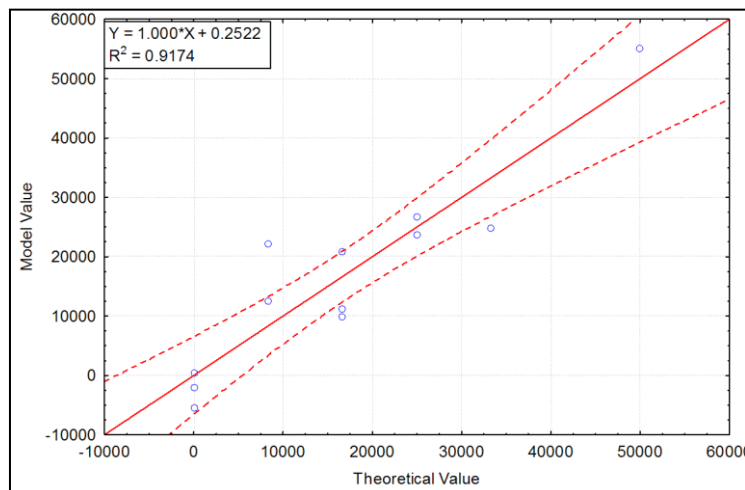


Figure B. 3: Calibration graph for the Zn metal using CLS model

B.2 Prediction Step of CLS Model

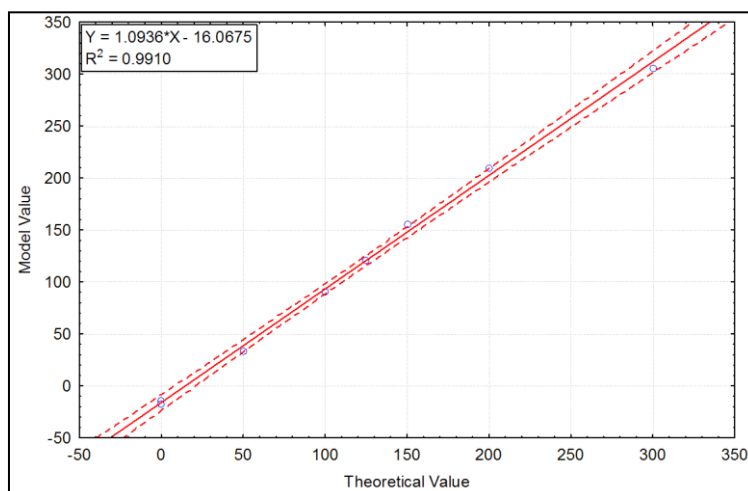


Figure B. 4: Graph for the prediction of Cu metal using CLS model

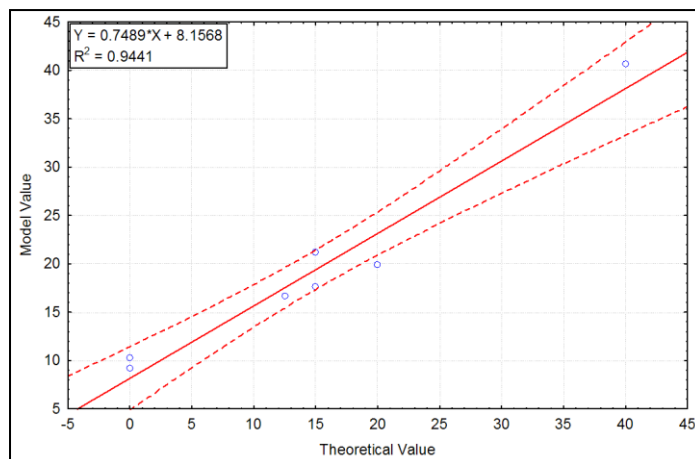


Figure B. 5: Graph for the prediction of Co metal using CLS model

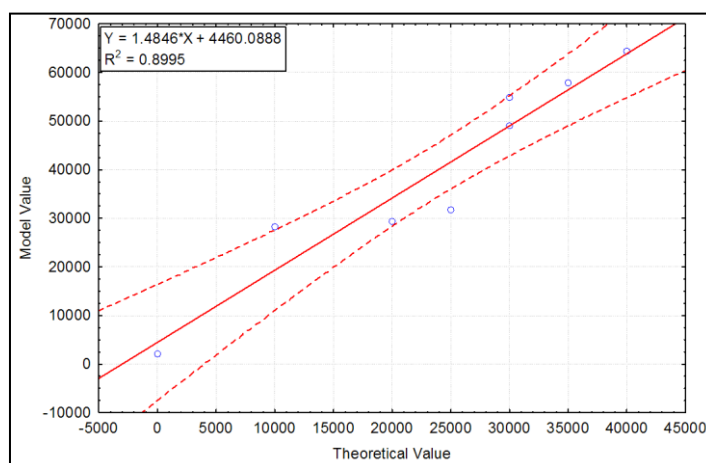


Figure B. 6: Graph for the prediction of Zn metal using CLS model

APPENDIX C: DERIVATIVE SPECTROSCOPY

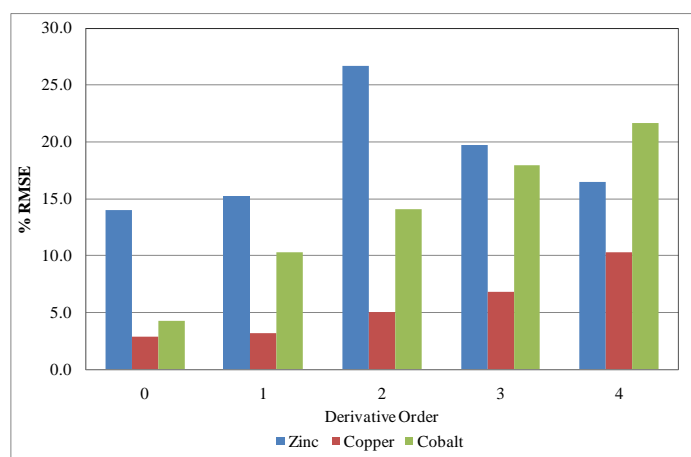


Figure C. 1: Evaluation of the derivative orders based on % RMSE

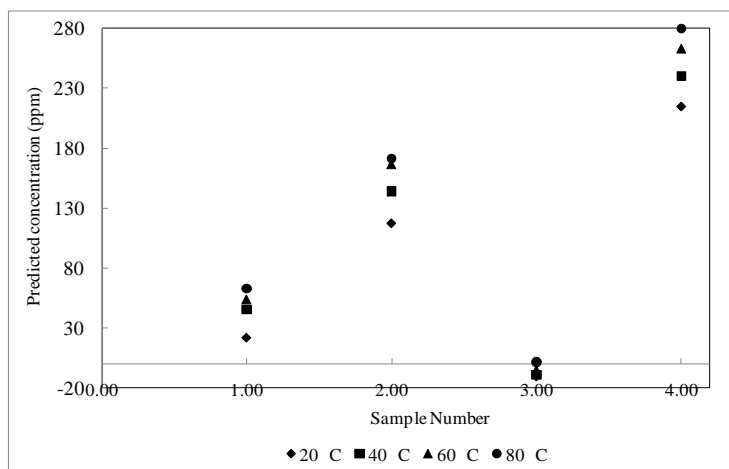
APPENDIX D: FACTORS AFFECTING CLS MODEL**D.1 Effect of the temperature**

Figure D. 1: Prediction ability of CLS model for copper metal at various temperatures

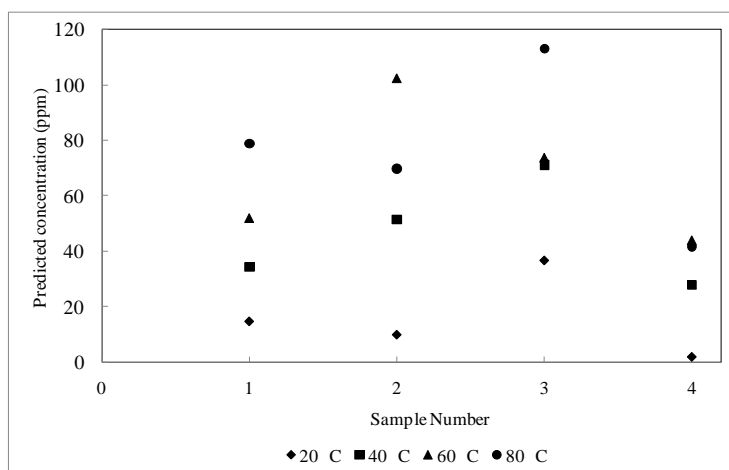


Figure D. 2: Prediction ability of CLS model for cobalt metal at various temperatures

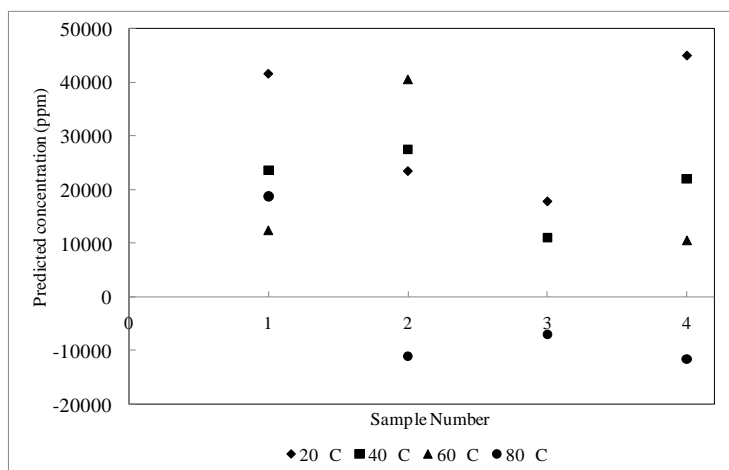


Figure D. 3: Prediction ability of CLS model for zinc metal at various temperatures

D.2 Effect of the Nickel concentration

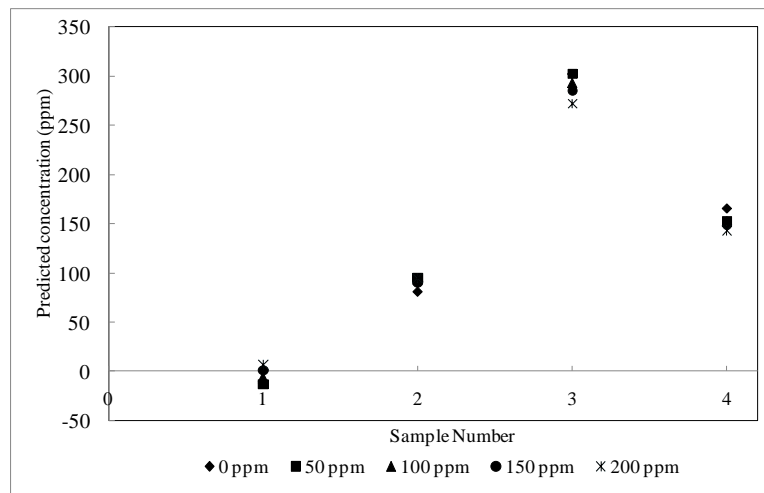


Figure D. 4: Prediction ability of ILS model for copper metal in presence of nickel

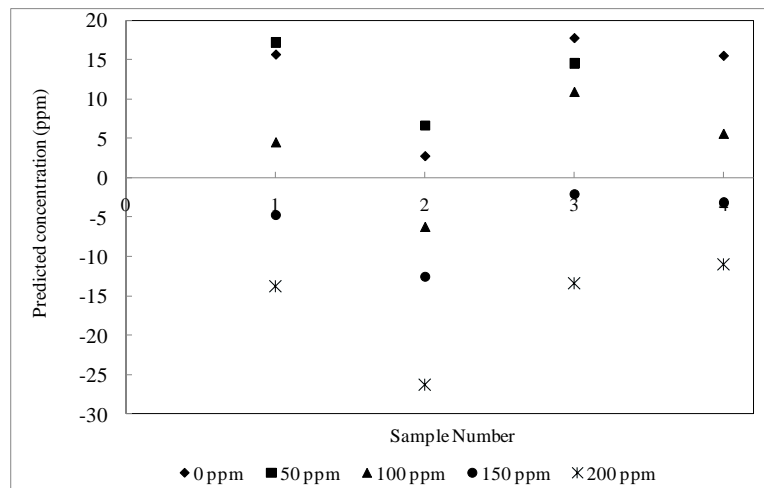


Figure D. 5: Prediction ability of ILS model for cobalt metal in presence of nickel

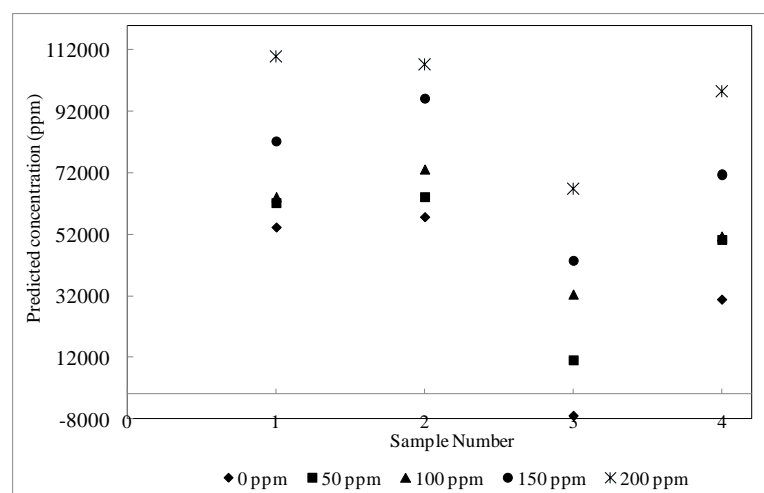


Figure D. 6: Prediction ability of ILS model for zinc metal in presence of nickel

APPENDIX E: SUPPLEMENTARY METHODS

E.1 PLS model evaluation

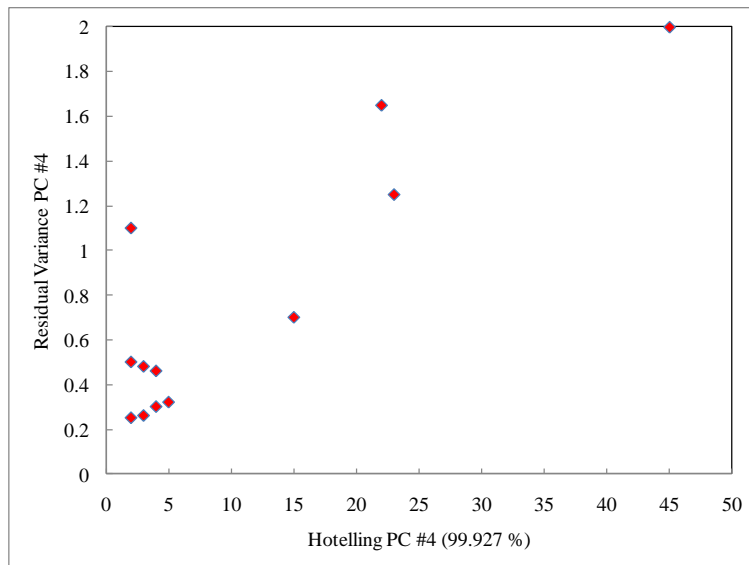


Figure E. 1: Residual plot for identification of outliers

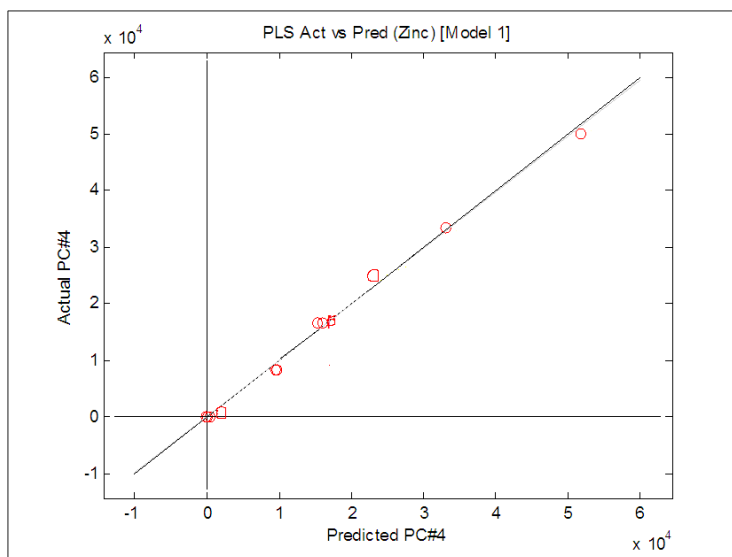


Figure E. 2: Calibration graph of zinc metal for the PLS model

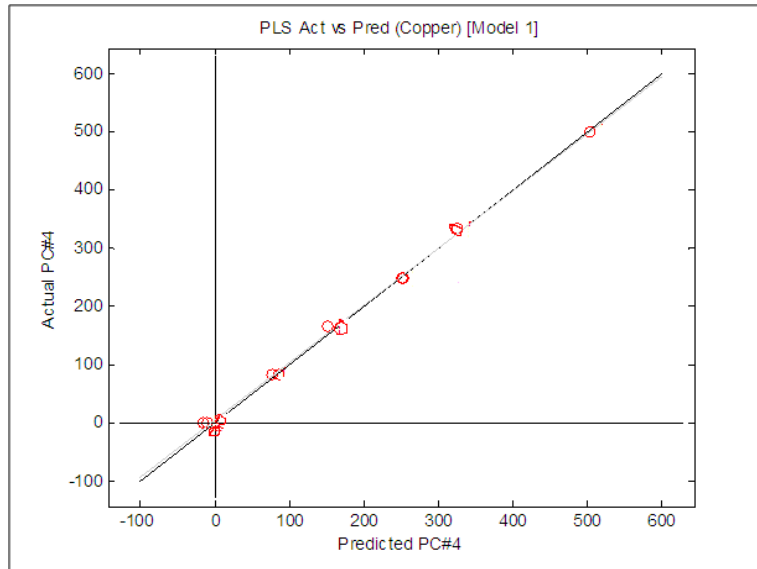


Figure E. 3: Calibration graph of copper metal for the PLS model

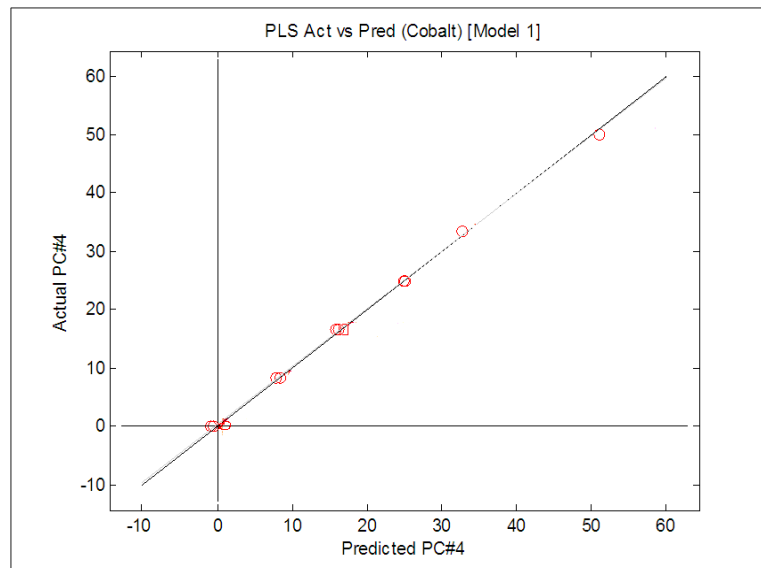


Figure E. 4: Calibration graph of cobalt metal for the PLS model

E.2 AAS experiments

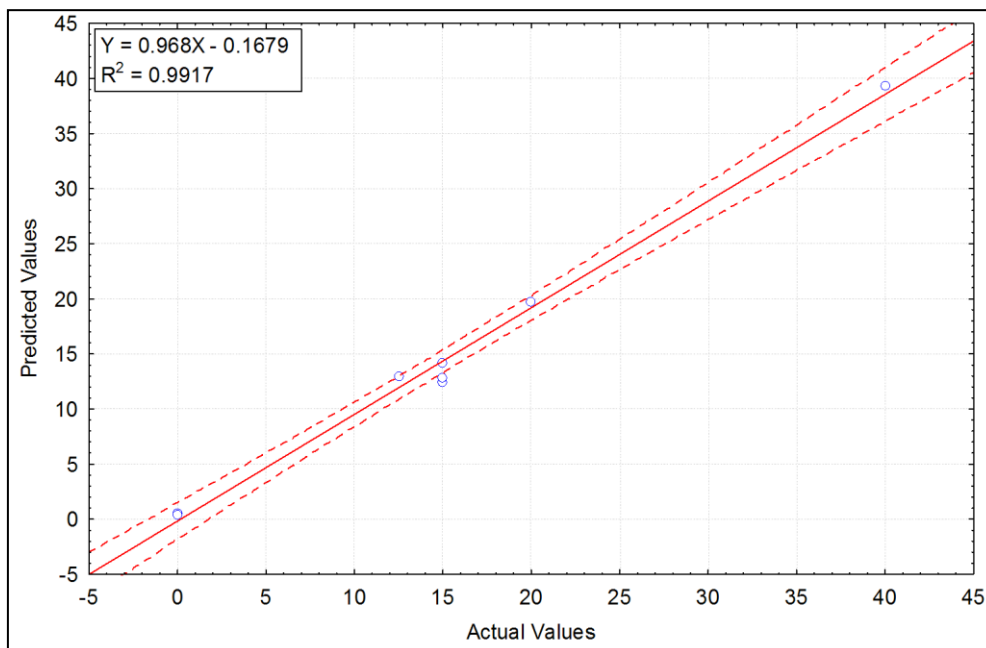


Figure E. 5: Predicted results for cobalt using the AAS technique

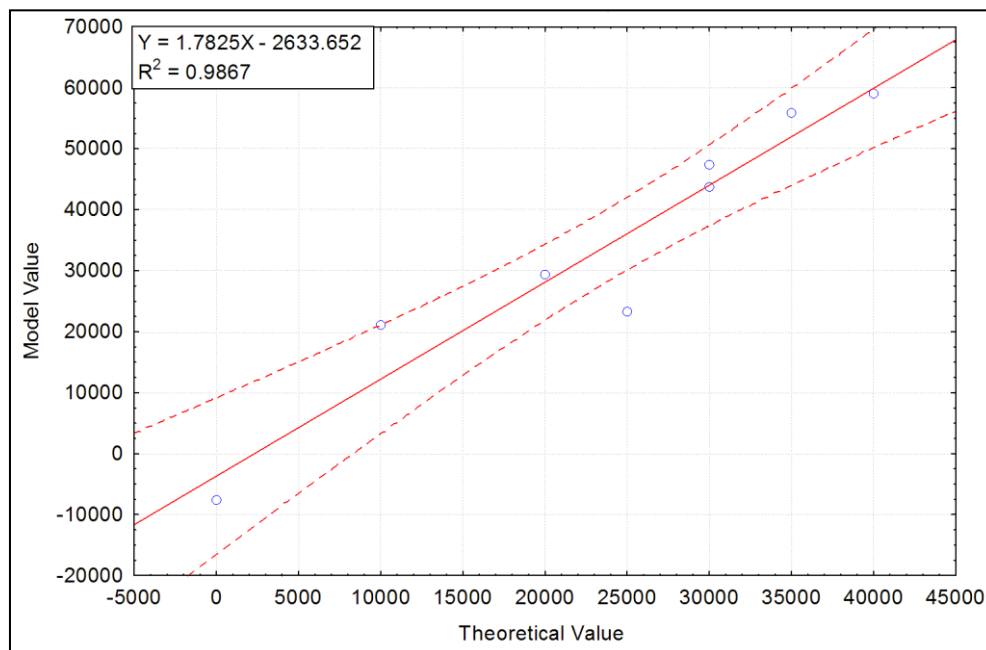


Figure E. 6: Predicted results for zinc using the AAS technique

APPENDIX F: PUBLICATIONS

Presentations

1. Phiri, M.J. and Aldrich, C., 2010: On-line monitoring of hydrometallurgical aqueous solution using diffuse reflectance spectrophotometer. *In: Proceedings of the 2nd International Symposium on the Processing of Zinc Ores and Concentrates (Zinc Processing '10)*, Cape Town, November 13-14.

Peer-reviewed Journal

2. Phiri, M.J. and Aldrich, C., 2010: On-line monitoring of hydrometallurgical aqueous solution using diffuse reflectance spectrophotometer. *Minerals Engineering Journal*. (Submitted for publication).